

AD-A040 008

TEXAS UNIV AT AUSTIN APPLIED RESEARCH LABS
THE SUPPRESSION OF SOUND BY SOUND OF HIGHER FREQUENCY.(U)
MAY 77 W L WILLSHIRE

F/G 20/1

UNCLASSIFIED

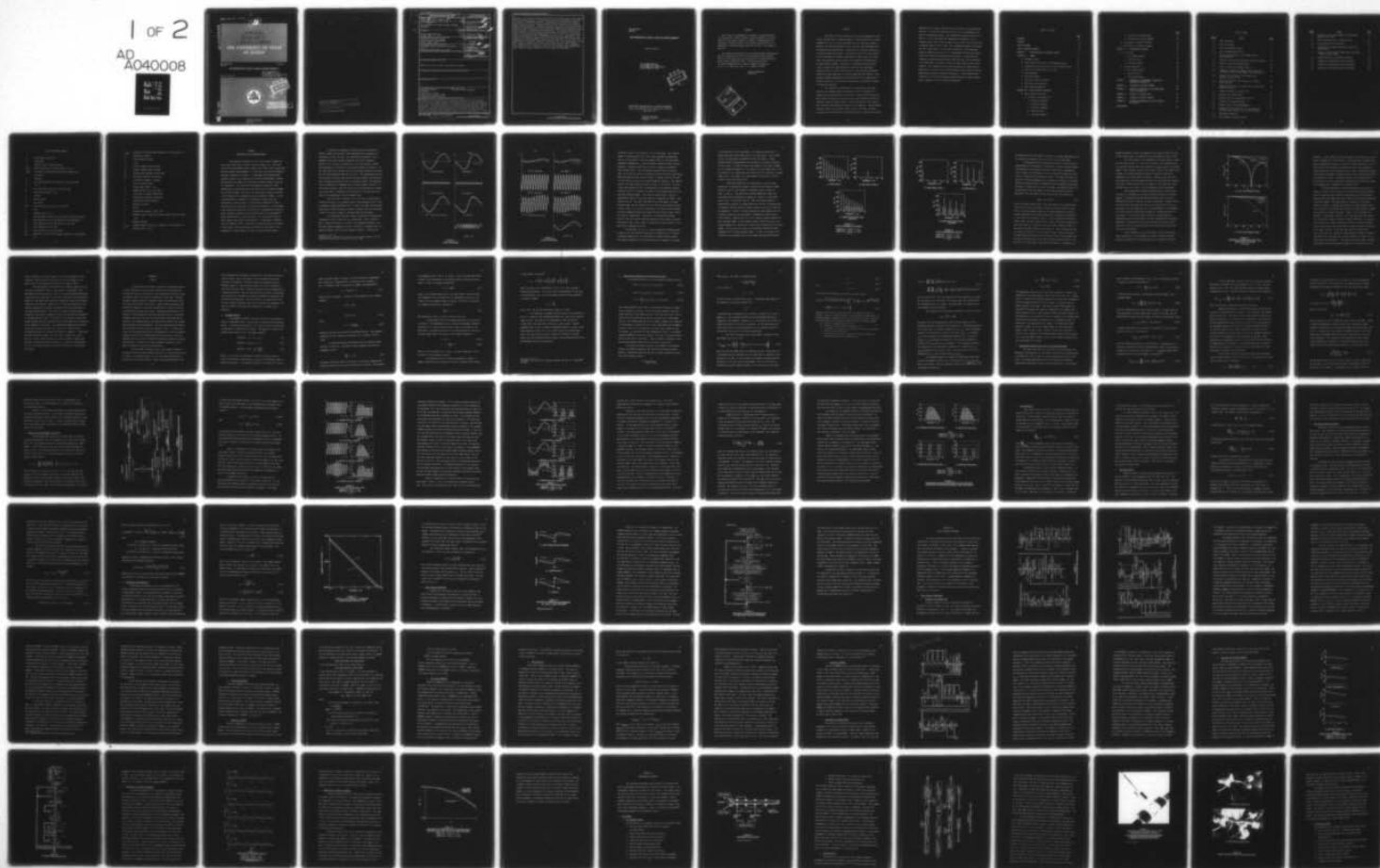
ARL-TR-77-22

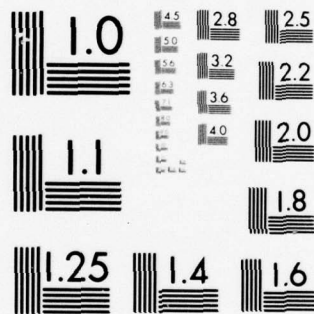
AFOSR-TR-77-0656

F44620-76-C-0040
NL

1 of 2

AD
A040008





MICROCOPY RESOLUTION TEST CHART
NATIONAL BUREAU OF STANDARDS-1963-A

AFOSR - TR - 77 - 0656

AD A 040008

APPLIED
RESEARCH
LABORATORIES

THE UNIVERSITY OF TEXAS
AT AUSTIN

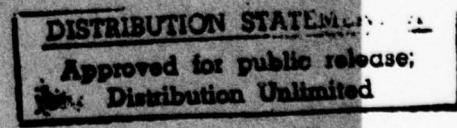
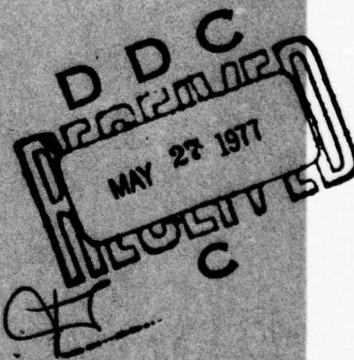
ARL-TR-77-22
May 1977

Copy No.

THE SUPPRESSION OF SOUND BY SOUND OF HIGHER FREQUENCY

William L. Willshire, Jr.

Office of Naval Research
Contract N00014-75-C-0867
Air Force Office of Scientific Research
Contract F44620-76-C-0040




DDC FILE COPY

APPROVED FOR PUBLIC
RELEASE; DISTRIBUTION
UNLIMITED.

AIR FORCE OFFICE OF SCIENTIFIC RESEARCH (AFSC)
NOTICE OF TRANSMITTAL TO DDC
This technical report has been reviewed and is
approved for public release IAW AFR 190-12 (7b).
Distribution is unlimited.
A. D. BLOSE
Technical Information Officer

REPORT DOCUMENTATION PAGE		READ INSTRUCTIONS BEFORE COMPLETING FORM
1. REPORT NUMBER AFOSR -TR-77-0656	2. GOVT ACCESSION NO.	3. RECIPIENT'S CATALOG NUMBER
4. TITLE (and Subtitle) THE SUPPRESSION OF SOUND BY SOUND OF HIGHER FREQUENCY.		5. TYPE OF REPORT & PERIOD COVERED INTERIM rept.
7. AUTHOR(s) WILLIAM L. WILLSHIRE, JR		6. PERFORMING ORG. REPORT NUMBER ARL-TR-77-22
		8. CONTRACT OR GRANT NUMBER(s) F44620-76-C-0040 N00014-75-C-0086
9. PERFORMING ORGANIZATION NAME AND ADDRESS UNIVERSITY OF TEXAS AT AUSTIN APPLIED RESEARCH LABORATORIES AUSTIN, TEXAS 78712		10. PROGRAM ELEMENT, PROJECT, TASK AREA & WORK UNIT NUMBERS 9781-02 61102F
11. CONTROLLING OFFICE NAME AND ADDRESS AIR FORCE OFFICE OF SCIENTIFIC RESEARCH/NA BLDG 410 BOLLING AIR FORCE BASE, D C 20332		12. REPORT DATE May 1977
14. MONITORING AGENCY NAME & ADDRESS (if different from Controlling Office)		13. NUMBER OF PAGES 131-135 p
		15. SECURITY CLASS. (of this report) UNCLASSIFIED
		16. DECLASSIFICATION/DOWNGRADING SCHEDULE
16. DISTRIBUTION STATEMENT (of this Report) Approved for public release; distribution unlimited.		
17. DISTRIBUTION STATEMENT (of the abstract entered in Block 20, if different from Report)		
18. SUPPLEMENTARY NOTES		
19. KEY WORDS (Continue on reverse side if necessary and identify by block number) NONLINEAR ACOUSTICS SIDE BANDS PLANE WAVES IN A TUBE SUPPRESSION OF SOUND BY SOUND MODULATION OF SOUND BY SOUND WEAK SHOCK THEORY ALGORITHM		
20. ABSTRACT (Continue on reverse side if necessary and identify by block number) The purpose of this research was to study the suppression of one sound by another sound of higher frequency. More specifically, the planar propagation in air of a finite amplitude tone (the pump) and a smaller amplitude tone (the weak signal) of lower frequency was investigated both theoretically and experimentally. Suppression is caused by an acoustic modulation process. The amount of suppression depends qualitatively on whether the pump frequency is lower than the weak signal frequency (Case I) or vice versa (Case II). Case I has been previously studied and large suppression of the weak signal has been		

obtained. Even though preliminary analytical work indicated that little suppression is possible in Case II, the present research was undertaken to determine the amount of suppression possible. Various exact and approximate preshock solutions were reviewed in the time domain (Earnshaw solution) and frequency domain (Fenlon solution). Postshock solutions were based on weak shock theory which was implemented in a computer algorithm, corrections for attenuation and dispersion were incorporated. Predictions thus obtained were compared to experimental results. The experiments, performed in a 30 m progressive wave tube, were restricted to Case II. For the weak signal, the range of source SPL was 104 to 121 dB and the range of frequency was 0.6 to 1 kHz. The corresponding ranges for the pump were 125 to 158 dB and 1.5 to 6.6 kHz, respectively. The measurement distances ranged from 3.9 m to 27 m. The agreement between experimental results and theoretical predictions was excellent. In particular the experiments confirmed the theoretical prediction that little suppression of the weak signal is obtained for Case II either before or after shock formation. The sidebands in both cases form around the high frequency and its harmonics. Thus another general conclusion is that the low frequency signal modulates the high frequency signal, regardless of their respective amplitudes.



UNCLASSIFIED

ARL-TR-77-22
May 1977

THE SUPPRESSION OF SOUND BY SOUND OF HIGHER FREQUENCY

William L. Willshire, Jr.

Office of Naval Research
Contract N00014-75-C-0867
Air Force Office of Scientific Research
Contract F44620-76-C-0040



APPLIED RESEARCH LABORATORIES
THE UNIVERSITY OF TEXAS AT AUSTIN
AUSTIN, TEXAS 78712

APPROVED FOR PUBLIC
RELEASE; DISTRIBUTION
UNLIMITED.

404434 ELL

FOREWORD

This report is an adaptation of William L. Willshire's thesis, "The Suppression of Sound by Sound of Higher Frequency," which was written for the degree of Master of Science in Engineering at The University of Texas at Austin. Mr. Willshire was enrolled in the Department of Mechanical Engineering, and the date of his degree is May 1977.

The research was carried out at the Applied Research Laboratories and was supported by the Office of Naval Research under Contract N00014-75-C-0867 and by the Air Force Office of Scientific Research under Contract F44620-76-C-0040. Technical monitors were Dr. Walter Madigosky and Dr. Logan E. Hargrove for ONR, and Lt.Col. R. C. Smith and Lt.Col. L. W. Ormand for AFOSR.

David T. Blackstock
Supervisor

Approved for	Write Section	<input checked="" type="checkbox"/>
NTS	Diff Section	<input type="checkbox"/>
Doc		
UNCLASSIFIED		
DECLASSIFICATION		
BY	DISTRIBUTION/AVAILABILITY CODES	
Doc	AVAIL. AND/OR SPECIAL	
A		

ABSTRACT

The purpose of this research was to study the suppression of one sound by another sound of higher frequency. More specifically, the planar propagation in air of a finite amplitude tone (the pump) and a smaller amplitude tone (the weak signal) of lower frequency was investigated both theoretically and experimentally. Suppression is caused by a modulation of the weak signal by the pump. The acoustic energy of the weak signal is not lost (absorbed) but rather redistributed to other parts of the spectrum. The modulation process leads to the formation of sidebands about the high frequency signal. The amount of suppression depends qualitatively on whether the pump frequency is lower than the weak signal frequency (Case I) or vice versa (Case II). Case I has been previously studied and large suppression of the weak signal has been obtained. Even though preliminary analytical work indicated that little suppression is possible in Case II, this research was undertaken to determine the amount of suppression possible.

The theoretical investigation was concerned with both Case I and Case II; a general notation was adopted so that the analysis of a single solution was applicable to both cases. Various exact and approximate preshock solutions were reviewed in the time (Earnshaw solution) and frequency (Fenlon solution) domains. These solutions were then compared with each other and ranked with regard to their exactness. Because general solutions valid in the postshock region were not available, postshock solutions were developed based on weak shock theory. Weak shock theory was

implemented in a computer algorithm with corrections for attenuation and dispersion. Predictions obtained from the use of the program were compared to experimental results. The experimental work was restricted to Case II. For the weak signal the experiments (performed in a 30 m progressive wave tube) covered a range of source SPL of 10^4 to 121 dB and a frequency range of 0.6 to 1 kHz. The corresponding ranges for the pump were 125 to 158 dB and 1.5 to 6.6 kHz, respectively. The measurement distances ranged from 3.9 m to 27 m. The agreement between experimental results and theoretical predictions was excellent. In particular the experiments confirmed the theoretical prediction that little suppression of the weak signal is obtained for Case II either before or after shock formation. The sidebands in both cases form around the high frequency signal and the energy for the sideband formation comes primarily from the high frequency signal (including its harmonics). Thus another general conclusion is that the low frequency signal modulates the high frequency signal, regardless of their respective amplitudes.

TABLE OF CONTENTS

	<u>Page</u>
FOREWORD	ii
ABSTRACT	iii
LIST OF FIGURES	vii
LIST OF IMPORTANT SYMBOLS	ix
CHAPTER I - INTRODUCTION AND LITERATURE REVIEW	1
CHAPTER II - THEORY	14
A. Earnshaw Solution	15
B. Exact Preshock Solutions for Two-Frequency Source	19
C. Approximate Preshock Solutions for Two-Frequency Source	23
D. Effect of the Weak Signal on the Pump	27
E. Shock Relations	37
F. Weak Shock Theory	38
G. Weak Shock Computer Algorithm	40
H. Attenuation and Dispersion	42
I. Major Computer Algorithm	45
CHAPTER III - MAJOR COMPUTER ALGORITHMS	50
A. Major Computer Algorithms	50
1. Flowchart for Program C500	50
a. Subroutine WAVEPROP	57
b. Subroutine TIMEFRE	57
c. Subroutine RESAMPLE	59
d. FFT Subroutine	60
e. Subroutine HANGEN2	63

	<u>Page</u>
2. Flowchart for Program GRAPH	63
3. Flowchart for Program TIMEPLOT	67
B. Calibration of Computer Programs	70
C. Flexibility of Computer Programs	72
CHAPTER IV - EXPERIMENTAL APPARATUS	75
A. The Systems	75
1. The Transmit System	75
2. Plane Wave Pipe	77
3. The Receive System	82
B. Test and Evaluation	83
1. The Transmit System	83
2. Plane Wave Pipe	86
3. The Receive System	91
CHAPTER V - COMPARISON OF EXPERIMENTAL RESULTS AND THEORETICAL PREDICTIONS	93
CHAPTER VI - CONCLUSIONS AND FINAL COMMENT	102
APPENDIX A - LISTINGS OF PROGRAM C500 AND SUBROUTINES USED BY PROGRAM C500	106
APPENDIX B - LISTINGS OF PROGRAM GRAPH	110
APPENDIX C - LISTINGS OF PROGRAM TIMEPLOT	112
APPENDIX D - ALTERNATE REPRESENTATION OF THE IMPROVED FM SOLUTION	114
BIBLIOGRAPHY	119

LIST OF FIGURES

<u>Figure</u>	<u>Title</u>	<u>Page</u>
1.1	Case I Waveforms	3
1.2	Case II Waveforms	4
1.3	Case I Experimental Spectra	7
1.4	Case II Experimental Spectra	8
1.5	Theoretical Suppression of Weak Signal before Shock Formation	11
2.1	Flowchart for Exact and Approximate Preshock Solutions	28
2.2	Effect of Pump on Weak Signal Case I	30
2.3	Effect of Pump on Weak Signal Case II	32
2.4	Comparison of Fenlon and Improved FM Solutions for the Effect of Pump on Weak Signal, Case I and Case II	36
2.5	Viscous (Y_v) and Thermal (Y_t) Boundary Layer Thickness for Air at STP	44
2.6	Effects of Absorption and Dispersion on A Small-Signal Sawtooth	46
2.7	Simplified Flowchart for Program C500, The Weak Shock Computer Algorithm	48
3.1	Detailed Flowchart for Program C500	51
3.2	Flowchart for Program GRAPH	64
3.3	Example Output of Program GRAPH, Case II	68
3.4	Flowchart for Program TIMEPLOT	69
3.5	Example Output for Program TIMEPLOT	71
3.6	Comparison of Predictions for the Suppression of the Weak Signal for Case II (no losses included)	73
4.1	Experimental Apparatus	76
4.2	Block Diagram of Transmit System	78

<u>Figure</u>	<u>Title</u>	<u>Page</u>
4.3	Exploded View of Flange Assembly with Measuring Microphone and Plug	80
4.4	Driver Mounting Yokes for Plane Wave Pipe	81
4.5	Block Diagram of Receive System	84
4.6	Comparison of Kirchhoff Attenuation Theory with Observed Data	87
4.7	Demerit of the Fiberglass Tangent Taper and Insert of Tangent Taper in Pipe	88
5.1	Example Spectrum of Experimental Waveform	94
5.2	Comparison of Experimental Data with Theory	96
5.3	Comparison of Experimental Data with Theory	98
5.4	Comparison of Experimental Data with Theory	100

LIST OF IMPORTANT SYMBOLS

c_o	small-signal sound speed
c	sound speed
c_p	specific heat at constant pressure
D_x, D_t	partial derivative of D with respect to x or t
E_w, E_p	the quantity E associated with the weak signal (w) or the pump (p)
f	frequency
I_n	n th order modified Bessel function of the first kind
j	$= \sqrt{-1}$
J_n	n th order Bessel function of the first kind
k	acoustic wave number $= \omega/c_o$
p	pressure
Pr	Prandtl number
r	pipe radius
SPL	sound pressure level (dB re 0.00002 N/m^2)
t	time
t'	retarded time $= t - x/c_o$
u	combined signal of pump and weak signal in particle velocity
u_p'	pump signal by itself in the absence of the weak signal
u_w'	weak signal by itself in the absence of the pump
u_{op}	source amplitude of the pump
u_{ow}	source amplitude of the weak signal
$u_{m,n}$	amplitude of a particular frequency component in the spectrum of u

u_{weak}	amplitude of the weak signal component in the spectrum of u
x	propagation distance
\bar{x}	shock formation distance
y	$= \omega_p t'$
Y_v	viscous boundary layer thickness
Y_t	thermal boundary layer thickness
α_b	boundary layer absorption coefficient
α_m	mainstream absorption coefficient
β	nonlinearity parameter of medium
γ	ratio of specific heats
ϵ	acoustic Mach number $= u/c_0$
ϵ_m	Neumann factor, $\epsilon_0=1$, $\epsilon_m=2$ if $m \geq 1$
κ	coefficient of thermal conductivity
λ	dilatational viscosity coefficient
μ	coefficient of shear viscosity
ν	kinematic viscosity
ρ	density
σ	dimensionless distance $= \beta \epsilon k x = x/\bar{x}$
Φ	parameter used to indicate the time a wavelet left the origin
Φ	$= \omega_p \Phi$
ω	angular frequency
$\omega_{m,n}$	angular frequency of the $u_{m,n}$ component of the spectrum of u
Ω	frequency ratio $= f_w/f_p$

CHAPTER I

INTRODUCTION AND LITERATURE REVIEW

The nonlinear interaction of two or more acoustic signals has been a very active area of study in the past decade or so. In a noteworthy early investigation Thuras, Jenkins, and O'Neil¹ (1935) showed that when two intense tones propagate in a plane wave tube, sum and difference frequency components are created. In 1956 Ingard and Pridmore-Brown² reported a study of the interaction of two intersecting beams of intense sound and used the phrase "the scattering of sound by sound" to describe the interaction. In a theoretical investigation Westervelt³ (1957) claimed that the interaction would take place only for collinear propagation of the two beams. The work on the scattering of sound by sound led to the invention of the parametric array by Westervelt⁴ (1960). In turn, a recent spinoff of research on the parametric array has been the "absorption of sound by sound," a term coined by Westervelt⁵ (1973) to describe the use of one sound to decrease the amplitude of a second sound. A more descriptive phrase for the phenomenon is "suppression of sound by sound" because the energy lost by the second sound is not absorbed but rather redistributed to other frequencies. For an excellent review of works related, both directly and indirectly, to suppression of sound by sound see Schaffer⁶ (1975). Suppression of sound by sound is the subject of this thesis. More specifically, the subject of this thesis is the suppression of a small signal by a higher frequency intense signal.

An underwater experiment with spherical waves performed by Moffett, Konrad, and Corcella⁷ (1972) demonstrated the phenomenon of suppression of sound by sound. The experiment was intended to test a parametric array whose primary frequencies were widely separated. Moffett et al. found that the amplitude of the high frequency primary was decreased by 17 dB when the low frequency primary was turned on. On the other hand, little decrease in the low frequency primary was observed when the high frequency primary was turned on. The explanation given for the decrease in the first case was that the high frequency primary underwent a frequency modulation by the low frequency primary. The modulation caused a production of sidebands about the high frequency "carrier" - at the carrier's expense. When the roles of the two primaries were reversed (the second case), a modulation still occurred, but one that had little effect on the amplitude of the low frequency wave.

The experiments of Moffett et al. show that two qualitatively different cases are to be considered when a finite amplitude tone is used to suppress a smaller amplitude tone.* In Case I the high intensity wave, which will be called the pump, is lower in frequency than the weak signal. In Case II the pump is higher in frequency than the weak signal.

The interaction processes in Case I and Case II are graphically illustrated in Fig. 1.1 and Fig. 1.2, respectively. Here u (vertical axis) is particle velocity, t is time, x is propagation distance, c_0 is the small signal propagation velocity, $t' = t - (x/c_0)$ is retarded time, ω is angular frequency, and \bar{x} is shock formation distance. In general the

*Moffett et al. studied the interaction of two intense signals, but the distinction between the two cases may still be made.

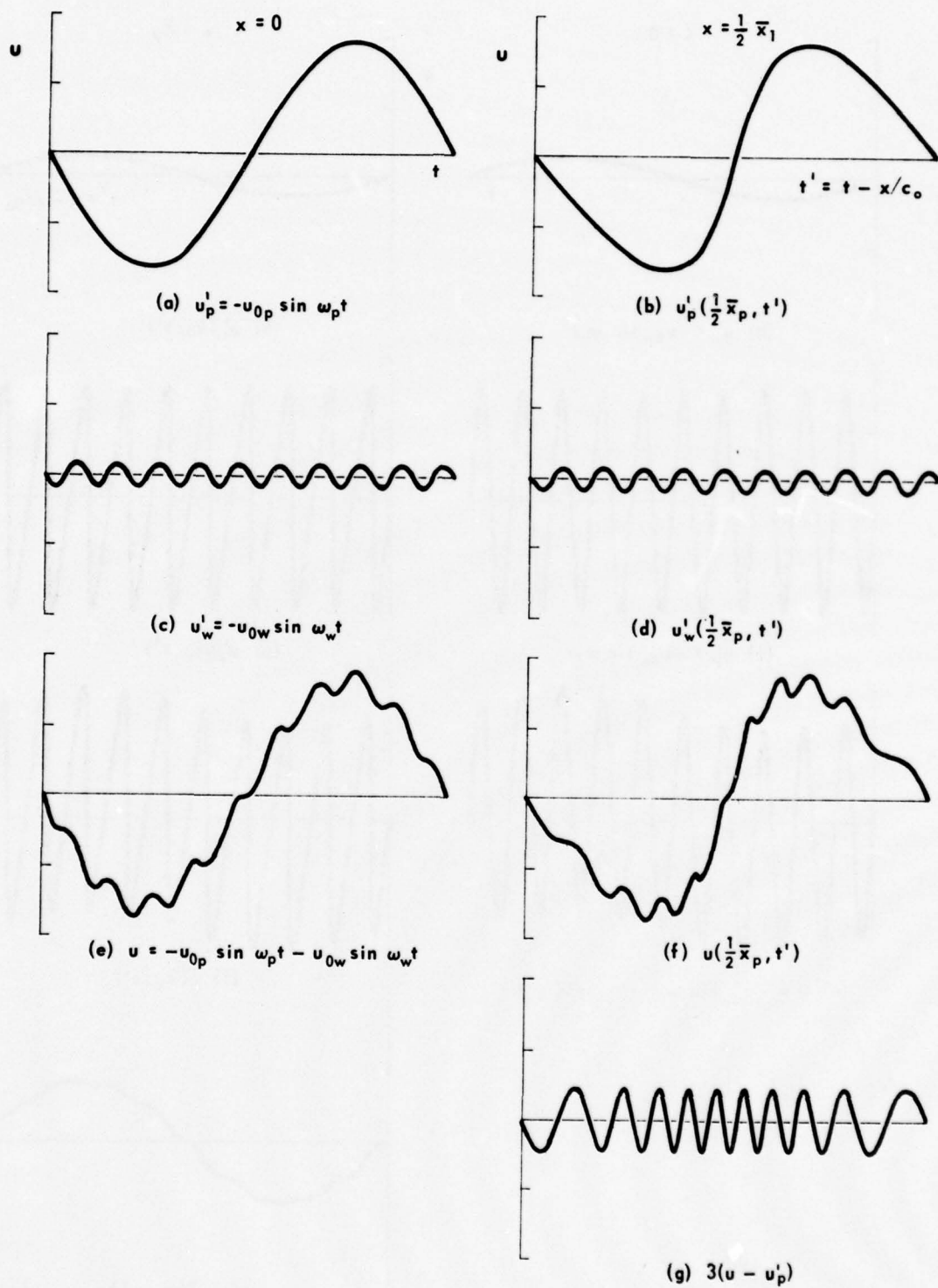


FIGURE 1.1
CASE I WAVEFORMS

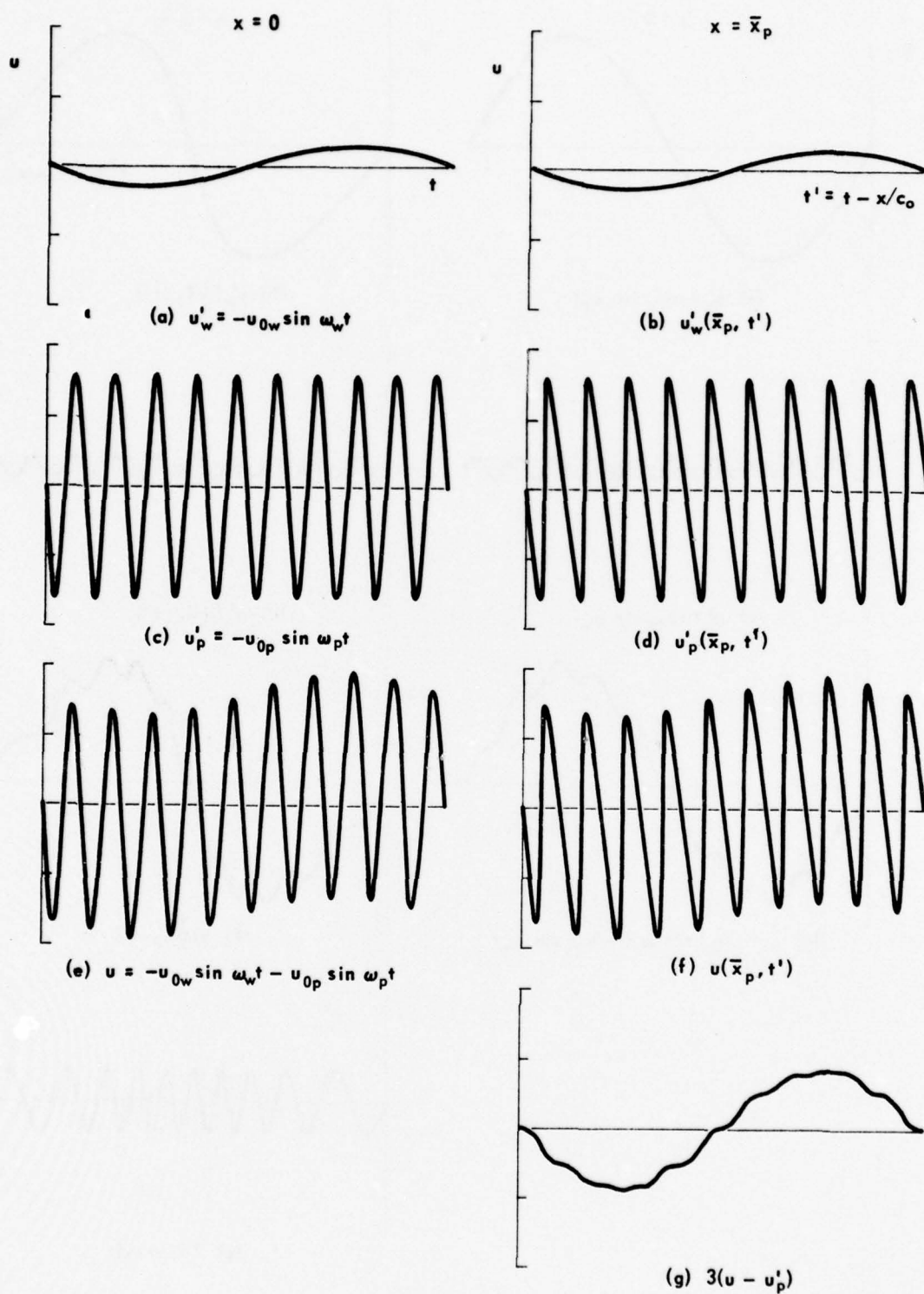


FIGURE 1.2
CASE II WAVEFORMS

subscript p refers to the pump and w to the weak signal. The combined signal is represented by u , u_p' is the pump propagated independently, that is, in the absence of the weak signal, and u_w' is the weak signal propagated independently. A zero preceding a subscript refers to source amplitude. Lossless theory⁸ has been used to compute the waveforms. First consider Case I. The low frequency pump by itself is shown in Figs. 1.1(a) and (b), first at the source ($x=0$) and then after some finite amplitude distortion has occurred ($x=\bar{x}_p/2$). Figures 1.1(c) and (d) show the weak signal by itself at the same propagation distances. The combined signal at the same distances is given in Figs. 1.1(e) and (f). The distorted pump waveform [1.1(b)] is subtracted from the distorted combined waveform [1.1(f)] to illustrate the effect the pump distortion has on the weak high frequency signal. The result is shown in Fig. 1.1(g); an amplification factor of 3 has been applied to emphasize the result. Next consider Case II. The source waveforms for the weak signal, the high frequency pump, and the combination of the pump and weak signal are shown in Figs. 1.2(a), (c), and (e), respectively. The three source waveforms are shown propagated separately an equal distance ($x=\bar{x}_p$) in Figs. 1.2(b), (d), and (f), respectively. Subtraction of the distorted waveform [1.2(d)] from the distorted combined waveform [1.2(f)] leads to the waveform shown in Fig. 1.2(g). Again, an amplification factor equal to 3 has been used to emphasize the result.

Through Figs. 1.1 and 1.2 a simple qualitative explanation may be given for the two different observations of Moffett et al. In Case I a frequency modulation of the weak signal is clearly visible [1.1(g)]. The frequency modulation is successful because the frequency of the pump

is less than that of the weak signal: the nonlinear distortion of a single pump cycle affects many cycles of the weak signal. Little variation of the weak signal is achieved for Case II, however. A high frequency ripple at approximately the frequency of the pump is observed in Fig. 1.2(g). In fact, the effect most apparent in the Case II figure is a low frequency modulation of the pump by the weak signal [Fig. 1.2(f)]. The distortion of a single pump cycle influences only a fraction of a weak signal cycle. The ripple on the weak signal is the result of the distortion of successive pump cycles.

Additional insight into the suppression of sound by sound interaction is obtained by viewing the process in the frequency domain. Figures 1.3 and 1.4 show spectra of waveforms similar to those in Figs. 1.1 and 1.2. The spectra are actually sample data taken from experiments that are described in Chapter IV. Figure 1.3 illustrates Case I; Fig. 1.4 illustrates Case II. When one acoustic signal is suppressed by a second, the energy taken from the first is redistributed to sidebands centered around the higher frequency wave, and, in Case II, its harmonics. In Case I the pump modulates the high frequency wave and transfers energy from the weak signal to sidebands located at $\omega_2 \pm n\omega_1$ (n an integer). Again in Case II, the low frequency signal modulates the high frequency signal, but the sideband energy (located at $m\omega_2 \pm \omega_1$, m an integer) appears to be drawn from the pump and its harmonics, not the weak signal. In both cases the energy for the sideband formation primarily originates from the high frequency signal. In Case I the energy redistributed to the sidebands from the weak signal substantially decreases

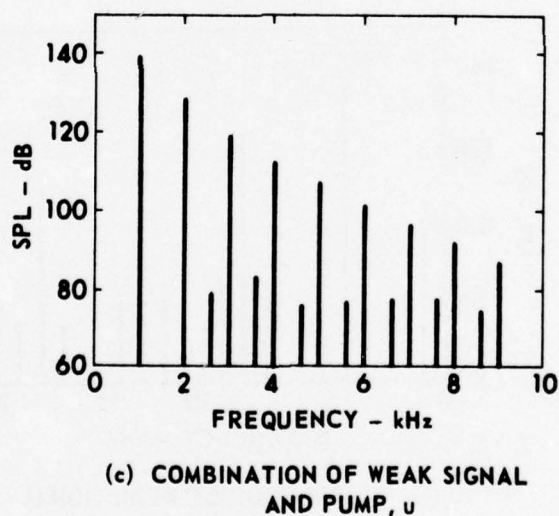
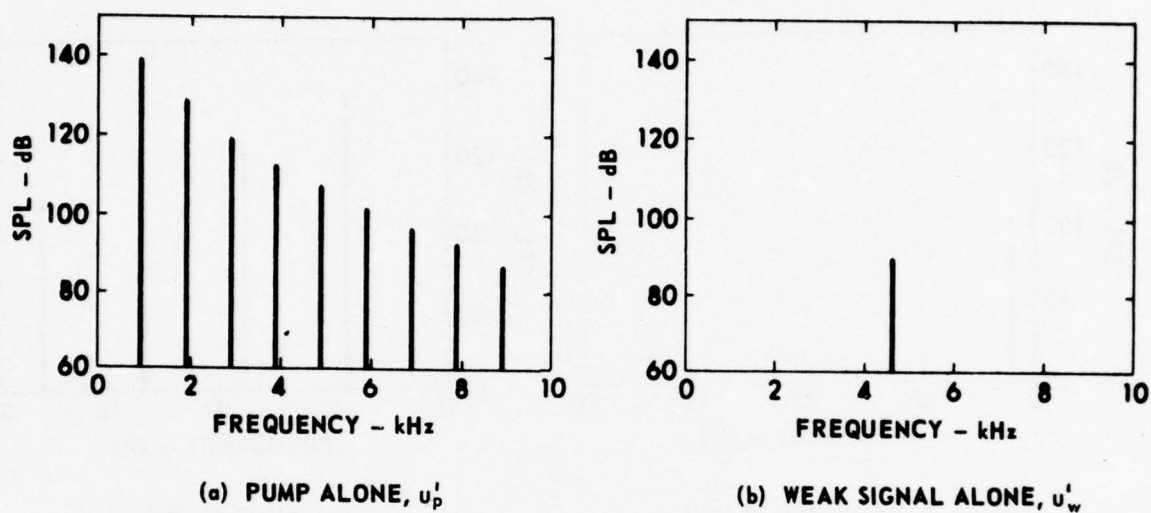


FIGURE 1.3
CASE I EXPERIMENTAL SPECTRA

SOURCE $SPL_p = 145$ dB, $f_p = 1$ kHz

SOURCE $SPL_w = 100$ dB, $f_w = 4.6$ kHz
 $x = 7.9$ m

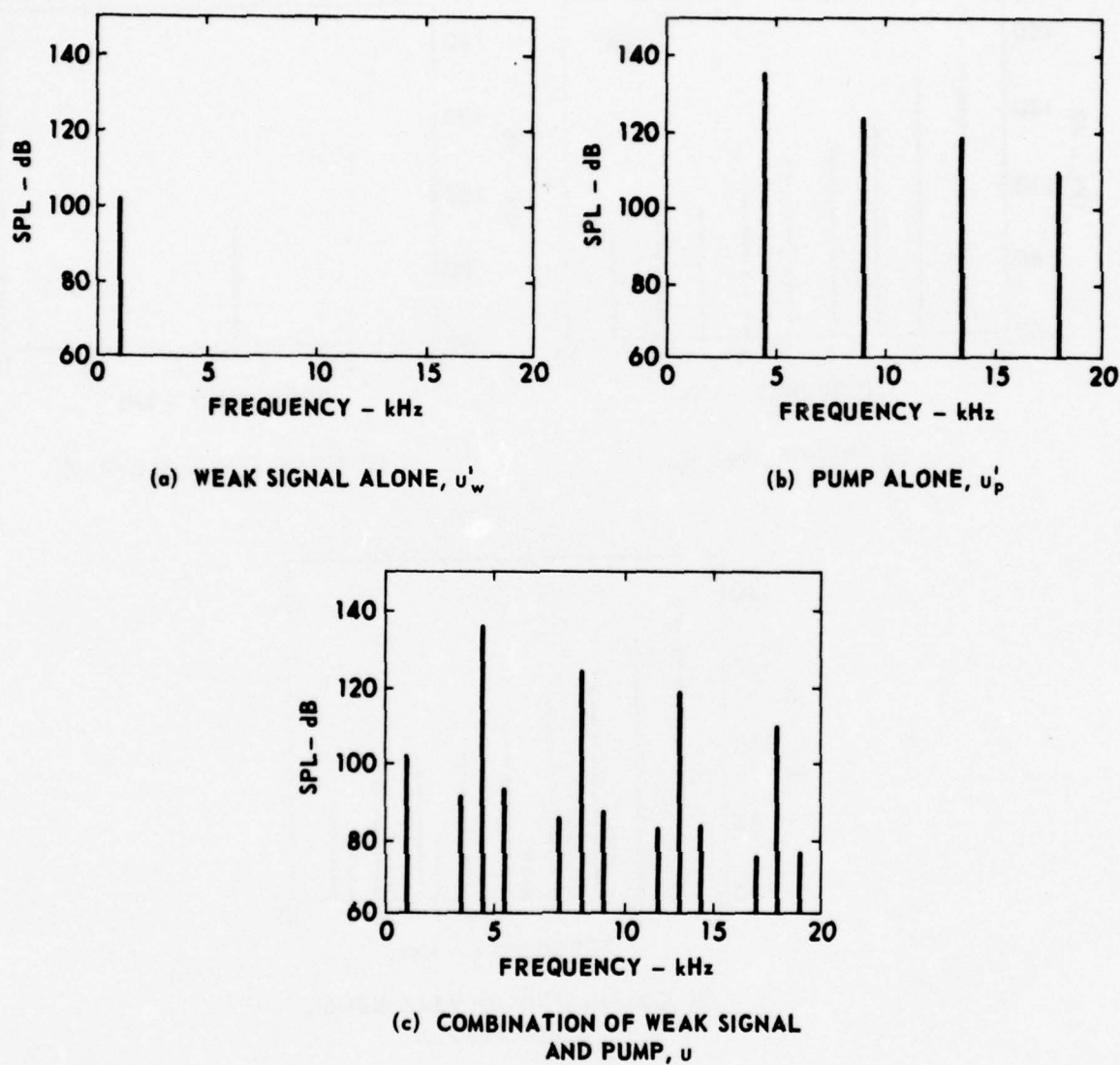


FIGURE 1.4
CASE II EXPERIMENTAL SPECTRA

SOURCE $SPL_w = 104$ dB, $f_w = 1$ kHz

SOURCE $SPL_p = 140$ dB, $f_p = 4.5$ kHz

$x = 4.2$ m

the amplitude of the weak signal; in Case II the energy redistributed from the pump and its harmonics has little effect on their amplitudes.

Although qualitative discussions are useful to achieve a basic understanding of the phenomenon of suppression of sound by sound, further understanding of the phenomenon requires a quantitative investigation. A way to begin the investigation is to use a solution by Fenlon for distortion of sound from a two-frequency source.⁹ Although his solution is limited to lossless propagation and to distances less than \bar{x} , it provides important information about the parameters that are significant and about the amount of suppression that may be obtained. The predicted result for the amplitude of the weak signal for both cases, provided the source amplitude of the weak signal is much less than that of the pump, is

$$u_{\text{weak}} = u_{\text{ow}} J_0(\Omega \sigma_p) \quad , \quad (1.1)$$

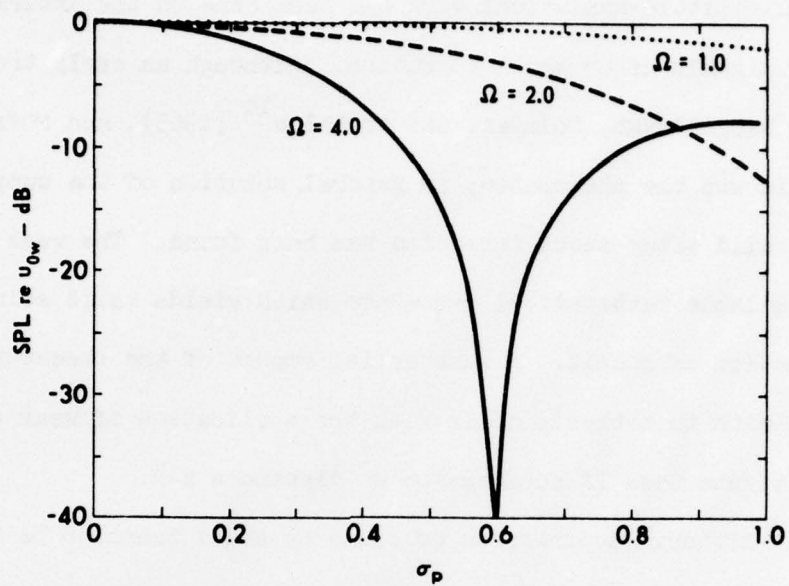
where the subscript weak refers to the weak signal of the combined waveform, J_0 is the zero order Bessel function of the first kind, Ω is the ratio of the weak signal frequency to the pump frequency, and $\sigma_p \equiv x/\bar{x}_p$. Complete suppression of the weak signal may be achieved at the zeroes of J_0 , the first one occurring at $\Omega \sigma_p = 2.4$. Here a quantitative difference between Case I and Case II may be seen. First note that the prediction is valid only when $\sigma_p < 1$. Even with this restriction, however, in Case I Ω may easily be chosen large enough that $\Omega \sigma_p = 2.4$. Thus a complete null may in theory be achieved. In an experimental study of Case I interaction, Schaffer⁶ observed reductions of as much as 40 dB in the weak signal when he varied the product $\Omega \sigma_p$ over a range including the null value 2.4. In Case II, on the other hand, Ω has values less than one. Therefore, the

largest permissible value of the argument of the Bessel function is $\Omega\sigma_p=1$. At this extreme value, the reduction of the weak signal is only 2.4 dB.

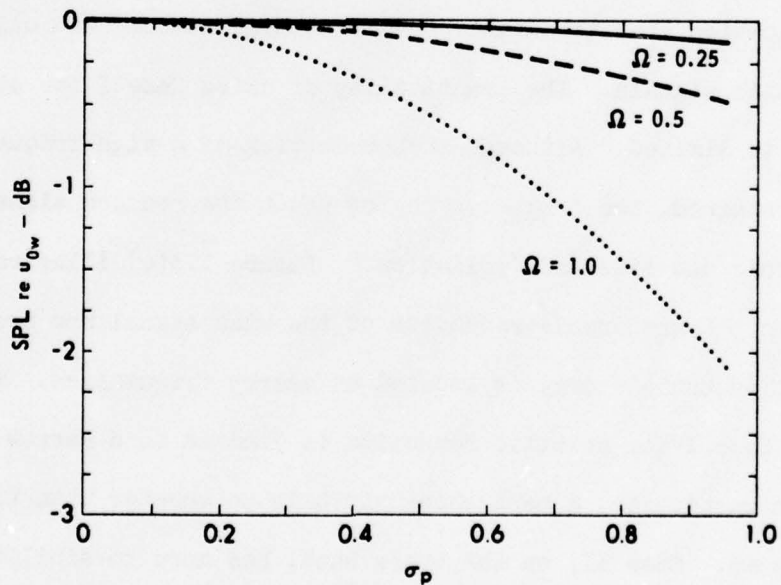
The effectiveness of the suppression of the weak signal is shown for both cases in Fig. 1.5. Plot (a) is for Case I; the horizontal axis is σ_p and the vertical axis is the decrease $[20 \log_{10} J_0(\Omega\sigma_p)]$ in the weak signal. Three different values of Ω are used. When $\Omega=4$, the range of the argument of the Bessel function includes its first zero, and total suppression of the weak signal is achieved. Figure 1.5 plot (b) shows the suppression of the weak signal for Case II. Three different values of Ω are used. Within the limits of the validity of the theory and within possible values of Ω , there is little suppression of the weak signal.

Other quantitative approaches besides Fenlon's solution have been used to investigate the nonlinear interaction between two acoustic signals. A frequency modulation (FM)-type solution has been used by Schaffer⁶ and others to describe the Case I interaction. Schaffer found that FM solution and Fenlon solution give the same prediction for the amplitude of the weak signal but not for the amplitudes of the sidebands. In the FM solution the sidebands are symmetric in magnitude about the weak signal. In the Fenlon solution, however, the amplitudes are asymmetrical about the weak signal; the upper sidebands have the larger amplitudes. An FM solution may also be derived for the Case II interaction but, as with the Fenlon solution, the FM solution is valid only for shock free waveforms.

Little suppression of the weak signal of Case II takes place before shocks form. An investigation is needed to determine whether additional suppression of the weak signal can be achieved after shock



(a) CASE I (LOW FREQUENCY PUMP),



(b) CASE II (HIGH FREQUENCY PUMP),

FIGURE 1.5
THEORETICAL SUPPRESSION OF WEAK SIGNAL
BEFORE SHOCK FORMATION

$$\Omega = \omega_w / \omega_p$$

formation. Little analytical work has been done on the interaction of two acoustic signals after shock formation. Although an early treatment was given by Naugol'nykh, Soluyan, and Khokhlov¹⁰ (1963), and Moffett et al.¹¹ (1977) discuss the phenomenon, no general solution of the suppression problem valid after shock formation has been found. The weak shock method is an available mathematical procedure which yields valid solutions beyond the formation of shocks. A substantial amount of the theoretical work involved with this thesis deals with the application of weak shock theory to investigate Case II suppression at distances $x > \bar{x}$.

Although suppression of sound by sound seems to be much more effective in Case I than in Case II, at least for the shock-free region, Case II is generally more attractive when applications are considered. An application that immediately comes to mind is the controlled reduction of acoustic signals. The practicality of using Case I for acoustic control is limited. Although much reduction of a high frequency signal can be obtained, the frequency region about the reduced signal is swamped by harmonic and sideband "pollution." Figure 1.3(c) illustrates the situation. Considerable reduction of the weak signal has been achieved, but much acoustic energy is located at nearby frequencies. The application of Case I for acoustic reduction is limited to a narrow frequency band, in particular, a band whose width is no greater than the frequency of the pump. Case II, on the other hand, has more possibilities; Fig. 1.4(c) shows why. Because the pump frequency in Case II is greater than that of the weak signal, the acoustic pollution is higher in frequency than the weak signal. If the pump can reduce the lower frequency weak signal, additional acoustical energy will be required that is not

close in frequency to the weak signal. The reduction bandwidth is the frequency of the pump minus the frequency of the weak signal, but the pump in Case II has a greater frequency than the pump in Case I.

The work presented in this thesis is a logical extension of the work done by Schaffer⁶ on Case I. The subject of this thesis is the suppression of sound by sound for Case II. General theoretical models and solutions which are applicable to both Case I and Case II are developed in Chapter II. The models and solutions are compared to each other and their limitations are discussed. Chapter III is a detailed description of the computer programs which implement weak shock theory with provisions for attenuation and dispersion. The intent is to give the reader enough insight into the computer programs so that he can use them with confidence in a minimum amount of time. For readers who do not want or desire this insight, Chapter III may be skipped without interfering with the continuity of the remainder of the thesis. The experimental apparatus and its calibration and accuracy are described in Chapter IV. Theoretical and experimental results are presented and compared in Chapter V. Conclusions and final comments are made in the last chapter, Chapter VI. Appendices A, B, and C contain listings of the major computer programs used. Appendix D contains a detailed derivation of an alternate representation for one of the preshock solutions discussed in Chapter II, the improved FM solution.

CHAPTER II

THEORY

The theoretical tools used to describe the interaction between a finite amplitude tone and a second, weaker tone are presented here. Although the subject of this thesis is the suppression of sound by sound for Case II, much of the theory is applicable to both cases. Whenever possible a general notation is employed so that the theoretical results are useful for both Case I and Case II. Three possible approaches were mentioned in Chapter I to describe the interaction: Fenlon's solution, an FM solution, and weak shock theory. Theoretical descriptions of the behavior of finite amplitude sound are frequently limited to shock-free waveforms, and such is the case for both Fenlon's solution and the FM solution. The solution based on weak shock theory, however, can accommodate waveforms with discontinuities. All three solutions may be derived from an implicit solution called the Earnshaw solution. In weak shock theory, the Earnshaw solution must be supplemented by a shock propagation equation derived from the Rankine-Hugoniot shock relations. Thus the Earnshaw solution is used to describe the continuous sections of waveform between discontinuities, and the shock propagation equation is used to make the connections across the discontinuities.

In this chapter the general form of the Earnshaw solution is reviewed, and then two exact preshock solutions for a two-frequency source are given: the Earnshaw solution for the time domain and the Fenlon solution for the frequency domain. Various useful approximations of the

exact solutions are then made and compared with each other and with the exact solutions. Next, the behavior of the interaction after shock formation is considered. The shock relations are combined with the Earnshaw solution to form weak shock theory, and then the equations of weak shock theory are cast in difference equation form and implemented in a computer subroutine. Next the importance and the effect of attenuation and dispersion are considered, followed by mathematical formulations for attenuation and dispersion. The last section of the chapter deals with the major computer algorithm, C500, which calculates the propagation of a wave; the effect of attenuation and dispersion is included in the algorithm.

A. Earnshaw Solution

The Earnshaw solution⁸ is an exact solution of the equations of motion for progressive waves. The solution is first reviewed for gaseous fluids. A convenient approximation of the solution is then obtained which is applicable to liquids as well as gases. The equations of motion for a lossless perfect gas are (see, for example, Banta¹²)

$$\text{Continuity: } \rho_t + u\rho_x + \rho u_x = 0 \quad (2.1)$$

$$\text{Momentum: } \rho(u_t + uu_x) + p_x = 0 \quad (2.2)$$

$$\text{Equation of state: } \frac{p}{p_0} = \left(\frac{\rho}{\rho_0} \right)^\gamma, \quad (2.3)$$

where ρ , u , and p are the instantaneous values of density, particle velocity, and pressure, respectively, ρ_0 and p_0 are the ambient values of density and pressure, x is propagation distance, t is time, and γ is the

ratio of specific heats of the gas. If the wave motion is progressive, say, restricted to outgoing waves, the following first integral of Eqs. 2.1 through 2.3 may be obtained (for example, see Blackstock¹³),

$$u_t + (c_0 + \beta u)u_x = 0 \quad , \quad (2.4)$$

where $\beta = (\gamma + 1)/2$ for gases. A solution of this equation for the boundary condition

$$u(0, t) = f(t)$$

is

$$u(x, t) = f(\varphi) \quad , \quad (2.5a)$$

where

$$\varphi = t - \frac{x}{c_0 + \beta u} \quad . \quad (2.5b)$$

Equations 2.5a and 2.5b constitute the Earnshaw solution. The parameter φ represents the time a point on a waveform, i.e., a wavelet, left the origin.

An important physical interpretation may be obtained directly from Eqs. 2.4 and 2.5b. Inspection of these equations shows that the propagation speed is

$$\frac{dx}{dt} = c_0 + \beta u \quad . \quad (2.6)$$

In general, different points, or wavelets, of a waveform propagate with different speeds, and the result is distortion of the wave. The variation

in propagation speed is due to two things. First, the sound speed varies because of the nonlinearity of the pressure-density relation; the sound speed c is (see, for example, Blackstock¹⁴)

$$c = c_0 + \frac{\gamma - 1}{2} u \quad , \quad (2.7)$$

where c_0 is the small signal value of the sound speed. Second, because the propagation of an acoustical wave is longitudinal, the wave is convected by its own passage through the medium. The effect of convection on propagation speed may be expressed as

$$\frac{dx}{dt} = c + u \quad . \quad (2.8)$$

The combination of Eqs. 2.7 and 2.8 results in Eq. 2.6.

An approximate form of the Earnshaw solution is often used for convenience. The approximate form is obtained by performing a binomial expansion of Eq. 2.5b and keeping terms of order ϵ only, where ϵ , the Mach number, is defined as the ratio of the maximum particle velocity to the small signal speed. The result of the binomial expansion is

$$u = f(\varphi) \quad (2.9a)$$

$$\varphi = t' + \frac{\beta x}{c_0^2} f(\varphi) \quad , \quad (2.9b)$$

where t' is the retarded time, $t - (x/c_0)$. By common usage Eqs. 2.9 are referred to as the Earnshaw solution.

The Earnshaw solution is equally applicable to liquids. A general expression for the equation of state for lossless perfect fluids

is (for example, see Beyer¹⁵)

$$p - p_0 = A \frac{\rho - \rho_0}{\rho_0} + \frac{B}{2!} \left(\frac{\rho - \rho_0}{\rho_0} \right)^2 + \frac{C}{3!} \left(\frac{\rho - \rho_0}{\rho_0} \right)^3 + \dots ,$$

where the values of the coefficients, A, B, C, etc., are in general empirically determined. To the same order of approximation as that used in the derivation of Eq. 2.9b, the Earnshaw solution is made applicable to liquids by taking

$$\beta = 1 + \frac{B}{2A}$$

in Eq. 2.9b. For air the ratio B/2A is equal to $(\gamma-1)/2$.

It is important to remember the restrictions on the validity of Eqs. 2.9. Because of the approximations made, Eq. 2.9b is valid only for values of $\epsilon \ll 1$. Note that $\epsilon=0.1$ corresponds to a SPL of 174 dB re 0.00002 N/m^2 in air and a SPL of 284 dB re $1 \text{ } \mu\text{Pa}$ in water.* Another important point is that by itself the Earnshaw solution, in either of the forms presented in Eqs. 2.5 or 2.9, is valid only for continuous waveforms. The solution may be used to predict the formation of shocks. Beyond the shock formation distance, however, the waveforms predicted with the Earnshaw solution are multivalued.

* Throughout this thesis the reference pressure for SPL is $= 0.00002 \text{ N/m}^2$ for air.

B. Exact Preshock Solutions for Two-Frequency Source

The Earnshaw solution for the two-frequency boundary condition

$$u(0,t) = u_{op} \sin \omega_p t + u_{ow} \sin \omega_w t \quad (2.10)$$

is

$$u(x,t') = u_{op} \sin \omega_p \varphi + u_{ow} \sin \omega_w \varphi \quad (2.11a)$$

$$\varphi = t' + \frac{\beta x}{c_o} \left(u_{op} \sin \omega_p \varphi + u_{ow} \sin \omega_w \varphi \right) \quad (2.11b)$$

The notation adopted is as follows. The subscript w denotes the signal and the subscript p the pump. A zero preceding a subscript indicates source amplitude of the particular tone. The first term in Eq. 2.11a is referred to as the pump term u_p and the second one as the weak signal term u_w . The combined particle velocity signal, composed of the pump and the weak signal, is referred to as u . When a particular tone propagates by itself, that is, in the absence of the other tone, a prime is used. For example, u_p' represents the pump propagated by itself. An important frequency parameter is the ratio $\Omega = \omega_w / \omega_p$. For Case I Ω is greater than 1, while for Case II Ω is less than 1. The w-p notation is adopted so that the derivations which follow hold for both Case I and Case II.

As noted in an earlier section, the validity of the Earnshaw solution is limited to distances $x < \bar{x}$, where \bar{x} is the shock formation distance. Fenlon⁹ has shown that the shock formation distance for waves from a two-frequency source is

$$\bar{x} = \frac{1}{\beta \epsilon_p k_p + \beta \epsilon_w k_w} \quad ,$$

where $k=\omega/c_0$. The region of validity becomes

$$x < \frac{1}{\beta \epsilon_p k_p + \beta \epsilon_w k_w}$$

or, in terms of σ ,

$$\sigma_p < 1 - \sigma_w \quad .$$

For the work done in this thesis, $\sigma_p \gg \sigma_w$. A reasonable approximation of the limitation set by shock formation is

$$\sigma_p < 1 \quad .$$

A convenient way to display data as a function of distance is to plot it against σ_p . The theoretical predictions and experimental results are displayed in this fashion. Normally $\sigma=1$ is the dividing line between the absence and presence of shocks in a waveform. For the particular waves studied here $\sigma_p < 1$ is a good approximation for the shock-free regions of the waveform, but $\sigma_p + \sigma_w < 1$ is the exact relationship.

The effect of the pump on the weak signal is expressed by the weak signal term of Eq. 2.11a,

$$(u_w)_{\text{EARN}} = u_{ow} \sin \left[\omega_w \left(t' + \frac{\beta x}{c_0} (u_{op} \sin \omega_p \phi + u_{ow} \sin \omega_w \phi) \right) \right] \quad , \quad (2.12)$$

where the subscript EARN denotes the Earnshaw solution. This portion of the Earnshaw solution represents the weak signal and its harmonics in the presence of the pump. It also includes the sidebands resulting from the interaction of the pump with the weak signal. But, Eq. 2.12 does not describe the complete sideband formation of the interaction of the pump

$$\ell_0 = \alpha \ell \quad , \quad (B-23)$$

$$y = ct/\ell \quad , \quad (B-24)$$

and

$$u = y - \cos \gamma \quad . \quad (B-25)$$

In terms of these variables, the impulse response becomes

$$h(y, \vec{r}_0) = \frac{4\pi^2 C \exp[-2a(1-y \cos \theta_1)]}{\ell} \int_{y-1}^{y+1} \frac{du}{u} I_0 \left(2a \sin \theta_1 \sqrt{1 - (y-u)^2} \right) \\ \times \exp \left[-2au \cos \theta_1 - \ell_0 (y^2 - 1)/u \right] \quad . \quad (B-26)$$

Equation (B-26) completes the reduction of the impulse response of a parametric array to a single integral. This integral is complicated, and an exact analytic expression for it is not known at this time. However, this formulation of the impulse response is useful for several reasons:

- (1) $h(y, \vec{r}_0)$ is always positive or zero,
- (2) $h(y, \vec{r}_0)$ is a smooth function except at $y=1$,
- (3) the behavior of $h(y, \vec{r}_0)$ as y approaches 1.0 and as y approaches infinity is well known, and
- (4) the properties of $h(y, \vec{r}_0)$ imply that it will be possible to approximate $h(y, \vec{r}_0)$ by a polynomial in y .

$$\begin{aligned}
 u(x, t') = & \sum_{n=1}^{\infty} \frac{2u_{op}}{n\sigma_p} J_0\left(\frac{n\sigma_w}{\Omega}\right) J_n(n\sigma_p) \sin n\omega_p t' \\
 & + \sum_{m=1}^{\infty} \sum_{n=-\infty}^{\infty} \frac{2u_{ow}}{\left(m + \frac{n}{\Omega}\right)\sigma_w} J_m\left[\left(m + \frac{n}{\Omega}\right)\sigma_w\right] J_n\left[(m\Omega+n)\sigma_p\right] \sin(m\omega_w + n\omega_p)t' .
 \end{aligned}
 \tag{2.14}$$

The first term of Eq. 2.14 is an expression for the amplitude of the pump and its harmonics in the presence of the weak signal; the second term is the remaining portion of u , namely, the weak signal, its harmonics, and the sidebands of the interaction.

The frequencies of the spectral components of u are seen to be

$$\omega_{m,n} = \left| m\omega_w + n\omega_p \right| .$$

The indices for the frequencies are used to form a notation for the individual frequency components of the spectra of u . The general notation for the amplitude of a spectral component of u is $u_{m,n}$, where the angular frequency of the component is equal to the value of $\omega_{m,n}$. For example, $u_{1,0}$ is the amplitude of the weak signal component (ω_w). For Case II ($\omega_p > \omega_w$), $u_{1,-1}$ represents the amplitude of the component located at a frequency of $\omega_p - \omega_w$ because $\omega_w - \omega_p$ is negative. The components located at the frequencies of the pump and its harmonics are represented by $u_{0,n}$ ($\omega_{m,n}$ evaluated at $m=0$ is equal to $n\omega_p$). The first term of Eq. 2.14 is represented by $u_{0,n}$ and the second term by $u_{m,n} - u_{0,n}$.

The sideband formation is composed of contributions from both terms of the Earnshaw solution, Eq. 2.11a; therefore, $(u_w)_{\text{EARN}} \neq u_{m,n} - u_{0,n}$. Part of the energy to form the sidebands comes from the suppression of the weak signal represented as

$$u_{1,0} = \frac{2u_{ow}}{\sigma_w} J_1(\sigma_w) J_0(\Omega\sigma_p) \quad (2.15a)$$

$$\doteq u_{ow} J_0(\Omega\sigma_p) \quad . \quad (2.15b)$$

The approximate result, Eq. 2.15b, was used in Chapter I to predict the suppression of the weak signal for Case I and Case II (Eq. 1.1). Another source of energy for the sideband formation is the pump and its harmonics. The first summation term of Eq. 2.14 is equal to $J_0(n\sigma_w/\Omega)$ times the Fubini solution for the pump. (The Fubini solution (for example, see Blackstock¹⁷) describes the nonlinear propagation of the signal from a single frequency source.) The difference between the Fubini solution for the pump and $u_{o,n}$ of the Fenlon solution is a measure of the energy redistributed from the pump and its harmonics to the sidebands through the interaction of the pump and the weak signal. The difference becomes greater for larger n or for the higher harmonics of the pump, and is larger in Case II than in Case I because Ω in Case II is less than 1. For Case I more energy for the sideband formation comes from the suppression of the weak signal, whereas in Case II more energy is redistributed from the harmonics of the pump.

C. Approximate Preshock Solutions for Two-Frequency Source

The exact solutions, Eq. 2.11 and Eq. 2.13, are available for analytical investigations, but approximate solutions are often much easier to implement and just as useful for certain purposes as the exact solutions. The crudest approximate solution is reviewed first and more sophisticated approximate solutions are discussed later. An FM solution

may be obtained by approximating ϕ (Eq. 2.11b) in the Earnshaw solution.

If $u_{op} \gg u_{ow}$, ϕ may be approximated as

$$\phi \doteq t' + \frac{\beta x}{c_o} u_{op} \sin \omega_p \phi \quad . \quad (2.16)$$

In this case the pump term of the Earnshaw solution becomes, in the frequency domain,

$$u_p = u_{op} \sum_{n=1}^{\infty} \frac{2}{n\sigma_p} J_n(n\sigma_p) \sin n\omega_p t' \quad , \quad (2.17a)$$

which is recognized as the classic Fubini solution. In other words, in this approximation the weak signal has no effect on the pump. But the pump definitely affects the weak signal, as shown by the expression for u_w :

$$u_w = u_{ow} \sin(\omega_w t' + \Omega \sigma_p \sin \omega_p \phi) \quad . \quad (2.17b)$$

A further simplification is now made by letting $\phi \doteq t'$ in the inner sine function of Eq. 2.17. The result is

$$(u_w)_{FM} = u_{ow} \sin(\omega_w t' + \Omega \sigma_p \sin \omega_p t') \quad , \quad (2.18)$$

where the subscript FM refers to the FM solution. Replacing ϕ by t' in this way is justified in that the approximation is made in a term that is already just a correction to the phase of t' . A frequency domain representation of Eq. 2.18 is (for example, see Carlson¹⁸)

$$(u_w)_{FM} = u_{ow} \sum_{n=-\infty}^{\infty} J_n(\Omega \sigma_p) \sin[(\omega_w + n\omega_p)t'] \quad . \quad (2.19)$$

A better approximate solution, which may be called the improved FM solution, is obtained by not approximating ϕ by t' in the inner sine function of Eq. 2.17b. The following Bessel function frequency domain representation of Eq. 2.17b has been found by Blackstock (see Appendix D),

$$(u_w)_{I \text{ FM}} = u_{ow} \sum_{n=-\infty}^{\infty} \frac{\Omega}{\Omega + n} J_n[(\Omega + n)\sigma_p] \sin[(\omega_w + n\omega_p)t'] \quad , \quad (2.20)$$

where the subscript I FM denotes "improved FM solution."

Physical interpretation of the FM and improved FM solutions is important in understanding the usefulness of the solutions. The approximate ϕ equation (Eq. 2.16) used to derive these solutions contains many implicit assumptions: (1) the pump is not influenced by the presence of the weak signal and the pump term does not give rise to contributions to the sideband formation (the pump term is simply the Fubini solution), (2) the weak signal does not distort (neither Eq. 2.19 nor Eq. 2.20 contains harmonics of the weak signal), and (3) the sideband formation is due solely to the modulation of the weak signal by the pump. These assumptions are simplifying because it has been shown⁶ that both terms of the Earnshaw solution contribute to the sideband formation, the pump is affected by the presence of the weak signal, and the distortion of the weak signal is dependent on its amplitude.

A still better approximate preshock solution may be obtained from the Fenlon solution. The $m=0$ terms of Eq. 2.13b represent the amplitude of the pump and its harmonics,

$$u_{o,n} = \frac{2u_{op}}{n\sigma_p} J_0\left(\frac{n\sigma_w}{\Omega}\right) J_n(n\sigma_p) \quad , \quad n > 0 \quad . \quad (2.21)$$

If $n\sigma_w/\Omega \ll 1$, $J_0(n\sigma_w/\Omega) \approx 1$ and Eq. 2.21 reduces to the Fubini amplitudes. The $m=1$ terms of Eq. 2.13b represent the weak signal and the sidebands resulting from the mutual interaction of the pump and the weak signal,

$$u_{1,n} = \frac{2u_{ow}}{\sigma_w \left(1 + \frac{n}{\Omega}\right)} J_1 \left[\left(1 + \frac{n}{\Omega}\right) \sigma_w \right] J_n \left[(\Omega+n) \sigma_p \right] \quad (2.22)$$

$$\text{If } n\sigma_w/\Omega \ll 1 \text{ (or } \sigma_w \ll 1), \frac{2J_1 \left[\left(1 + \frac{n}{\Omega}\right) \sigma_w \right]}{\sigma_w \left(1 + \frac{n}{\Omega}\right)} = 1,$$

and Eq. 2.22 becomes

$$u_{1,n} = u_{ow} J_n \left[(\Omega+n) \sigma_p \right] \quad (2.23)$$

which is referred to as the approximate Fenlon solution (APP FEN). Unlike the previous approximate solutions, however, this expression includes sideband contributions from both the pump signal and the weak signal. The $m=2,3,\dots$, terms of Eq. 2.13a represent the higher harmonics of the weak signal and the sidebands resulting from their interaction with the pump and its harmonics. For $\sigma_w(m+n/\Omega) \ll 1$, the amplitudes of these "higher order" sidebands are very small. The improved FM solution (Eq. 2.20) differs from the approximate Fenlon solution (Eq. 2.23) by the factor

$$\frac{(u_w)_{\text{I FM}}}{(u_{1,n})_{\text{APP FEN}}} = \frac{\Omega}{\Omega + n} \quad (2.24)$$

The difference between the two solutions is small for Case I, where $\Omega > 1$, and for small n , but the two solutions differ considerably for Case II, where $\Omega < 1$, even for small n . As already noted, the reason there is a

difference between the two solutions is that in approximating ϕ by Eq. 2.16 the effect of the weak signal on the pump was not included in the improved FM solution.

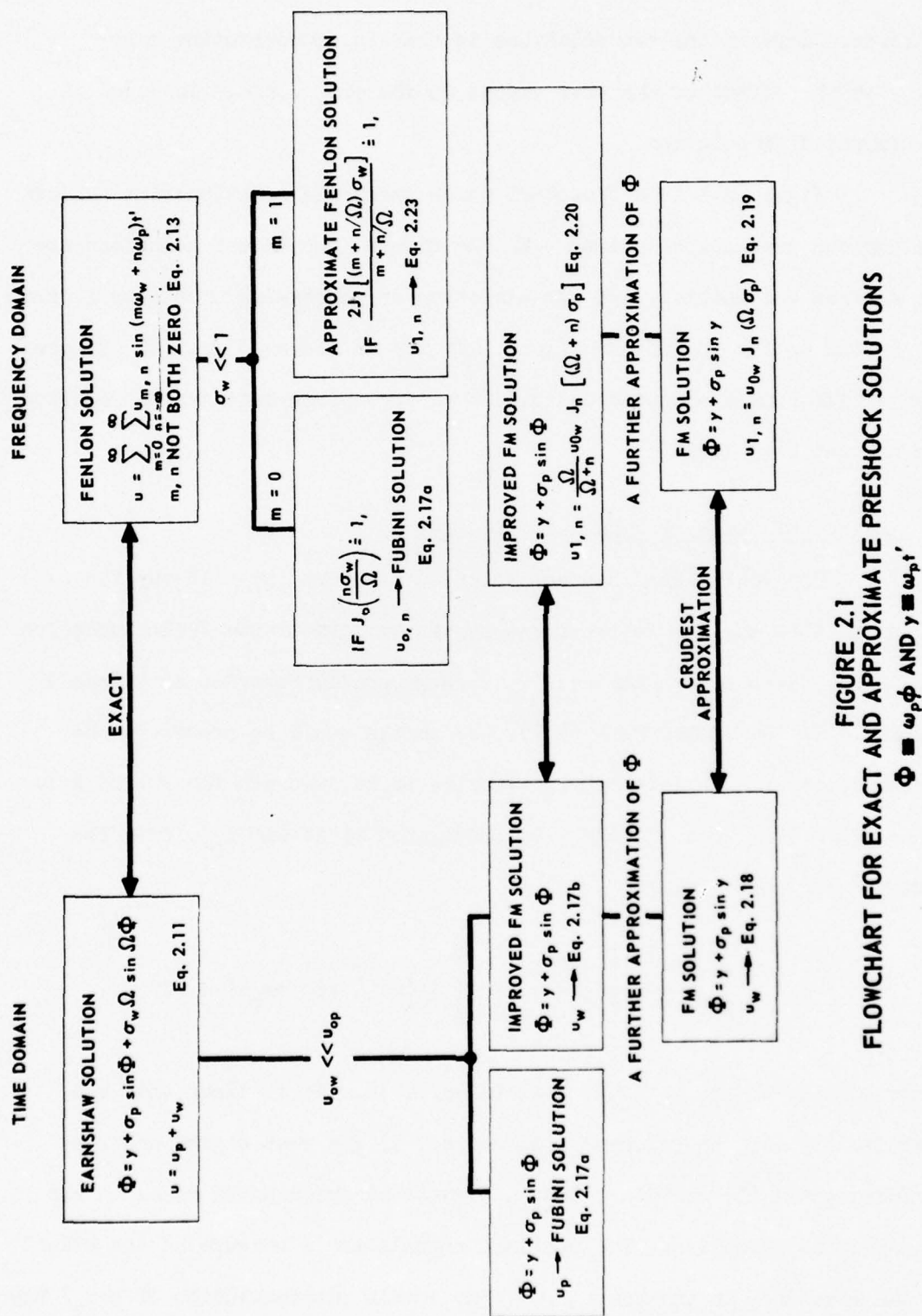
Figure 2.1 is a flowchart which shows the relationships between the various preshock solutions. In the figure, equivalent solutions are across from one another, and the direction of increasing exactness is from the bottom to the top of the figure. It may be observed from the figure that a time domain solution equivalent to the approximate Fenlon solution has not yet been found.

D. Effect of the Weak Signal on the Pump

The weak signal has an effect on the pump, seen in the factor $J_0(n\sigma_w/\Omega)$ that appears in the first summation term of the Fenlon solution (Eq. 2.14), even though the weak wave is generally regarded as a "small signal." If the factor were unity, the series would be precisely the Fubini solution. An interesting exercise is to subtract the Fubini solution, Eq. 2.17a, that is, the pump propagated by itself u_p' , from the complete Fenlon solution:

$$u - u_p' = \sum_{n=1}^{\infty} \frac{2u_{op}}{n\sigma_p} \left[J_0\left(\frac{n\sigma_w}{\Omega}\right) - 1 \right] J_n(n\sigma_p) \sin n\omega_p t' + DS, \quad ,$$

where DS stands for the double sum in Eq. 2.14. It is clear that $u - u_p'$ includes (1) all the sideband components, (2) the weak signal and its harmonics, and (3) certain residual signals at frequencies equal to the pump and its harmonics. The residual signals are a measure of the effect of the weak wave on the pump. The time domain representation of $u - u_p'$ may



be found from the Earnshaw solution. The effect of the weak signal on the pump is seen in the time domain by the sidebands due to the pump term of the Earnshaw solution. The time domain representation of the Fubini solution,

$$u_p'(x, t') = u_{op} \sin \omega_p \varphi, \quad (2.25a)$$

where

$$\varphi = t' + \frac{\beta x}{c_0} u_{op} \sin \omega_p \varphi, \quad (2.25b)$$

is subtracted from the complete Earnshaw solution (Eq. 2.11). This subtractive procedure is only valid for the complete Earnshaw solution. In the approximate Earnshaw solutions the approximation used for φ guarantees that $u_p = u_p'$; therefore, the subtractive procedure yields the weak signal term.

Figure 2.2 illustrates the predicted effect of the pump on the weak signal in Case I using the following solutions: the complete Earnshaw solution (Eq. 2.12), the FM solution (Eq. 2.18), the improved FM solution (Eq. 2.17b), and the specially constructed signal $u - u_p'$ (Eq. 2.11a minus Eq. 2.25a), which shows the effect of the weak signal on the pump. The four solutions are, respectively, (a), (b), (c), and (d) in the figure. The source amplitudes and frequencies are exaggerated to emphasize the effect of one signal on the other.

A comparison of the spectra in Fig. 2.2 reveals that the predicted amplitude of the weak tone is the same in every plot. For the FM solution the sideband formation is symmetric about the weak tone, but for the improved FM solution the formation is asymmetric. The higher

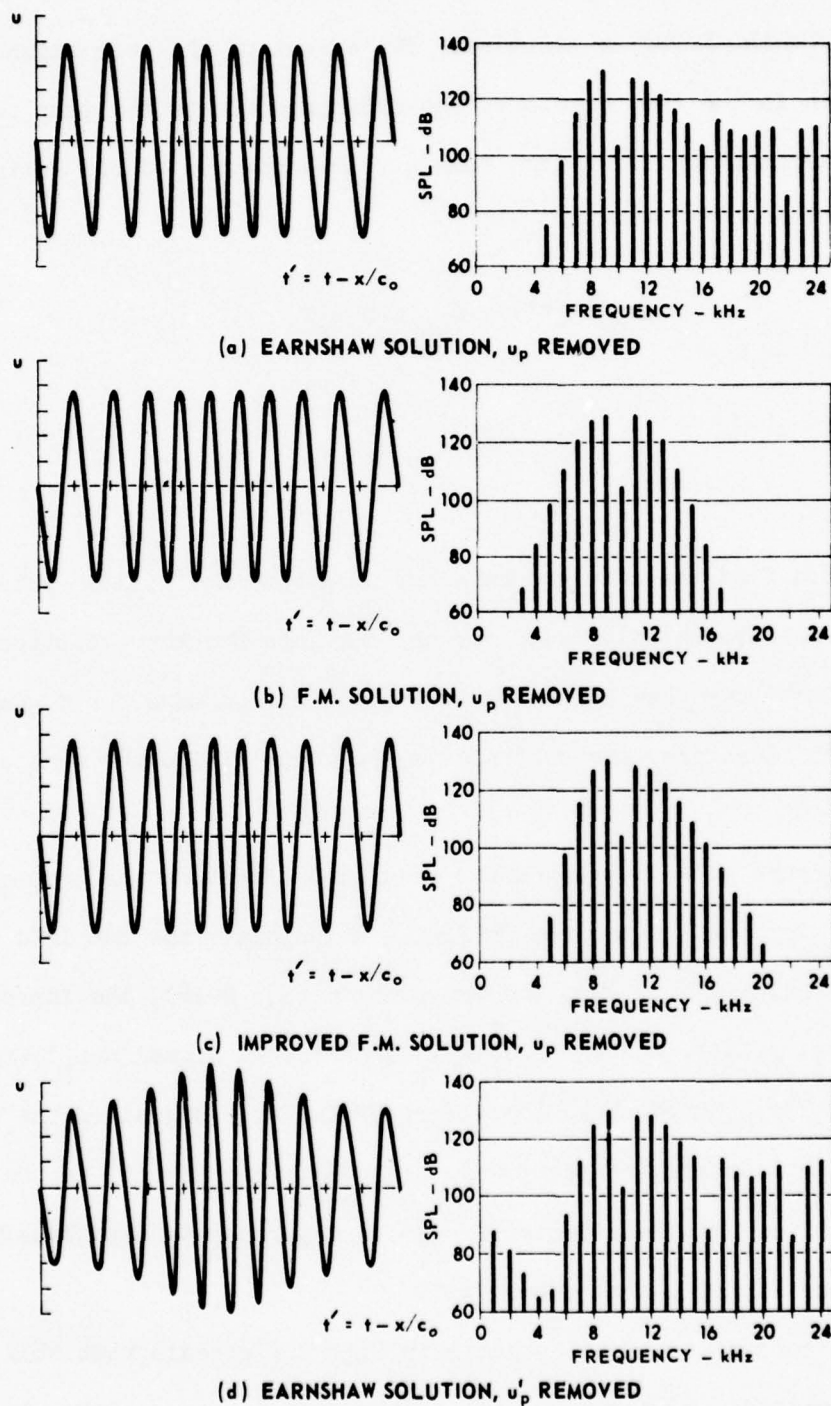


FIGURE 2.2
EFFECT OF PUMP ON WEAK SIGNAL CASE I
SOURCE SPL_p = 150 dB, f_p = 1 kHz
SOURCE SPL_w = 135 dB, f_w = 10 kHz
 x = 1.7 m

frequency sidebands are enhanced. In the complete Earnshaw solution the weak signal undergoes finite amplitude distortion at a rate depending on its amplitude, but in the FM solutions the weak signal does not distort no matter what its amplitude. The greater high frequency sideband formation in the Earnshaw solutions is partially a result of the harmonics of the weak signal interacting with the pump and its harmonics. The difference between plot (a) and plot (b) is more difficult to explain. Both the pump and weak signal terms in the Earnshaw solution contribute to the sideband formation caused by the mutual interaction between the tones. In plot (a), only the weak signal term of the Earnshaw solution is shown; therefore only the sidebands due to the effect of the pump on the weak signal are seen. The Earnshaw solution in plot (d) shows the effect of the pump on the weak signal and the effect of the weak signal on the pump. The observed sideband formation is due to both terms in the solution. The fundamental and harmonics of the pump (the residual signals described earlier) seen in the plot indicate that the presence of the weak signal has an effect on the finite amplitude distortion of the pump, as is very evident in the waveform of plot (d). The weak signal seems to be undergoing amplitude as well as frequency modulation. The amplitude modulation is not caused by the relatively large amplitude of the weak signal in this example; computations with weak signals of much smaller amplitude (100 dB down from pump amplitude) showed similar amplitude modulation.

Figure 2.3 illustrates the predicted effect of the pump on the weak signal in Case II. Plot (a) illustrates the Earnshaw solution (Eq. 2.12), plot (b) the FM solution (Eq. 2.18), plot (c) the improved FM

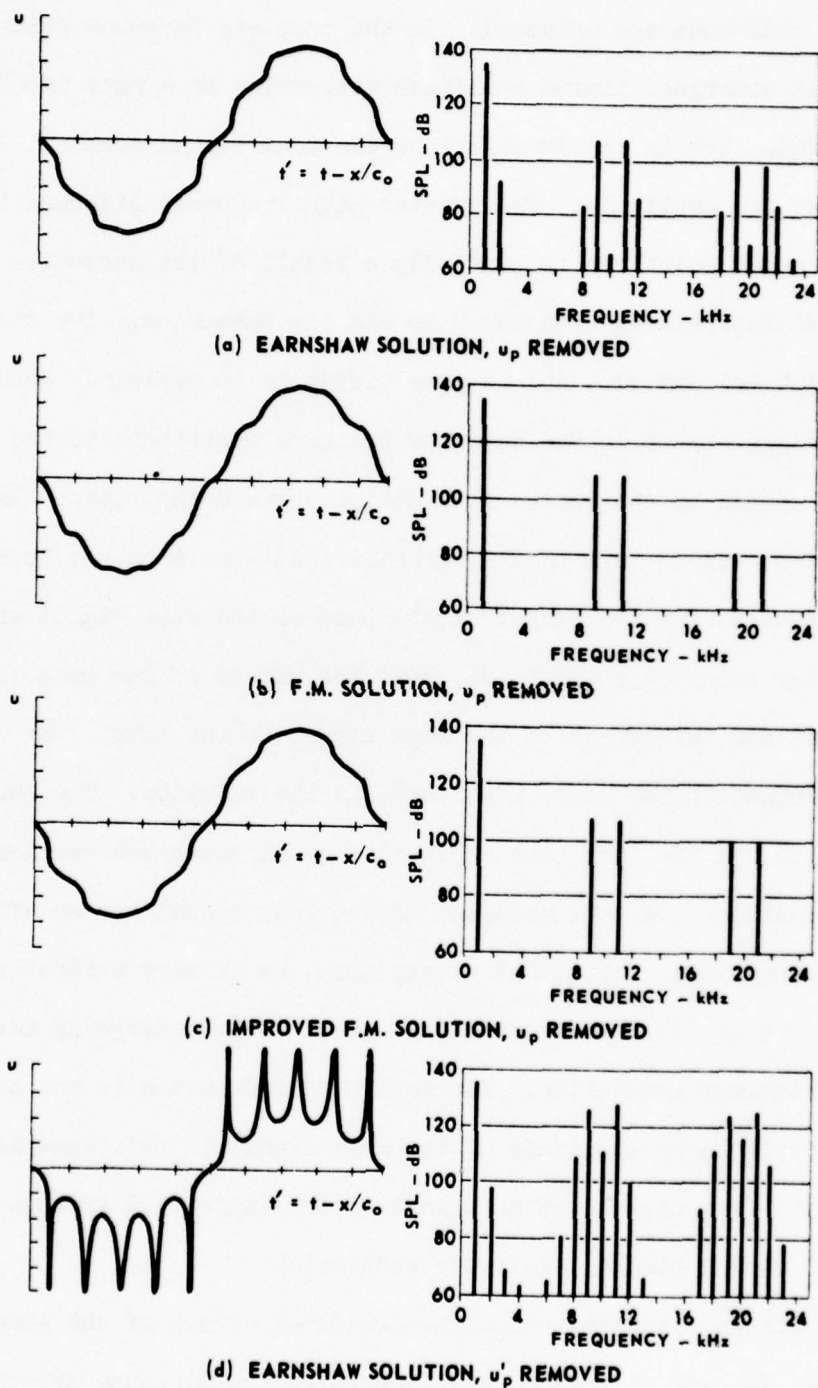


FIGURE 2.3
EFFECT OF PUMP ON WEAK SIGNAL CASE II

SOURCE $SPL_w = 135$ dB, $f_w = 1$ kHz

SOURCE $SPL_p = 150$ dB, $f_p = 10$ kHz

$x = 0.7$ m

solution (Eq. 2.17b), and plot (d) the signal $u-u_p'$. The source amplitudes and frequencies are exaggerated to emphasize the interaction between the tones.

Inspection of the spectra of Fig. 2.3 reveals that the predicted amplitude for the weak tone is the same for all the solutions. The FM solution sidebands are symmetric about the pump and harmonic frequencies; the improved FM solution sidebands are asymmetric (by a fraction of a decibel). In the improved FM solution the sidebands around the second harmonic of the pump are 20 dB larger than those for the simple FM solution. The finite amplitude distortion of both tones is incorporated in the complete Earnshaw solution but not in the approximate solutions. The distortion of the weak signal is observed in the Earnshaw solution plots [plots (a) and (d)]. The interaction of the pump with the harmonics of the weak signal is a cause of the greater sideband formation in the Earnshaw solutions. The sideband formation in plot (a) is due solely to the weak signal term of the two-frequency Earnshaw solution. The sidebands in plot (d) are due to both terms of the Earnshaw solution. Evidence of the effect of the weak signal on the pump is the energy located at frequencies equal to that of the pump and its second harmonic. Notice that the amplitude of the second harmonic component is larger than that of the pump. The sidebands in plot (d) are abnormally large compared to those in the other solutions. Only the sidebands from the weak signal term of the Earnshaw solution are contained in the other solutions. The effect of both tones on each other is best observed in the dramatic waveforms of plot (d). The period of the cusps is approximately the period of the pump (or the sidebands observed in the corresponding spectrum). The cusp

formation is not due to the relatively large amplitude of the weak signal in Fig. 2.3; cusps were predicted in calculations where the amplitude of the weak signal was 100 dB less than the pump amplitude.

Figures 2.2 and 2.3 demonstrate that the primary source of energy for the sidebands is different in the two cases. The suppression of the weak signal for both cases is described by Eq. 2.15a. The difference between the Fubini solution and the $u_{o,n}$ terms of the Fenlon solution (Eq. 2.14) is a measure of the amount of energy of the pump and its harmonics which is redistributed to the sidebands. The normalized difference between the two is

$$\frac{(u_{o,n})_{FEN} - (u_{o,n})_{FUB}}{(u_{o,n})_{FUB}} = 1 - J_0\left(\frac{n\sigma_w}{\Omega}\right) \quad , \quad (2.26)$$

where the subscript FUB refers to the Fubini solution, $n=1$ corresponds to the pump, and $n=2$ to the pump's second harmonic, etc. The smaller the difference between the solutions, the less pump energy is redistributed to the sidebands. For Case I, the argument of J_0 in Eq. 2.15a may be greater than one ($\sigma_p < 1$ but $\Omega > 1$) and may equal the first zero of J_0 . Therefore, much energy may be redistributed from the weak signal to the sidebands. On the other hand, for Case I little energy is redistributed from the pump and its harmonics so long as n is not large; Eq. 2.26 is approximately zero because $J_0(n\sigma_w/\Omega) \approx 1$ for $\sigma_w \ll 1$ and $\Omega > 1$. For Case II the roles of the primary and secondary sources of energy for the sideband formation are switched. The argument of J_0 in Eq. 2.15 has a limiting value of 1 ($\Omega < 1$ and $\sigma_p < 1$) for Case II, so that little suppression of the weak signal is achieved. On the other hand, the amount of energy redistributed from

the pump and its harmonics is greater. Even though $\sigma_w \ll 1$, the fact that $\Omega < 1$ means that the argument of J_0 in Eq. 2.26 may deviate substantially from zero and thus the value of J_0 may deviate correspondingly from unity.

The energy for the sideband formation in both Case I and Case II comes primarily from the higher frequency tone and its harmonics. In Case I the higher frequency tone is the weak signal and so a great deal of its energy is required to form the sidebands. In Case II the pump is the higher frequency tone. The sideband energy taken from it represents such a small percentage that the relative decrease in the amplitude of the pump and its harmonics is not very great.

Figure 2.4 illustrates the difference between the approximate Fenlon solution and the Bessel function representation of the improved FM solution due to Blackstock (see Appendix D). The approximate Fenlon solution spectra represent $u_{1,n}$ and the FM solution represents u_w . The ratio of the improved FM solution to the approximate Fenlon solution (Eq. 2.24) represents the difference between the two solutions. Plots (a) and (b) show that for Case I there is little difference between the two solutions (the ratio is approximately one for small n and $\Omega > 1$), but for Case II the difference is larger (with $\Omega < 1$, even for small n , the ratio is not equal to one). For Case II the predicted sidebands for the approximate Fenlon solution are much larger than those for the improved FM solution. Similarly large sidebands were also observed in Fig. 2.3(d). The two solutions with large sideband formations both incorporate to some degree the mutual sideband formation of the pump and the weak signal.

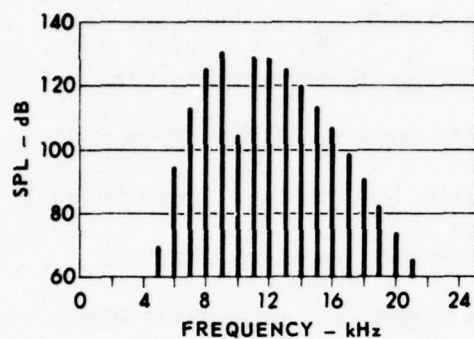
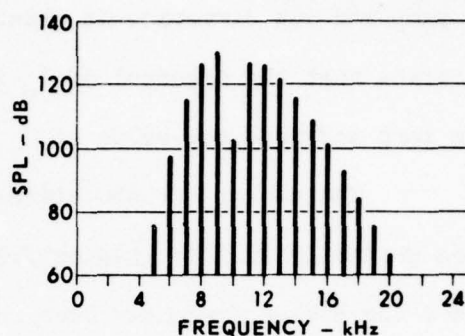
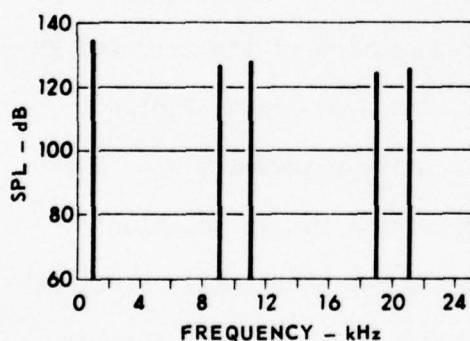
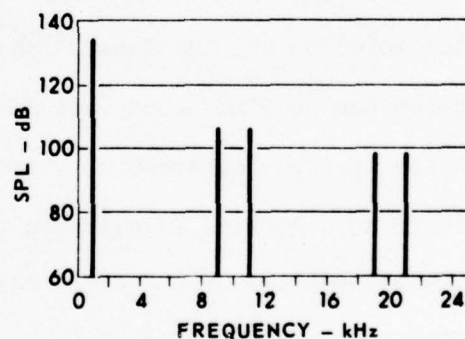
(a) APPROXIMATE FENLON SOLUTION, $u_{1,n}$ (b) IMPROVED FM SOLUTION, u_w **CASE I**SOURCE SPL_p = 150 dB, f_p = 1 kHzSOURCE SPL_w = 135 dB, f_w = 10 kHz x = 1.7 m(c) APPROXIMATE FENLON SOLUTION, $u_{1,n}$ (d) IMPROVED FM SOLUTION, u_w **CASE II**SOURCE SPL_w = 135 dB, f_w = 1 kHzSOURCE SPL_p = 150 dB, f_p = 10 kHz x = 0.7 m

FIGURE 2.4
COMPARISON OF FENLON AND IMPROVED FM SOLUTIONS FOR
THE EFFECT OF PUMP ON WEAK SIGNAL, CASE I AND CASE II

E. Shock Relations

When shocks form in a waveform, conservation equations must be applied across them to connect the continuous portions of the waveform on either side. The conservation equations commonly used are called the Rankine-Hugoniot shock relations. The relations may be combined to yield an expression for the propagation speed of a shock. The expression which is an approximation of the same order as the Earnshaw solution is (for example, see Pestorius⁸)

$$\left(\frac{dx}{dt}\right)_{\text{shock}} = c_0 + \frac{\beta}{2} (u_2 + u_1) \quad , \quad (2.27)$$

where $\left(\frac{dx}{dt}\right)_{\text{shock}}$ is the propagation speed of the shock, the subscript 2 refers to behind the shock, and the subscript 1 refers to in front of the shock. The propagation velocity of a wavelet in a continuous waveform is given by Eq. 2.6. A comparison of the two equations (Eqs. 2.6 and 2.27) shows that a shock travels with the mean speed of wavelets just behind and just ahead of it. Therefore wavelets behind the shock tend to catch up with the shock while the shock tends to overtake wavelets ahead of it.

The Earnshaw solution is valid only for progressive waves. Is this condition satisfied when a wavelet overtakes a shock, that is, is there a reflection of the wavelet which would negate the progressive wave assumption? Lighthill¹⁹ calculated that for weak shocks the departure from progressive wave flow is of the order Z^3 where Z is the shock strength defined as $(p_2 - p_1)/p_1$. Thus, to order Z^2 the formation of shocks does not invalidate the progressive wave assumption. When $\epsilon = 0.1$, the maximum value of Z is 0.0032. Therefore, for the purpose of this thesis, reflections

from shocks may be ignored. The Earnshaw solution may continue to be used for the continuous sections of a waveform.

If, when a wavelet overtakes a shock, or vice versa, there is no reflection, what is the consequence of the merger? The answer to this question is an important result of nonlinear acoustics. A shock is composed of at least two wavelets. One of the wavelets is associated with the peak (maximum pressure) of the shock and another wavelet is associated with the trough (minimum pressure) of the shock. These two wavelets, which may be used to describe a shock, may be referred to as the endpoint wavelets of the shock. In a wavelet-shock merger either the shock or the wavelet overtakes the other because of differing propagation speeds. A wavelet-shock merger is really the merging of one of the shock's endpoint wavelets with the third wavelet. When a wavelet overtakes a shock, the wavelet governs the amplitude of the shock, but when a shock overtakes a wavelet ahead of it the overtaken wavelet determines the amplitude of the shock. A similar process occurs between two shocks with differing propagation speeds which overtake one another. The result of the merging of two shocks is a single shock.

F. Weak Shock Theory

Weak shock theory is based upon the Earnshaw solution (Eq. 2.9) and the equation for the propagation speed of a shock (Eq. 2.27). The quantity ϕ in the Earnshaw solution has units of time, and the coefficient $\beta f(\phi)/c_0^2$ has units of time per distance. The shock propagation relationship connects the Earnshaw solution on one side of a shock to the Earnshaw solution on the other side of the shock. It would be very useful if the shock propagation equation were in units of time per distance. Inverting

Eq. 2.27 will produce the desired dimensions. Further usefulness is achieved by making a variable transformation from t , real time, to t' , the retarded time. The variable transformation is expressed by

$$\frac{dt'}{dx} = \frac{dt}{dx} - \frac{1}{c_o} \quad . \quad (2.28)$$

Substituting the inverse of Eq. 2.29 in this equation yields

$$\left(\frac{dt'}{dx} \right)_{\text{shock}} = \frac{1}{c_o + \frac{\beta}{2} (u_1 + u_2)} - \frac{1}{c_o} \quad . \quad (2.29)$$

Performing a binomial expansion to the same order as before and collecting terms yields

$$\left(\frac{dt'}{dx} \right)_{\text{shock}} = - \frac{\beta}{2c_o^2} (u_1 + u_2) \quad . \quad (2.30)$$

Equations 2.30 and 2.9 form weak shock theory.

In preparation for the implementation of weak shock theory in a computer algorithm, the following ideas need to be established. A waveform may be described as a collection of wavelets associated with a corresponding collection of retarded times, or as

$$u_i(t_i'), \quad i = 1, 2, 3, \dots, n \quad (2.31)$$

where n is the number of points in the waveform representation. To simplify this discussion and other descriptions, let time t refer to retarded time t' . The use of weak shock theory to propagate the wave represented by Eq. 2.31 results in a new waveform represented by the same

collection of wavelets, but a different collection of times. The new collection of times is calculated from Eqs. 2.9b and 2.30. The changed time relationships between the wavelets represents the distortion of the waveform. A shock is formed when two or more wavelets are associated with the same time or when a multivalued region is predicted in the waveform.

G. Weak Shock Computer Algorithm

Equations 2.30 and 2.9b form the mathematical basis for weak shock theory. The application of the equations was briefly discussed in the last section, but how is weak shock theory practically implemented? Analytical implementation is possible but usually very difficult to do except for the simplest of boundary conditions. In principle, implementation of weak shock theory by means of a computer algorithm is simple. Pectorius⁸ has developed a computer algorithm referred to as WAVEPROP which implements weak shock theory. WAVEPROP was initially designed to be used on random waveforms, but works equally as well on deterministic waveforms.

In WAVEPROP an input waveform is propagated a desired distance in incremental steps. The input waveform is represented as a collection of wavelets and their corresponding times. The values of the wavelets are stored in an array, called the U array, and the values of t' in a second array, called the T array. In the propagation of the initial waveform the first incremental distance produces a new T array associated with the U array. The spacing between the elements of the T array is initially uniform but, because of waveform distortion, the spacing between the T elements changes with every incremental propagation step. The input for the next propagation step is the output of the last step. A shock is

formed when two or more elements of the U array are associated with the same time. If more than two wavelets are associated with the same value of time, only the largest and smallest amplitude wavelets (the endpoint wavelets) are needed to represent the shock. The remaining wavelets associated with the shock are not necessary and are dropped from the arrays. Therefore, as a waveform undergoes propagation, the number of elements in the U and T arrays decreases.

The form of the weak shock theory equations implemented by the computer programs is not Eqs. 2.30 and 2.9b. Because of the step-by-step nature of the propagation process, Eq. 2.9b may be viewed in a new light. The elements of the T array before a propagation step are referred to as t'_{old} and the elements of the array after a propagation step are referred to as t'_{new} . With these definitions and a little rearranging, Eq. 2.9b becomes

$$t'_{new} = t'_{old} - \frac{\beta f(t'_{old}) \Delta x}{c_o^2}, \quad (2.32)$$

where $f(t'_{old})$ is the value of the wavelet associated with t'_{old} and Δx is the size of the incremental propagation step. Weak shock theory in the form of Eqs. 2.30 and 2.32 is in a convenient form to be implemented in the computer algorithm discussed. All that is needed is to express Eqs. 2.30 and 2.32 in difference equation form (due to Pestorius⁸). The difference equation representation of Eq. 2.32 is

$$t'[(k+1)\Delta x] = t'_s(k\Delta x) - \beta c_o^{-2} [t'(k\Delta x)] \Delta x, \quad (2.33)$$

and the difference equation representation of Eq. 2.30 is

$$t_s'[(k+1)\Delta x] = t_s'(k\Delta x) - \frac{\beta \Delta x c_o^{-2}}{2} \left\{ u_2[k\Delta x, t_s'(k\Delta x)] + u_1[k\Delta x, t_s'(k\Delta x)] \right\}, \quad (2.34)$$

where

Δx = incremental distance,

$t'[(k+1)\Delta x]$ = the value of t' after $k+1$ incremental distance steps,

t_s = the value of t' associated with a shock, and

$t_s'[(k+1)\Delta x]$ = the value of t_s' after $k+1$ incremental distance steps.

Equation 2.33 may be rearranged and substituted into Eq. 2.34 to obtain a simplified shock propagation equation

$$t_s'[(k+1)\Delta x] = \frac{t_2'[(k+1)\Delta x] + t_1'[(k+1)\Delta x]}{2}. \quad (2.35)$$

Equations 2.33 and 2.35 are the form of weak shock theory used by WAVEPROP to calculate the new times for a collection of wavelets.

H. Attenuation and Dispersion

Attenuation and dispersion need to be incorporated in the computer algorithms because the predictions generated are to be compared to experimental results. The experiments are performed in a plane wave tube, and the presence of the tube wall introduces appreciable attenuation and dispersion. In a normal sized duct, or a pipe, the effect of viscosity and heat conduction near the bounding surfaces is the dominant cause of attenuation over a wide frequency range. In a pipe there exists a viscous boundary layer across which the particle velocity associated with an acoustical signal undergoes a rapid transition from its mainstream

value to zero at the boundary. A thermal boundary also exists across which the propagation of an acoustical signal changes from adiabatic in the mainstream to isothermal at the boundary. These boundary layers are usually very thin. The mainstream is the part of the interior of the pipe where the boundary layer effects are not felt by the propagating acoustic signal. Figure 2.5 is a plot of boundary layer thickness versus frequency for air for both the thermal boundary and the viscous boundary. The viscous boundary layer (Y_v) is given by²⁰

$$Y_v = \sqrt{\frac{2\nu}{\omega}} \quad , \quad (2.36)$$

where ν is the kinematic viscosity of the medium. The thermal boundary layer thickness (Y_t) is equal to Y_v divided by the square root of the Prandtl number. In 1868 Kirchhoff published his derivation of an expression for the mainstream attenuation coefficient, α_m , and one for the boundary layer attenuation, α_b :²¹

$$\alpha_b = \frac{1 + \frac{\gamma - 1}{\sqrt{\text{Pr}}}}{rc_o} \frac{\nu\omega}{2} \quad , \quad (2.37)$$

$$\alpha_m = \frac{\omega^2 \nu}{2c_o^3} \left(\frac{\lambda + 2\mu}{\mu} + \frac{\lambda - 1}{\text{Pr}} \right) \quad , \quad (2.38)$$

where Pr is the Prandtl number defined as $c_p \mu / \kappa$, λ is the dilatational viscosity coefficient, μ is the coefficient of sheer viscosity, r is the radius of the pipe, κ is the coefficient of thermal conductivity, and c_p is the specific heat at constant pressure. If $\alpha_b \gg \alpha_m$ and $r \gg Y_v$, a pipe is referred to by Weston²² as a wide pipe. For the plane wave tube used

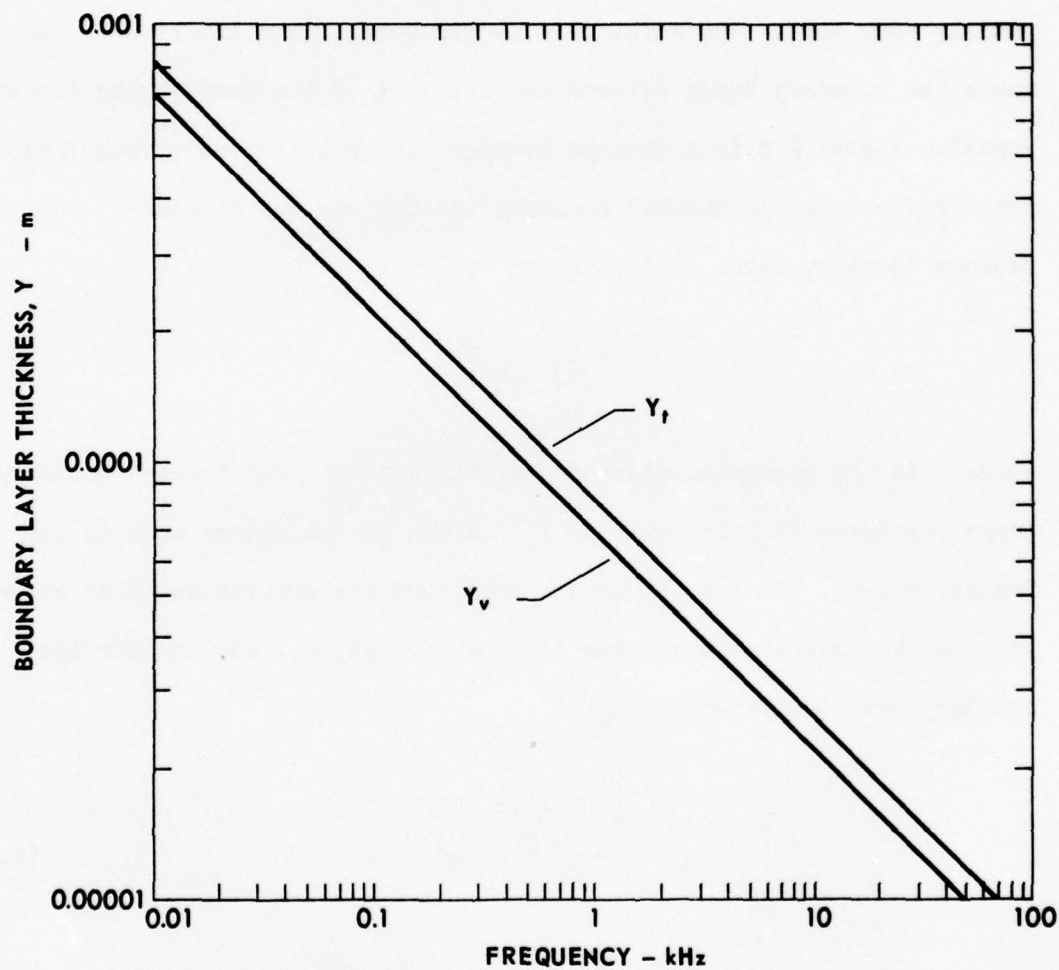


FIGURE 2.5
VISCOUS (Y_v) AND THERMAL (Y_t) BOUNDARY
LAYER THICKNESS FOR AIR AT STP

(5 cm diam) and for a tone of 5 kHz, the ratio of α_m/α_b is equal to 0.005. The next most important source of attenuation is relaxation effects in the medium. Attenuation due to relaxation is equal to the attenuation due to boundary layer effects (α_b) at frequencies of the order of 100 kHz.²³ Therefore, for the plane wave tube used and at the frequencies of the primaries (less than 5 kHz), the major cause of attenuation of the acoustic signals is viscous boundary layer effects.

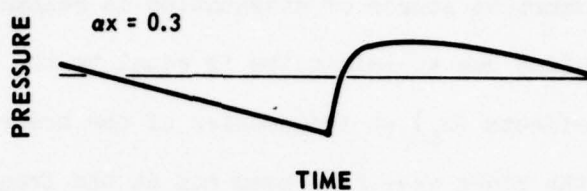
The viscous and thermal boundary layers cause dispersion as well as attenuation. In air for tubes, dispersion is expressed by

$$c(\omega) = c_o \left(\frac{1 - \alpha_b}{\omega} \right) \quad . \quad (2.39)$$

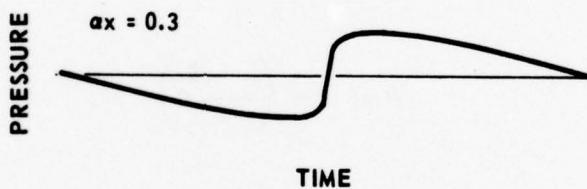
For a simple frequency source, the various harmonics get out of step with each other because of their varying phase velocities. Only for large frequencies is the phase velocity equal to c_o . The net result is that the peak of a shock becomes rounded while the trough stays sharp. An illustration due to Webster²⁴ of the effect of dispersion on a sawtooth is shown in Fig. 2.6.

I. Major Computer Algorithm

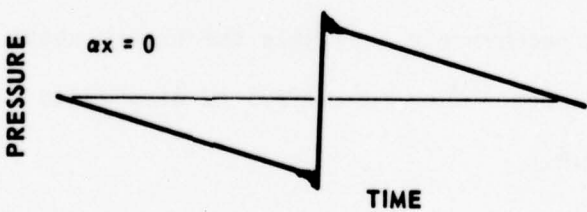
Program C500, the computer algorithm, which implements weak shock theory with attenuation and dispersion, is fairly involved. A detailed explanation of program C500 is presented in Chapter III, and a documented listing of the program and the subroutines used are presented in Appendix A. A brief outline is given here so the reader may gain a basic understanding of the program.



(a) BOTH ABSORPTION AND DISPERSION



(b) ABSORPTION ONLY



(c) LOSSLESS

FIGURE 2.6
EFFECTS OF ABSORPTION AND DISPERSION
ON A SMALL-SIGNAL SAWTOOTH

(Adapted from Webster²⁷)

Figure 2.7 is a simplified flowchart for program C500. The program begins with the initialization of program parameters including reading from data cards, the source SPLs, and frequencies of the two source tones and the desired propagation distance. The initial waveform is represented by a collection of wavelets, whose values are stored in the U array, and a corresponding collection of times, which are stored in the T array. The calculation of the initial waveform takes place next, and then the waveform is stored on disk. The initial waveform is propagated the desired distance by a series of incremental propagation steps. DO loop 8016 is the major DO loop of the program; each completion of the loop signifies the completion of one incremental propagation step. DO loop 8016 begins by recalling the waveform (the U and T arrays) from disk storage and writing the arrays on magnetic tape to be displayed later by program TIMEPLOT. The propagation of the waveform is achieved by calling subroutine WAVEPROP, the weak shock computer algorithm. The output waveform of WAVEPROP is then stored on disk. A call is made to subroutine TIMEFRE, which performs a fast Fourier transform (FFT) on the waveform so that the Fourier coefficients of the waveform may be calculated. The largest Fourier coefficients are then selected and their amplitudes and frequencies corrected for inaccuracies inherent in the FFT. Next, the corrected Fourier coefficients are written on a second magnetic tape to be processed later by program GRAPH. In the next section of the program a decision is made about applying attenuation and dispersion corrections. The corrections are made only every NATDIS number of trips through DO loop 8016. If attenuation and dispersion corrections are not made, control of the program returns to the beginning of DO loop 8016. The next

PROGRAM C500

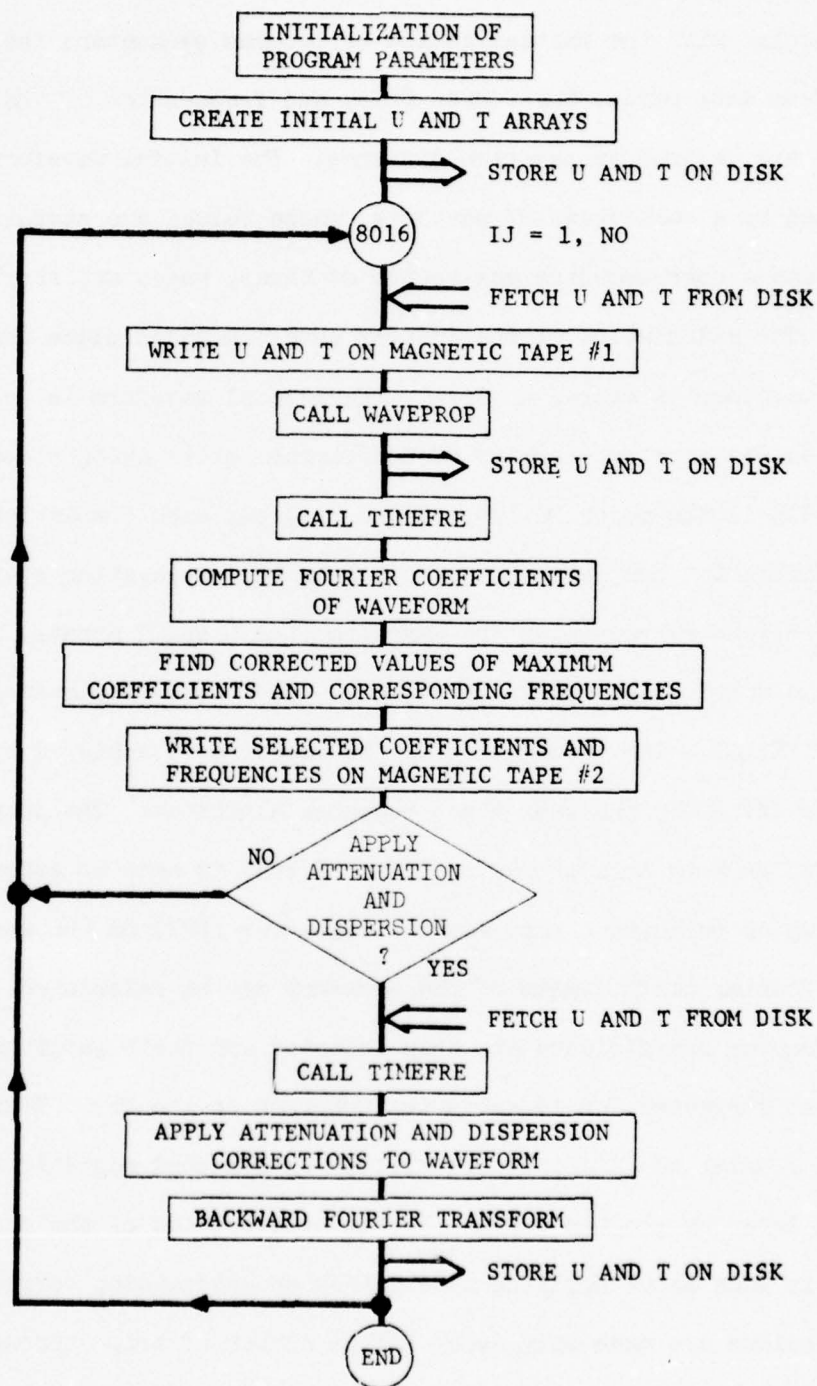


FIGURE 2.7
SIMPLIFIED FLOWCHART FOR PROGRAM C500,
THE WEAK SHOCK COMPUTER ALGORITHM

and last section of the program applies any corrections that are to be made. Here the waveform is recalled from disk storage and an FFT obtained (by a call to subroutine TIMEFRE) because the corrections are made in the frequency domain. An inverse FFT takes the signal back into the time domain. The corrected waveform is stored on the disk storage and control of the program returns to the beginning of DO loop 8016. The whole process in DO loop 8016 is repeated until the desired propagation distance is reached. An important aspect of program C500 is the use of disk storage. When attenuation and dispersion corrections are not made, the disk storage allows subroutine WAVEPROP to have the output of the last propagation as its input for the next propagation step. Example program outputs are presented in Chapter III.

Program C500 is used to calculate the theoretical predictions for comparison to the experimental results in Chapter V. In Chapter III the output of program C500 is compared to one of the exact preshock solutions for the same source conditions. The comparison (Fig. 3.6) shows that the results of the two solutions are equivalent; therefore, nothing is lost by using program C500 for $x < \bar{x}_p$. As a matter of fact, the use of program C500 is advantageous because it provides a simple method of incorporating attenuation and dispersion.

CHAPTER III

MAJOR COMPUTER ALGORITHMS

The computer algorithms used to implement weak shock theory with provisions for attenuation and dispersion are explained in detail here. This chapter is intended to help a user of the programs become familiar with the scope and limitations of the programs. A reader not desiring this insight may skip the present chapter without disrupting the continuity of the thesis. Program C500, which implements the weak shock method and also includes provisions for attenuation and dispersion, is discussed first. After the detailed flowchart for the program is explained, a discussion of the major subroutines and problems associated with the program is given. Also programs GRAPH and TIMEPLOT, which display the output of program C500, are discussed and their flowcharts explained; samples of the output of programs GRAPH and TIMEPLOT are included. The calibration of the three programs as a unit is discussed next. In the last section of the chapter the flexibility of these programs is considered for applications other than the very precise ones dealt with in this thesis.

A. Major Computer Algorithms

1. Flowchart for Program C500

It may be useful to recall the simplified flowchart for program C500 found in Chapter II (Fig. 2.4) before discussing the detailed flowchart for program C500, Fig. 3.1. That simplified flowchart and accompanying discussion serve as a good introduction to program C500 and

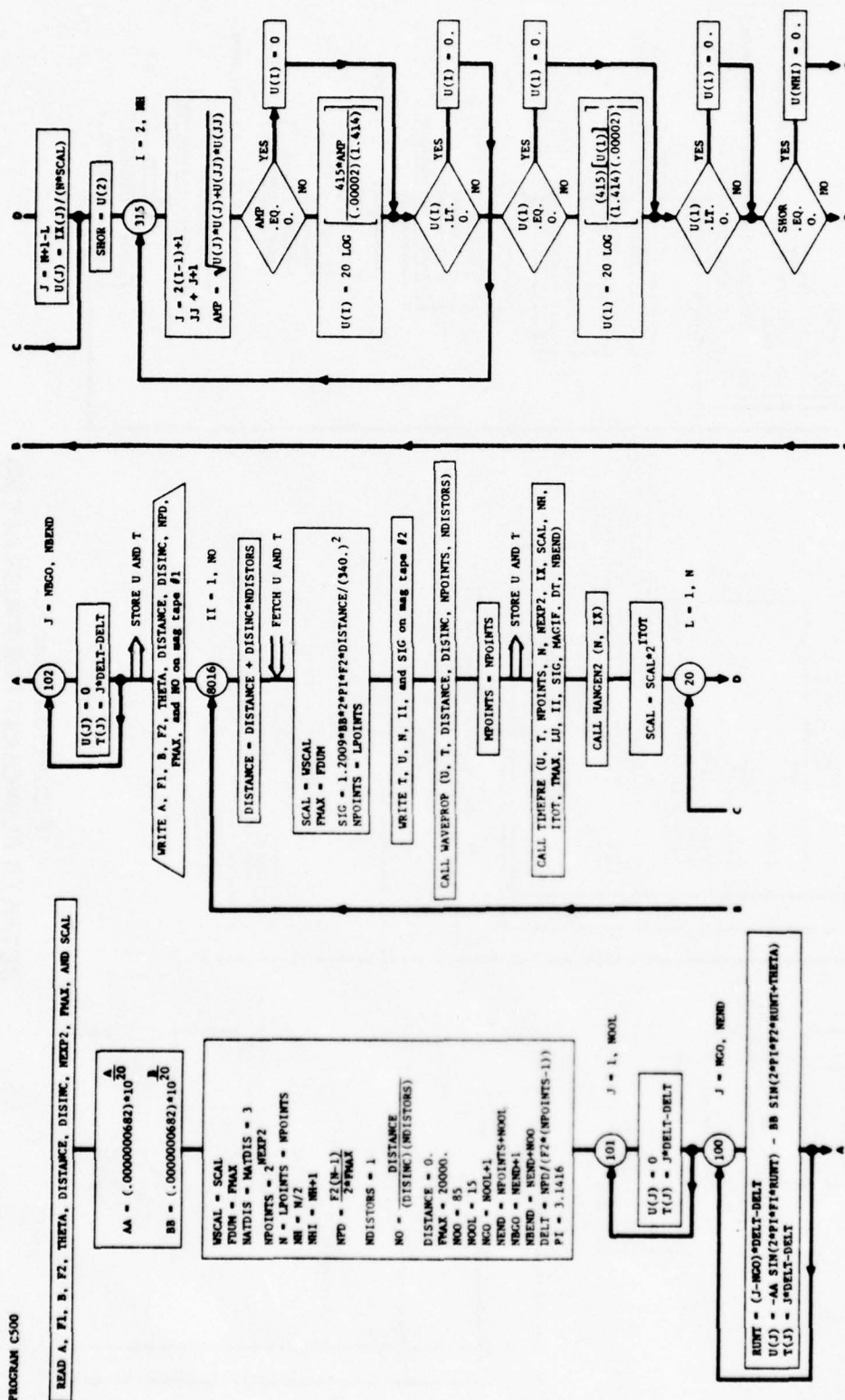


FIGURE 3.1
DETAILED FLOWCHART FOR PROGRAM C500

this chapter. Another aid in understanding the flowchart for program C500 is Appendix A, which is a documented listing of program C500 and its subroutines and definitions for the various program parameters.

The program parameters that determine the output of program C500 are read from data cards at the beginning of the program. The definitions of the parameters are found in Appendix A. An important relationship between DISTANCE (the desired propagation distance) and DISINC (the incremental propagation step size) is that the ratio DISTANCE/DISINC must be equal to an integer. Next, the source SPL of each tone (called A or B in the program) is used to obtain a source particle velocity amplitude. The vast majority of program parameters are then initialized. Some explanation, besides the definitions in Appendix A of a few parameters, is needed and will help to explain some basic idea behind the program. The number of points in the initial waveform is the even number NPOINTS. The initial waveform includes an even number NPD of pump wavelengths to help ensure zero or approximately zero endpoints. NDISTOR is the number of incremental propagation steps done in succession without stopping to Fourier transform the output waveform. NO is the number of (NDISTORS) \times (DISINC) propagation steps necessary to reach the desired propagation distance. The initial waveform is represented by a particle velocity array U and a time array T. The initial waveform is calculated by DO loop 100. The phase of the initial waveform is 180° to ensure that the shocks which form will form inward away from the endpoints of the arrays. Zero buffers are added to the beginning of the waveform (DO loop 101) and to the end of the waveform (DO loop 102) to allow for possible spreading out of the original time base caused by distortion when the wave

propagates. The initial waveform, which represents the boundary condition, is stored on disk so that a waveform may be recalled and operated on (e.g., transformed by FFT) without destroying the original waveform. Some of the input (deterministic) parameters and other program parameters are written on the spectrum output magnetic tape (magnetic tape No. 1) to identify the data on the tape.

The next section of the program consists of the remainder of the program and contains the major DO loop of the program, DO loop 8016. An incremental propagation of the waveform stored on disk is achieved by the completion of one trip through DO loop 8016; every completion of a loop represents the completion of a propagation step equal to $(NDISTORS) \times (DISINC)$. NO number of loops of DO loop 8016 have to be completed in order to propagate an initial waveform the desired distance. The DO loop has three major sections: the first calculates the Fourier transform of the output waveform of a propagation step; in the second, the major (local maxima) Fourier coefficients are selected from the output waveform spectrum and corrected values and frequencies are calculated for the selected coefficients; and the last section contains the implementation of the attenuation and dispersion corrections. The DO loop begins by incrementing DISTANCE by $(DISINC) \times (NDISTOR)$ for the calculation of σ_p (referred to as SIG in the program) for the next output waveform. The waveform on disk is recalled and written on magnetic tape No. 2 to be plotted by program TIMEPLOT later, if desired. A call to subroutine WAVEPROP achieves the propagation of the waveform through the weak shock method. The output waveform returned by WAVEPROP is then stored on disk. A fast Fourier transform (FFT) is performed on the output waveform by a call to

subroutine TIMEFRE. Subroutine TIMEFRE removes the zero buffers from the waveform and calls subroutine RESAMPLE. Subroutine RESAMPLE resamples the waveform to produce a desired number of equally spaced points in the U and T arrays. Still under the control of subroutine TIMEFRE, the resampled waveform undergoes an FFT and the real and imaginary parts of the Fourier coefficients are returned to the main program. A data window is applied to the frequency components of the waveform by a call to subroutine HANGEN2. A data window is used to ensure that the endpoints of the waveform are zero to reduce side lobes, aliasing, and leakage* inherent in a FFT. The real and imaginary parts of the frequency components are scaled to calibrated values by DO loop 20. Calibrated values are necessary so that the output of program C500 is compatible with experimental results. DO loop 315 calculates the magnitude of the real and imaginary points of the frequency components and DO loop 888 calculates their frequencies. The sections of the program between DO loop 888 and the end of DO loop 315 compute the first and last Fourier coefficient of the output waveform.

In the next section of the program, and of DO loop 8016, the major or local maximum frequency components of the spectrum of the waveform are selected. The chosen frequency components are corrected for the data window and for the inherent error of the FFT. The corrected amplitude and frequency of a Fourier coefficient are calculated by an interpolation scheme by Burgess.²⁵ The selection of the maximum frequency components is accomplished by DO loop 5, and is initiated by checking the frequency of a coefficient. If the frequency of the coefficient is greater than FMAX (the largest frequency of interest), DO loop 5 is

* To be defined and discussed in the FFT subroutine section.

terminated and the remaining section of the program is executed. When a maximum frequency component is located, the interpolation is between the maximum component and the larger of the two components to the left and right of the maximum. The corrected amplitude of a frequency component is stored in an even numbered element of the FT array and the frequency of the component is stored in the next larger odd element of the FT array. The array containing the corrected Fourier coefficients and frequencies is written on magnetic tape No. 1, with the value of σ_p associated with the spectrum. Magnetic tape No. 1, or the spectrum output tape, is processed by program GRAPH.

The corrections for attenuation and dispersion are applied in the last section of the program and the third section of DO loop 8016. The corrections are not applied after every propagation step because to do so would introduce errors due to resampling (resampling problems are discussed in the subroutine RESAMPLE section). When the corrections are not applied, the control of the program execution is returned to the beginning of DO loop 8016. An important point about program C500 is that when attenuation and dispersion corrections are not applied, the input waveform for the next propagation step is the output of the last propagation step which has been stored on disk. DO loop 815 implements the corrections for attenuation and dispersion only when a given number, called NATDIS, of completions of DO loop 8016 have been executed. Before the corrections are made, the waveform is recalled from disk storage and subroutine TIMEFRE is called to transform the signal to the frequency domain. The corrections are made and then an inverse FFT is taken to get back into the time domain. DO loop 816 scales the corrected waveform to

calibrated values. The waveform amplitude has to be calibrated so that the finite amplitude distortion predicted by weak shock theory for the wave is correct. DO loop 818 shifts the elements of the U and T arrays forward to make room for the right-hand zero buffer which was removed by subroutine TIMEFRE. A zero buffer is added to the right end of the corrected waveform by DO loop 821; a zero buffer at the left end is added by DO loop 817. Next, the corrected waveform with zero buffers is stored on disk, and the signal is returned to the beginning of DO loop 8016 until the desired propagation distance is reached.

a. Subroutine WAVEPROP

Subroutine WAVEPROP is the weak shock method subroutine. An input waveform, described in terms of a U array and a T array, is propagated an incremental distance according to weak shock theory. WAVEPROP renumbers the elements of the arrays as shock-wavelet merging causes a decrease in the total number of elements in the arrays. Equally spaced data points are not required. The original version of WAVEPROP performed all the necessary DISINC steps to propagate the initial waveform the desired distance with one call to WAVEPROP. The present form of WAVEPROP performs NDISTORS number of DISINC steps with every call to WAVEPROP. For a complete explanation of WAVEPROP see Pestorius.⁸

b. Subroutine TIMEFRE

Subroutine TIMEFRE was specifically written for C500. TIMEFRE performs the actual transformation from the time domain to the frequency domain. The zero buffers are checked to see if they are large enough. If they are, the zero buffers are removed from the U array prior to a call

to the FFT and the elements of the U and T arrays are renumbered, but the time relationships between the elements of the arrays are maintained. If the zero buffers are not large enough (they no longer exist), the program execution is stopped and one of the following messages is printed:

RIGHT ZERO BUFFER NOT LARGE ENOUGH

if the right-hand zero buffer is not large enough, or

LEFT ZERO BUFFER NOT LARGE ENOUGH

if the left-hand zero buffer is too small. It is then necessary to increase NOO or NOOL depending on which of the zero buffers is in question. NOO and NOOL are the number of zeroes, respectively, in the right and left zero buffers. The number of remaining zeroes in the two buffers is printed with every call to TIMEFRE. NET is the number of zeroes in the left buffer, and LET in the right buffer. TIMEFRE's calling sequence is

CALL TIMEFRE (U, T, NPOINTS, N, NEXP2, IX, SCAL, NH,
ITOT, TMAX, LU, II, SIG, MAGIF, DT),

where

N is the desired number of elements in U or T after a call
to RESAMPLE,

$$NEXP2 - N = 2^{NEXP2},$$

IX is the integer array where U is stored to perform the
integer Fourier transform on U,

SCAL is the multiplicative scaling factor used on the U array
before it is stored in IX,

$$NH = N/2,$$

ITOT is a scaling factor returned by the integer forward FFT,

TMAX is the length of the time data before FFT,

LU is a look-up table for the FFT,

II is the number of the last incremental step taken,

MAGIF is a dummy variable,

DT is the spacing in the time data after RESAMPLE,

and the remaining variables have been previously defined. A call to TIMEFRE causes a call to RESAMPLE and a call to IFFTFD. Subroutine TIMEFRE returns the real and imaginary parts of the Fourier coefficients to the main program in the U array.

c. Subroutine RESAMPLE

Subroutine RESAMPLE used in program C500 is very nearly identical to the version used by Pestorius.⁸ The only difference is that the internal storage for the computational steps has been changed to allow the storage area to be used by other parts of program C500. Besides resampling the data points, calls to RESAMPLE have an unfortunate side effect. In the process of obtaining more (or less) array elements which are equally spaced, the waveform defined by the arrays becomes "undistorted." The distortion of a waveform is represented by the changed spacing of the elements of the T array: the elements near a shock become bunched up and elements near a rarefaction are spread apart. A call to RESAMPLE, however, produces even spacing in the T array; even with an interpolation scheme, the resulting waveform is undistorted (the shocks are not as sharp). In program C500 the undistortion of a waveform is a problem only when attenuation and dispersion are applied. When attenuation and dispersion are not applied, the input to WAVEPROP is the previous output, which has been stored on disk. To minimize the RESAMPLE problem, not every incremental propagation step is followed by attenuation and

dispersion corrections. Pestorius⁸ has a detailed discussion on selecting a value of NATDIS, the number of DISINC between corrections for attenuation and dispersion.

d. FFT Subroutine

The Fourier transform routine, the forward transform IFFTDF or the backward transform IFFTDB, is an integer routine. The reason an integer FFT is used on a floating point array is that it saves computational time. Before a call to IFFTDF is made in subroutine TIMEFRE, the U array is scaled up by SCAL so as to maintain the desired number of significant digits before the truncation involved in the transition from floating point to integer number occurs. The FFT routines are designed for harmonic analysis of the frequency composition of waveforms. The frequencies of interest in a two-frequency interaction are in general not harmonically related. An FFT routine may be used to find nonharmonically related frequency information by making the fundamental sought by the FFT small. The hope is that the harmonics of the fundamental will fall near the true component frequencies. Using a small fundamental is a "shotgun" approach that may lead to erroneous results. If a true component frequency does not fall directly in the middle of the main lobe of a harmonic of the fundamental, the amplitude of the Fourier coefficient returned by the FFT will be incorrect. Instead of the correct value for the frequency component, two false components are returned by the FFT. A $\sin(x)/x$ interpolation is performed between the two false values to get the correct amplitude and frequency of the component. The interpolation scheme used also corrected for the Hanning data window.²³ If the length of a given

set of time data is T , the fundamental frequency Δf associated with an FFT of the data is

$$\Delta f = 1/T \quad .$$

A long length of data is required for a small Δf .

Another problem encountered with an FFT is aliasing. An FFT has a maximum frequency for which a Fourier coefficient can be correctly calculated. The frequency of the last Fourier coefficient that may be calculated with an FFT is called the Nyquist or cutoff frequency.

$$\text{Nyquist Frequency} = 1/(2\Delta t) \quad ,$$

where Δt is that sampling rate given by $\Delta t = T/n$, where n is the number of points in the time data. If the time data has real frequency components which are greater than the Nyquist frequency, aliasing occurs. A frequency greater than the Nyquist frequency is folded over to a frequency less than the Nyquist frequency. If the Nyquist frequency is 10 kHz and there is a real frequency component at 15 kHz, the Fourier transform will fold the 15 kHz into a 5 kHz component in the spectrum of the waveform. The folding over of frequency components greater than the Nyquist frequency by a Fourier transform may be represented by

$$F_{\text{apparent}} = F_{\text{true}} - (M) * (F_{\text{Nyquist}})$$

where F_{apparent} is the folded over frequency, F_{true} is the real frequency, F_{Nyquist} is the Nyquist frequency for the Fourier transform for a certain input, and M is a positive integer such that F_{apparent} is between 0 Hz and the Nyquist frequency. Aliasing is a potential problem in the present work because of the large amplitudes of the pump harmonics; the more

remote harmonics may exceed the Nyquist frequency. However, the problem is really important only when the folded over frequency falls upon a frequency of interest. Aliasing may be detected by changing the Nyquist frequency by a known amount; this change will cause any aliasing to be shifted a corresponding amount.

Leakage is also a problem with an FFT. Leakage is caused when the values of particle velocity associated with endpoints of the time data are not the same, causing false frequency components to appear throughout the spectrum of the waveform. The result of an FFT of a finite length waveform is not a true Fourier transform of the waveform but a transform of a waveform in which the original waveform is periodically extended to infinity in the time domain. Discontinuities at the periodically extended waveform cause leakage, and leakage causes side lobes to form around the main Fourier coefficients. One way to solve the leakage problem is to ensure that the signal is zero at each endpoint. The initial time data is constructed so that there is an integral number of periods of the pump. The phase of the input data is selected so that the shocks which are formed by the pump form inward, away from the endpoints of the signal. When a dispersion correction is applied to an intermediate waveform, the phase of the frequency components of the waveform is changed. The endpoints of the waveform are then not necessarily zero. Zero buffers are then required to allow the nonzero endpoints of the signal to distort out of the time base (beyond the time endpoints). A Hanning data window is applied to the data to ensure zero endpoints before an FFT is taken. But data windows distort the data they are applied to; therefore, the data have to be corrected after a data window has been used. With all the problems

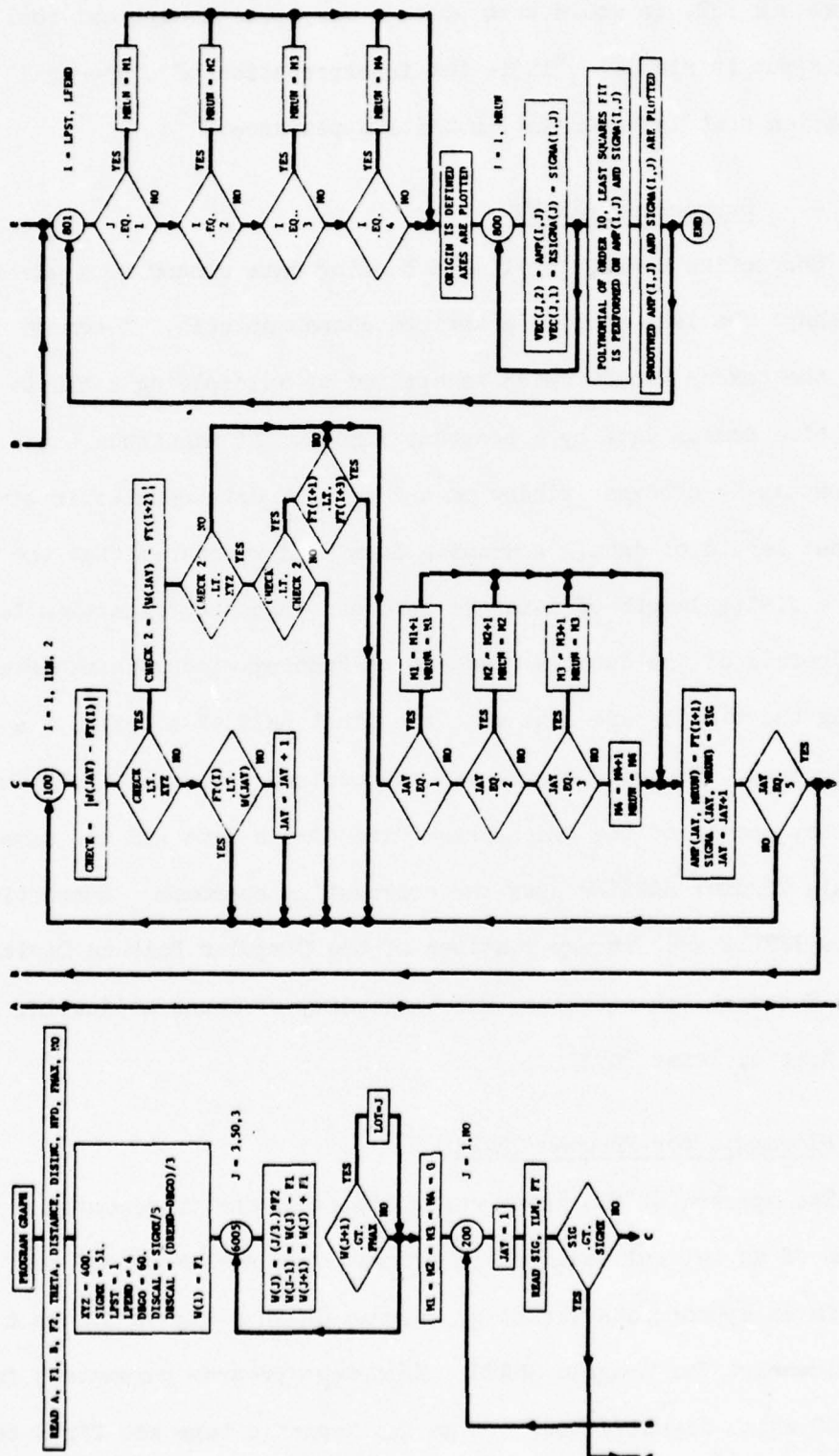
inherent with a FFT, it would seem to be a very poor analytical tool. Burgess has put it nicely: "It is the interpretation of a spectral representation that is important, not its appearance."²⁵

e. Subroutine HANGEN2

Subroutine HANGEN2 applies a Hanning data window to a waveform, so as to shape the data to give a desired characteristic. A common data window is the boxcar window which is applied by multiplying a finite length of time domain data by a constant function of magnitude one. The effect of applying a boxcar window on a length of data results in simply the original length of data. A Hanning data window ensures that the endpoints of a finite length of data are zero and that the transition to zero at the endpoints of the data is gradual. A Hanning window is achieved by multiplying the time domain data with the first half of a cycle of a sine function squared. The same result may be obtained through convolution in the frequency domain of the transformed time domain data and the sine squared data window; HANGEN2 uses the convolution approach. Subroutine HANGEN2 and IFFTDF are library routines of the Computer Science Division of Applied Research Laboratories, The University of Texas at Austin, Box 8029, Austin, Texas 78712.

2. Flowchart for Program GRAPH

The spectra of the waveforms produced by the incremental propagation of an initial waveform in program C500 are processed and displayed in an appropriate format by program GRAPH. Figure 3.2 is a detailed flowchart for program GRAPH. Important program parameters from program C500 which identify the data on the magnetic tape are first read



from the program C500 output spectrum tape; program GRAPH variables are initialized in the next section of the program (Appendix B is a documented listing of program GRAPH which includes the definitions of the program variables). A few of the parameters warrant additional explanation. A numerical filter is employed to select specific frequency components from the spectra of program C500; XYZ is the bandwidth of the numerical filter. The amplitude for a particular frequency component is found as a function of σ_p . Each selected frequency component is associated with a spectral number: the lowest frequency component has a spectral number of 1, the next lowest 2, etc. The output of GRAPH consists of plots of the amplitude of the frequency components corresponding to the spectral numbers as a function of σ_p . DO loop 6005 calculates the center frequencies for the numerical filter and stores them in the W array; the center frequencies are really the frequencies of interest in the interaction of the weak signal and the higher frequency pump ($\omega_w, \omega_p, \omega_p \pm n\omega_w$; n an integer). The numerical filtering is accomplished by DO loop 200, DO loop 100 being the actual filter. Each trip through loop 200 is started by reading a spectrum from the magnetic tape. Each spectrum is searched for frequency components which fall within XYZ Hz from the center frequencies. If more than one frequency component is found within XYZ Hz from a center frequency, the component which has the greatest amplitude is chosen. The selected frequency components are stored in the AMP and SIGMA arrays according to their spectral numbers. For example, the amplitude of the third Fourier coefficient found within the bandwidth of the second smallest center frequency is stored in the AMP(2,3) element of the AMP array, and the corresponding value of σ_p for this coefficient is stored

in the SIGMA(2,3) element of the SIGMA array. Each time a component is associated with a spectral number, an index for that spectral number is incremented by one, the final value of an index equaling the number of selected components for that particular spectral number. The indexes are called M1, M2, M3, and M4 for the first four spectral numbers. The remaining portion of program GRAPH, DO loop 801, does the plotting. The program parameters LPST and LPEND determine the number of plots to be created by program GRAPH. The first plot corresponds to a spectral number equal to LPST, and the last plot has a spectral number equal to LPEND.

The actual plotting of arrays AMP and SIGMA is straightforward and needs no explanation. However, before the elements of array AMP for a particular center frequency are plotted, a polynomial least squares best fit of the data is performed. The parameter KK in program GRAPH is equal to the order of the polynomial fit; KK had a value of 10 here. A polynomial fit of the data is necessary for two reasons. Attenuation and dispersion corrections are not applied at every incremental propagation step, but when corrections are made, a stair-step decrease is caused in the amplitudes of all the frequency components. The polynomial fitting smooths the plots of the amplitude of a frequency component versus σ_p . The second reason a polynomial fit is necessary is that it connects elements of an array corresponding to a frequency component in a natural, reasonable manner. Every spectrum searched will not produce frequency components for every spectral number; therefore, larger jumps might exist in σ_p between consecutive elements in SIGMA than caused by the propagation increment. Nothing is known between two consecutive points in the AMP

array except the points are expected to be joined by a smooth curve.

Figure 3.3 shows an example output from program GRAPH.

3. Flowchart for Program TIMEPLOT

The waveforms produced by the incremental propagation of an initial waveform by WAVEPROP in program C500 are displayed in an appropriate format by program TIMEPLOT. Program TIMEPLOT simply removes the left zero buffers from selected waveforms and plots the first portion of the particle velocity waveform as a function of time. Figure 3.4 is a flowchart for program TIMEPLOT; Appendix C gives a documented listing of the program, including definitions for the program parameters. The program parameters are initialized in the beginning of the program. Two of these parameters, IHOP and TMAX, require a little explanation. IHOP-1 is equal to the number of waveforms skipped between the waveforms which are plotted, and TMAX is the length of the portion of the plotted waveform. Loop 100 is the major loop of program TIMEPLOT. The loop is begun by reading a waveform from a magnetic tape. The index of loop 100 is compared to IHOP, and if the two are equal the waveform is plotted and IHOP is increased by an amount equal to its original value; if the two are not equal the index of loop 100 is incremented and the next waveform is read from the magnetic tape. After a particular waveform has been selected to be plotted, the zeroes in the left zero buffer are counted by loop 308. The final value of the loop index JJ, less one, is equal to the number of zeroes in the left zero buffer. DO loop 310 removes the left zero buffer; TSLIP is the amount the time axis is slipped backward when the left zero buffer is removed to retain the correct time relationship between the elements of the remaining waveform. DO loop 555 determines the number of

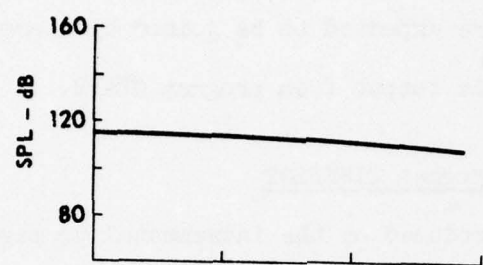
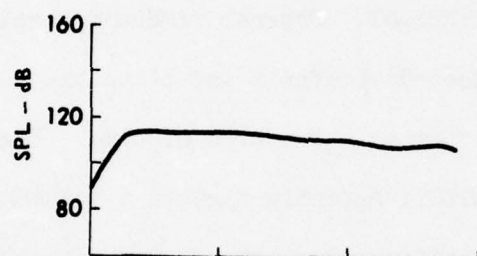
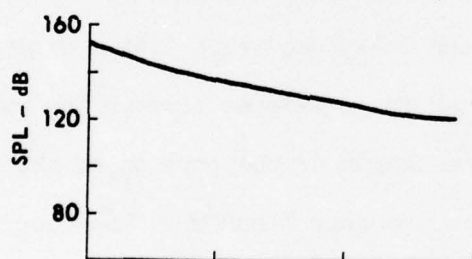
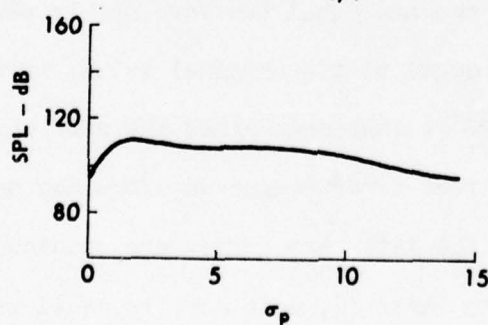
(a) WEAK SIGNAL ($u_{1,0}$)(b) FIRST LOWER SIDEBAND ($u_{-1,1}$)(c) PUMP ($u_{0,1}$)(d) FIRST UPPER SIDEBAND ($u_{1,1}$)

FIGURE 3.3
 EXAMPLE OUTPUT OF PROGRAM GRAPH, CASE II
 SOURCE $SPL_w = 115$, $f_w = 1.0$ kHz
 SOURCE $SPL_p = 151$, $f_p = 3.5$ kHz

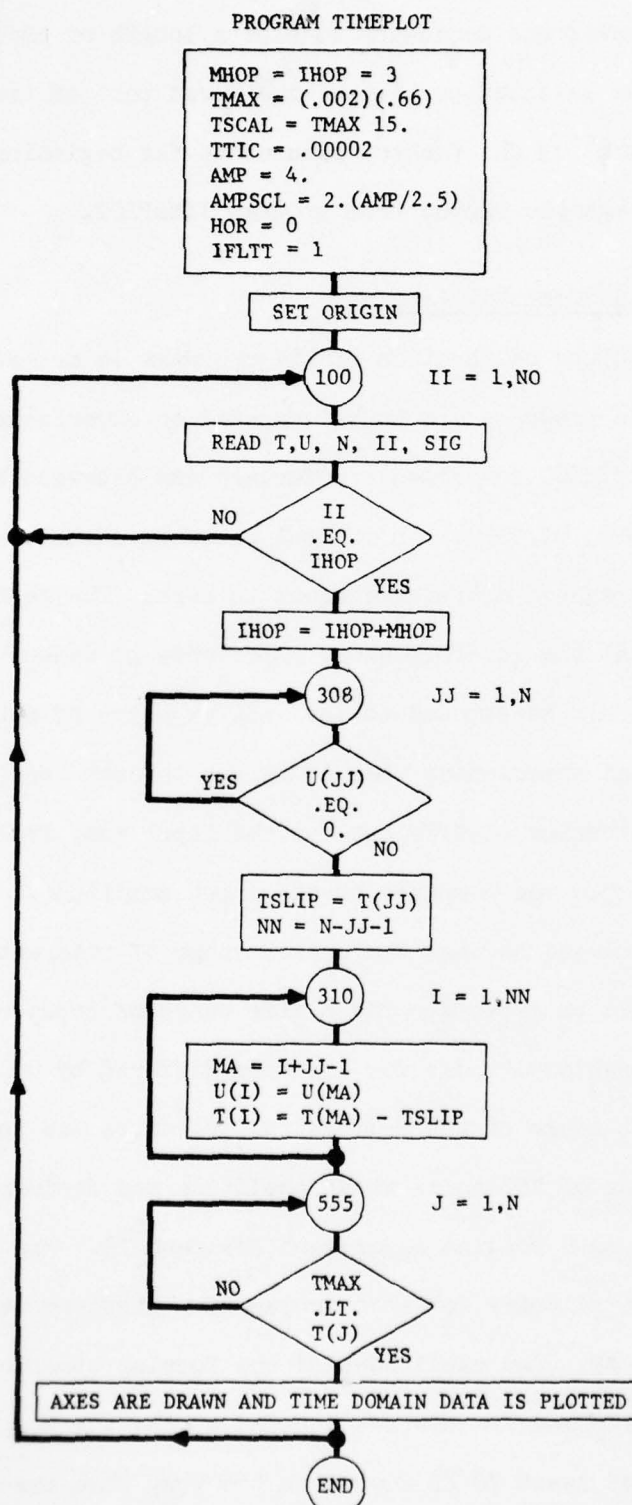


FIGURE 3.4
FLOWCHART FOR PROGRAM TIMEPLOT

elements of the waveforms necessary to plot a length of the waveform equal to TMAX. Then the selected portion of the first part of the waveform is plotted, and control of the program returns to the beginning of loop 100. Figure 3.5 is an example output from program TIMEPLOT.

B. Calibration of Computer Programs

The absolute calibration of the programs is necessary because the results of the programs are to be compared to experimental results. The calibration of C500 concerned the forward and backward FFTs taken during the execution of C500. An initial waveform composed of a tone of known SPL was propagated a distance equal to zero. The zero propagation distance meant that the waveform would experience no distortion or attenuation but would be exposed to the vast majority of mathematical procedures a signal experiences when it is run through the program. The amplitude of the Fourier coefficient for the input tone from the spectrum of the output of C500 was compared to the input amplitude. The frequency of the tone was changed so that the entire range of interest in the frequency domain could be checked. For a wide range of input amplitudes, the input and output amplitudes for the tone differed by no more than 0.01 dB. The next stage of the calibration procedure was to input a waveform consisting of two tones whose amplitude and frequency were similar to those used in a routine experiment for Case II. The difference in input and output amplitudes for zero propagation distance was always found to be within 0.02 dB. The amplitudes of the Fourier coefficients corresponding to the sideband frequencies located at the sum and difference frequencies were at least 70 dB down from the pump when the pump was 149 dB and the propagation distance was zero. The final stage of the

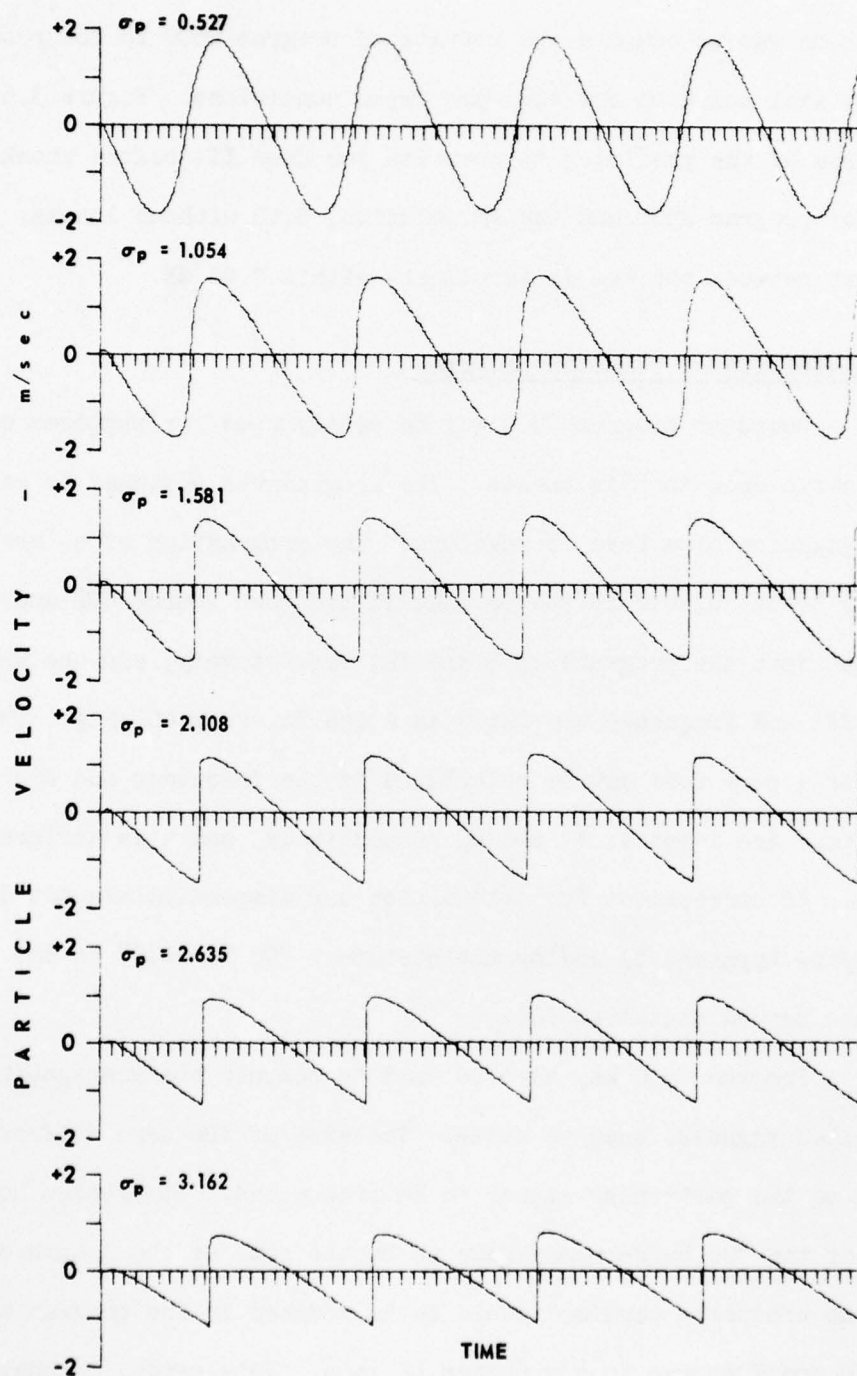


FIGURE 3.5
EXAMPLE OUTPUT FOR PROGRAM TIMEPLOT

SOURCE $SPL_w = 115$ dB, $f_w = 1$ kHz

SOURCE $SPL_p = 149$ dB, $f_p = 3.5$ kHz

EACH DIVISION REPRESENTS 0.00002 sec
ON HORIZONTAL AXIS

calibration was to compare the results of program C500 to the results of an analytical solution for the same input conditions. Figure 3.6 is a comparison of the predicted suppression for Case II (before shock formation) for program C500 and the FM solution, both without losses. The agreement between the two is excellent--within 0.02 dB.

C. Flexibility of Computer Programs

Computer program C500 may be easily used for purposes other than the specific ones in this thesis. The program was designed to calculate the propagation of a Case II waveform. The propagation of a Case I waveform may be calculated by the program if the pump source SPL and frequency are input into the programs as B and F2, respectively, and the weak tone source SPL and frequency are input as A and F1, respectively. The propagation of a pure tone may be calculated if the frequency and source SPL of the tone are input as F2 and B, respectively, and A is assigned a value of zero. If corrections for attenuation and dispersion are not desired, they may be bypassed by adding the statement "GO TO 8016" to the program, two lines beyond statement 701.

Program C500 may also be used to compute the propagation of more complicated signals, such as noise. The size of the zero buffers needed depends on the particular signal to be propagated. For random noise the length of the two buffers may have to be the same as the length of the data. An arbitrary waveform could be introduced in the program and stored in the U and T arrays in any number of ways: data cards, an analytical expression, digitized analog data, etc. Program C500 is flexible in what constitutes an acceptable input waveform; program GRAPH is flexible in the frequency components it searches for. The center frequencies of the

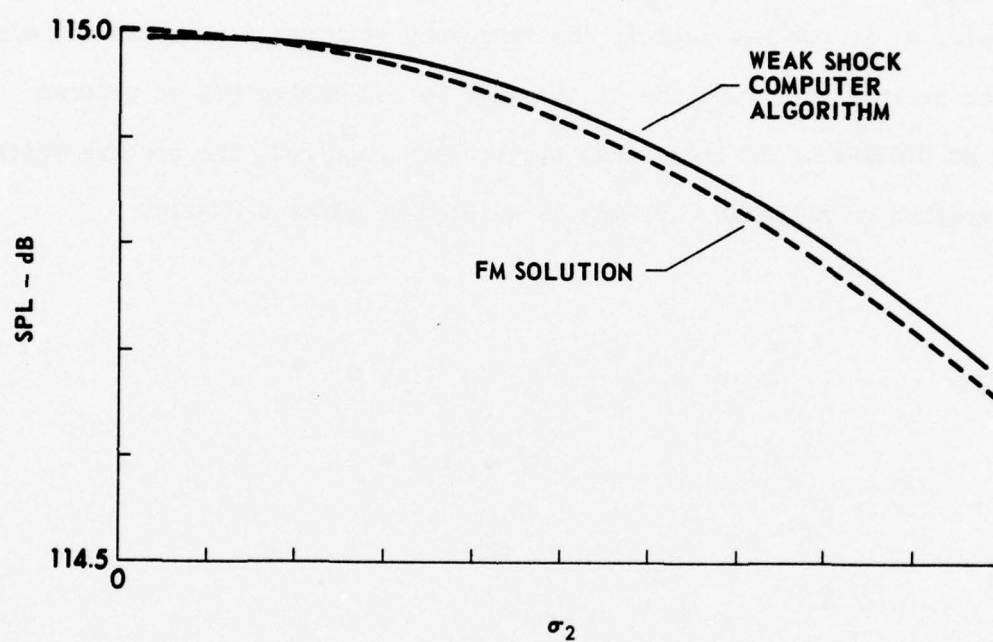


FIGURE 3.6
COMPARISON OF PREDICTIONS FOR THE SUPPRESSION OF
THE WEAK SIGNAL FOR CASE II (NO LOSSES INCLUDED)

SOURCE $SPL_w = 115$ dB, $f_w = 1$ kHz

SOURCE $SPL_p = 150$ dB, $f_p = 4.5$ kHz

numerical filter in program GRAPH are stored in the W array. The amplitude of any desired frequency component may be plotted as a function of σ_p by changing the values stored in the elements of the W array. For a single or double frequency, waveform σ_p is calculated using the corresponding ϵ of the source SPL input as B. For noise or other complicated signals, σ_p is not meaningful; the frequency components of these signals may be plotted as a function of distance by redefining SIG in program C500 as DISTANCE. If individual spectra are required, the spectra which are written on magnetic tape may be printed or plotted easily.

CHAPTER IV

EXPERIMENTAL APPARATUS

The experimental apparatus and procedures are described here, and the experimental measurements are reported in the next chapter. The experimental apparatus is divided into three parts: the transmit system, the plane wave pipe, and the receive system. The equipment used in each system is listed and, if necessary, its function explained. Special problems experienced with individual pieces of equipment are discussed. The second half of the chapter includes the checking and testing of each part of the experimental apparatus. Figure 4.1 (adapted from Webster²⁶) is a general diagram for the experimental setup.

A. The Systems

1. The Transmit System

The following list of equipment was used in the transmit system:

- a. Bruel and Kjaer (B&K) type 1022 beat frequency oscillator (BFO),
- b. General Radio (GR) type 1310-A oscillator,
- c. Dukane type 1A921 200 W power amplifiers,
- d. University type ID-75 75 W horn driver,
- e. Hewlett Packard 5300B timing system,
- f. Hewlett Packard 350C attenuator set,
- g. Tektronix 545B dual channel oscilloscope,
- h. JBL Model 375-H horn drivers (with aluminum diaphragm),
- i. JBL Model 375-H horn driver (with phenolic diaphragm),

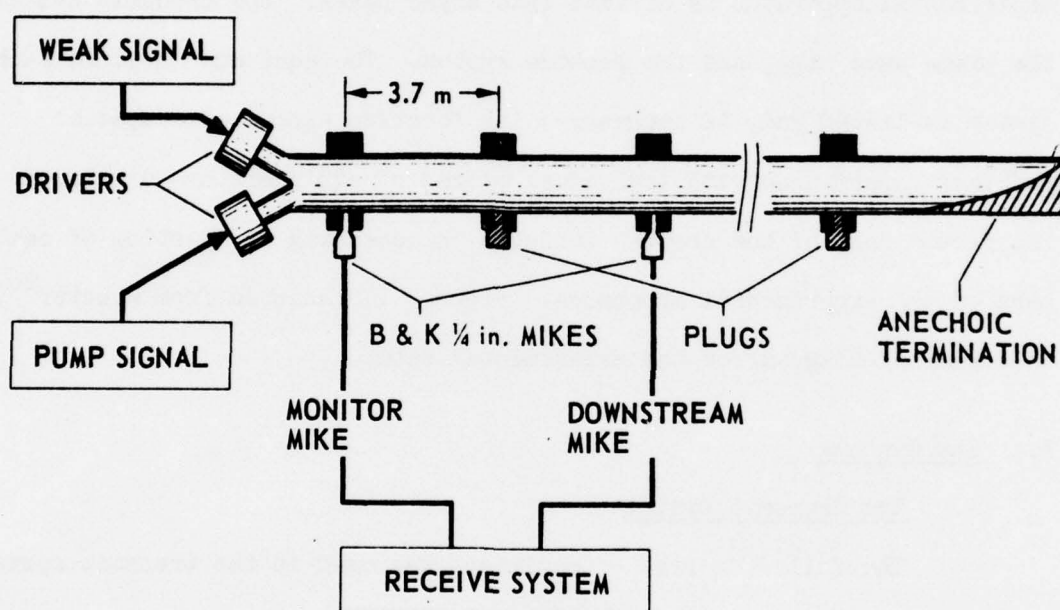


FIGURE 4.1
EXPERIMENTAL APPARATUS

(Adapted from Webster²⁶)

- j. Pearson Electronics, Inc., model 110 current loop,
- k. Hewlett Packard 400 EL FET voltmeter, and
- l. Hewlett Packard 3580A spectrum analyzer.

The transmit system was further divided into two separate subsystems: one to produce the pump signal and another to produce the weak signal. Separate oscillators, amplifiers, and drivers were used to produce the two signals independently to decrease the intermodulation distortion (IM) between the signals in the transmit system. Figure 4.2 is a diagram of the transmit system showing the use of the listed equipment. Some comment about the two types of JBL horn drivers is necessary. The JBL 375-H driver with an aluminum diaphragm has a flat frequency response from 300 Hz to 8600 Hz, with a maximum input of no more than 25 W. The JBL 375-H driver with a phenolic diaphragm has a flat frequency response from 300 Hz to 4.5 kHz, with a maximum input of 60 W. Two different arrangements of drivers were used to produce the two acoustic signals. In one case the weak signal was produced by a University ID-75 driver and the pump signal by the phenolic diaphragm JBL 375-H driver. In the second arrangement an aluminum diaphragm JBL 375-H driver produced the weak signal, and three drivers of the same type, operating in parallel, produced the pump signal. The first arrangement of drivers was used in the first experiments. After the failure of the phenolic diaphragm JBL 375-H driver, the second arrangement of drivers was used.

2. Plane Wave Pipe

The plane wave tube was used to ensure planar progressive propagation of the acoustic signals. This particular tube has been used in several previous investigations.^{6,8,24,27} The tube consists of eight

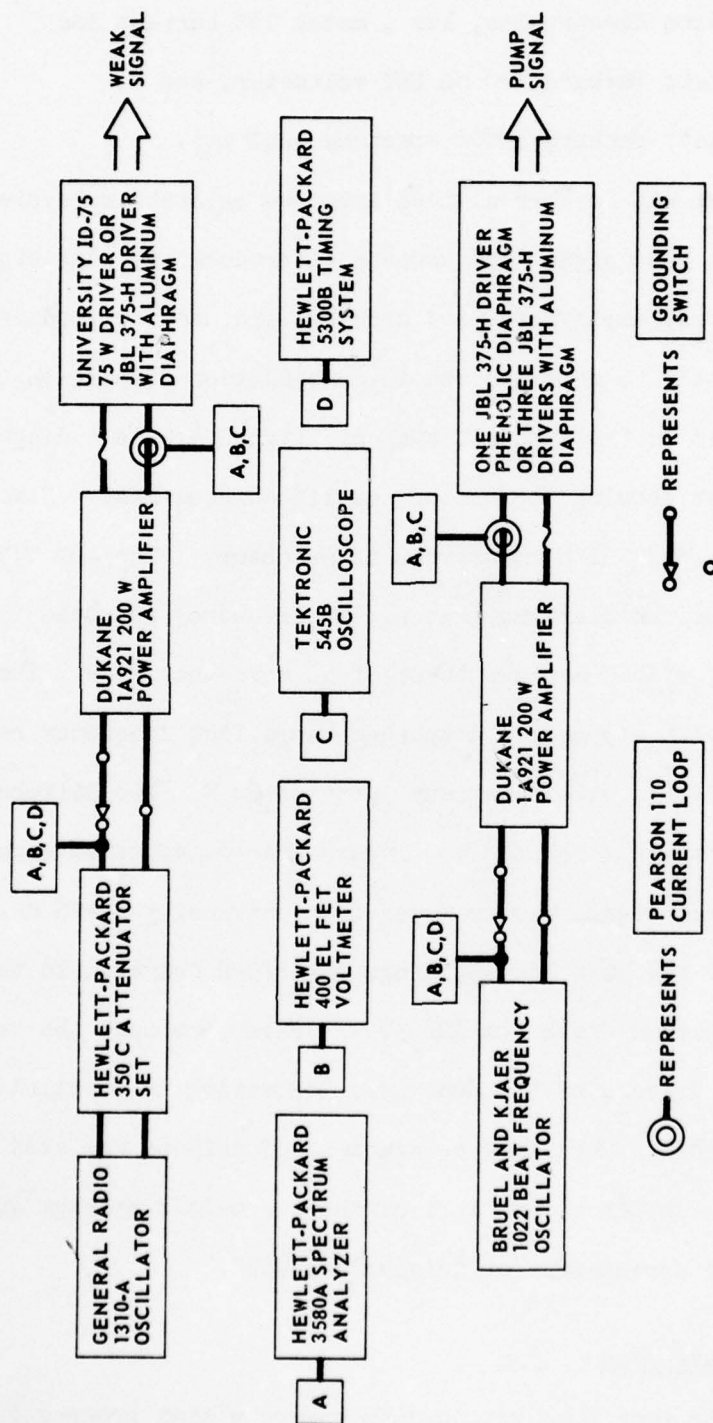


FIGURE 4.2
BLOCK DIAGRAM OF TRANSMIT SYSTEM

3.66 m (12 ft) lengths of aluminum pipe with an inside diameter of 5 cm. Both ends of each pipe have specially made connecting flanges affixed with three set screws. Each set of flanges has three steel alignment pins which help ensure a smooth junction between two consecutive pieces of pipe. Each pair of connecting flanges also contains a microphone port. Figure 4.3 is a picture of one of the flange assemblies. When a microphone port is not in use, an aluminum plug is inserted in the port. When a microphone is to be used in a certain port, a teflon collar is inserted in the port. A B&K 1/4 in. microphone may then be inserted in the collar so that the microphone diaphragm is flush with the inside surface of the pipe. The eighth section of pipe has a 2 m tapered fiberglass wedge. The termination helps satisfy the progressive wave approximation.

The two different arrangements of drivers used to produce the acoustical signal required two different driver mounts for the plane wave tube. When a two-driver source was used, a single Y yoke was employed to connect the drivers to the end flange. A double Y yoke was used when a four-driver source was required. The yokes made a gradual transition from the dimensions of the mouth of each driver to the dimensions of the inside of the pipe. The propagation distances of the observed waveforms are measured from the point in the yokes at which the complete pump signal is formed. The single yoke is shown in Fig. 4.4a, and the double yoke in Fig. 4.4b. In both pictures the first microphone location (called the monitor microphone location), with a 1/4 in. microphone inserted, may be seen. In neither picture are the drivers connected to the power amplifiers, but the black conductor in the lower left corner is the transmission line from the amplifiers. Both pictures also show that the entire

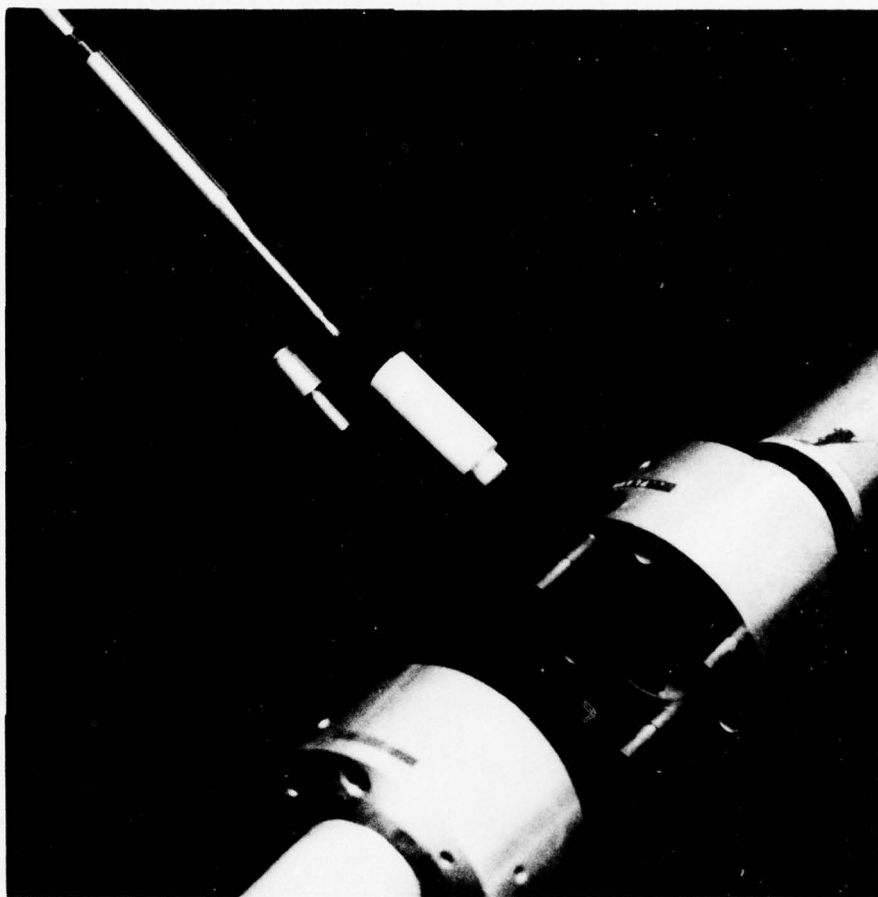
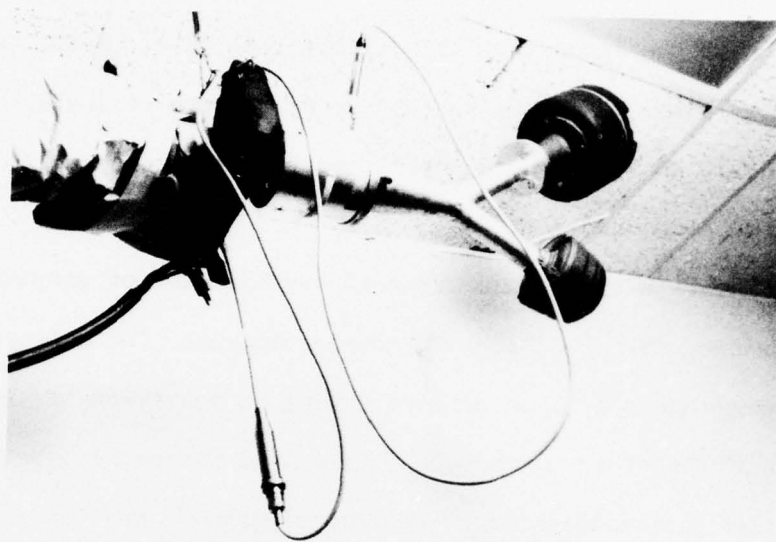
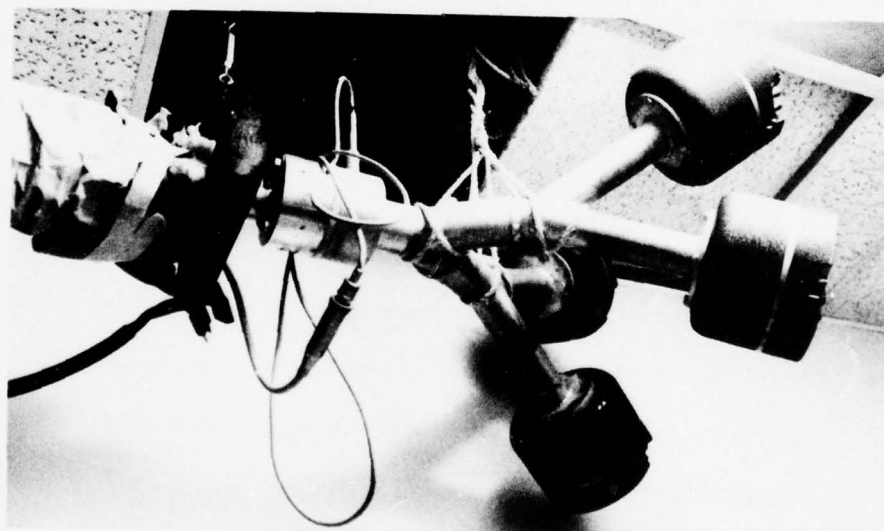


FIGURE 4.3
EXPLODED VIEW OF FLANGE ASSEMBLY WITH
MEASURING MICROPHONE AND PLUG
(THE PROTECTIVE GRID SHOWN ON THE MICROPHONE
WAS REMOVED BEFORE THE MICROPHONE WAS
INSERTED IN THE HOLDER AND FLANGE)

(Taken from Schaffer⁶)



(a) TWO DRIVER, SINGLE YOKE



(b) FOUR DRIVER, DOUBLE YOKE

FIGURE 4.4
DRIVER MOUNTING YOKES FOR PLANE WAVE PIPE

plane wave tube is suspended from the ceiling in a hall. Noise control treatment of the plane wave tube was necessary because of leakage of the acoustic signals. In Fig. 4.4 the noise control treatment may be seen (fiberglass insulation and duct seal).

The separate electronic transmit systems did not completely eliminate undesired mixing of the two source signals. The drivers connected through acoustical paths were acting as receivers of the acoustical signals of the other drivers.⁶ This mutual interaction between the sources produced intermodulation of the two signals in the drivers themselves. The weak signal drivers were particularly affected by the pump signal. The branch of the yoke which held the small signal driver was filled with size 00 steel wool to change the acoustic impedance of the branch. The steel wool decreased, by approximately 5 dB, the amplitude of the received pump signal by the small signal driver.

3. The Receive System

The following list of equipment comprised the receive system:

- a. Bruel and Kjaer 4136 1/4 in. condenser microphones,
- b. Bruel and Kjaer 2619 field effect transistor (FET) preamplifiers,
- c. Bruel and Kjaer 2803 dual channel microphone power supply,
- d. Bruel and Kjaer 4220 microphone calibrator,
- e. Bruel and Kjaer A00029 30 m microphone extension cables,
- f. Hewlett Packard 3580A spectrum analyzer,
- g. Hewlett Packard 400 EL FET voltmeter,
- h. Tektronix 545B dual channel oscilloscope, and
- i. Honeywell 500 2X-Y recorder.

AD-A040 008

TEXAS UNIV AT AUSTIN APPLIED RESEARCH LABS
THE SUPPRESSION OF SOUND BY SOUND OF HIGHER FREQUENCY.(U)
MAY 77 W L WILLSHIRE

F/G 20/1

F44620-76-C-0040

UNCLASSIFIED

ARL-TR-77-22

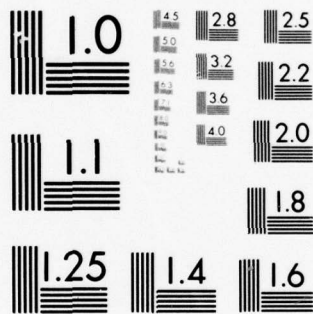
AFOSR-TR-77-0656

NL

2 OF 2

AD
A040008





MICROCOPY RESOLUTION TEST CHART
NATIONAL BUREAU OF STANDARDS-1963-A

Figure 4.5 is a diagram of the receive system. A microphone was always in the monitor port (the microphone port in the driver mount) to continuously monitor the output of the drivers. To observe the propagation of a wave as a function of distance, a second microphone was alternately used in the seven remaining microphone ports. The second microphone is called the downstream microphone. At the beginning and end of an experiment, both microphones were calibrated with a B&K 4220 pistonphone.

B. Test and Evaluation

1. The Transmit System

A useful way to evaluate the transmit system is the "black box approach." In the black box approach, once a desired waveform has been observed at the monitor microphone location, the manner in which the waveform is produced is of no consequence. The propagation distances are not measured with respect to the monitor microphone position, but the monitor microphone port is the closest observation point of the source waveform. Whatever is observed downstream from the monitor microphone is due to the waveform observed there, or some phenomenon downstream, and is not due to the transmit system. Valid, reliable experimental results depend on the accuracy of the receive system.

Getting a desired waveform at the monitor microphone location is not a trivial problem. Once a desired waveform is produced, it also has to be stable and reproducible. A desirable waveform is an acceptable approximation of a pure tone. If the second harmonic of a tone is at least 20 dB smaller in amplitude than the fundamental, the waveform of the tone is deemed satisfactory. Before a wave propagates to the monitor microphone location, it experiences distortion from three sources:

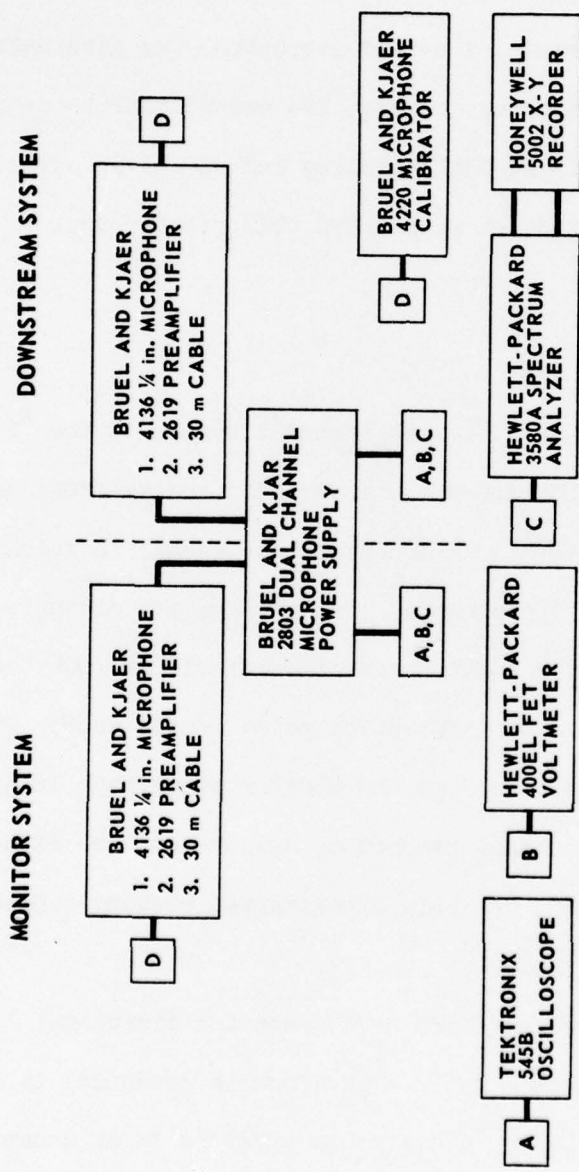


FIGURE 4.5
BLOCK DIAGRAM OF RECEIVE SYSTEM

(1) distortion in the transmitting electronics, (2) distortion in the drivers, and (3) finite amplitude distortion with propagation. For these reasons pure tones are very difficult to produce at the levels necessary for finite amplitude research. For the experiments reported in Chapter V, in all cases, the second harmonic was more than 35 dB down from the fundamental in the electrical signals to the drivers. The requirement that the second harmonic be at least 20 dB down from the fundamental at the monitor microphone location was met in all of the experimental runs except one. In this run the pump had an amplitude of 149 dB and a frequency of 3.5 kHz and the second harmonic at the monitor was only 10 dB down from the fundamental. The JBL 375-H driver with an aluminum diaphragm was found to be prone to strong distortion at 3.5 kHz.

The amplitudes required from the drivers (especially the JBL 375-H driver with an aluminum diaphragm) in producing the desired acoustic signals often led to fatigue and eventual breakdown of the drivers. Evidence that a driver was experiencing an input overload was the inconstant output amplitude from the driver and the abnormally high second harmonic. A necessary safeguard to protect a driver was a quick blow fuse on the output of the amplifier which just barely permitted operation at the desired energy requirement. Another precaution was to use an input grounding switch on the input to the amplifiers. As an experiment progressed, the downstream microphone was moved to various locations to obtain waveforms as a function of propagation distance. The acoustic signal in the pipe was turned off when the microphone was moved. The signal to the drivers was quieted by grounding the input to the amplifiers, and therefore the amplifiers remained on during the numerous

microphone location changes. Before the input was either grounded or turned on, the amplitude of the input signal was decreased by at least 20 dB so that any transient caused by throwing the grounding switch would not be severe; large transients may cause the voice coil of a driver to exceed its maximum allowable outward excursion and may possibly damage the driver. The JBL 375-H driver failed in two ways. A fusible link to the voice coil melted (resulting in no response from the driver) or the voice coil assembly overheated and broke down (resulting in a burning phenolic odor from the driver mouth).

2. Plane Wave Pipe

In Chapter II it was shown that the major contributor to attenuation in the pipe was attenuation due to boundary layer effects (Eq. 2.37). Under normal experimental conditions (temperature 23°C, relative humidity 50%, and atmospheric pressure 752 mm Hg) the theoretical value of α_b is $3.60 \times 10^{-4} \sqrt{f}$ Np/m. Schaffer⁶ performed an experiment in the plane wave tube to measure α_b ; Fig. 4.6 is a plot of the results. The experimental value of α_b was found to be $3.37 \times 10^{-3} \sqrt{f} - 0.00558$ Np/m. In the theoretical work performed in this thesis, the experimental value of α_b is used.

The absorbing termination in the last section of pipe was critical in satisfying the progressive wave assumption, especially for the pump because of its large amplitude. A paper by Burns²⁸ served as the basis for an experimental study of various materials for, and shapes of, end terminations.²⁹ A tone burst scheme was used to evaluate different materials and shapes for the termination. Figure 4.7 is a plot of the data for the best all-purpose termination found. The plot is for a

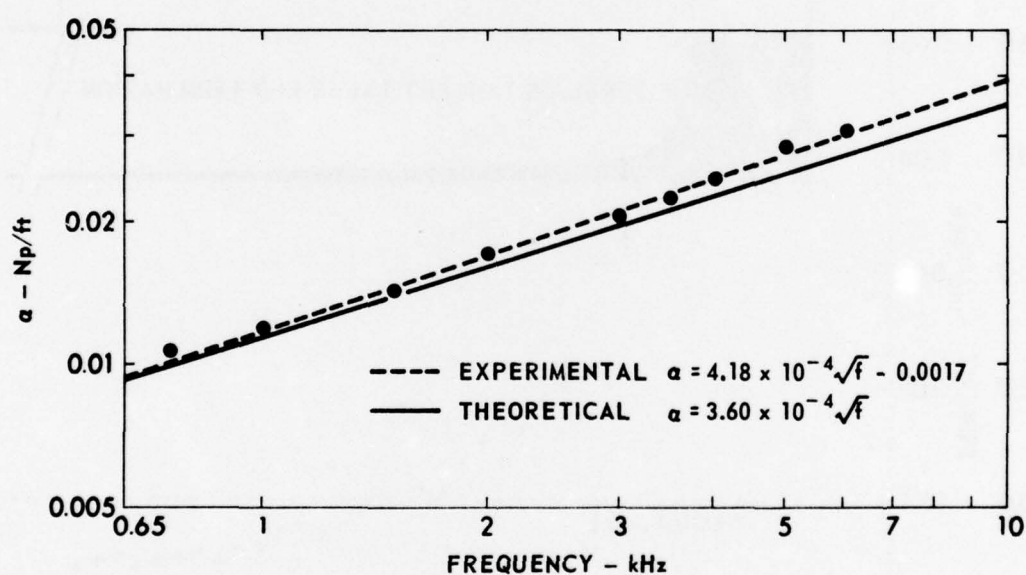


FIGURE 4.6
COMPARISON OF KIRCHHOFF ATTENUATION THEORY WITH OBSERVED DATA

(Taken from Schaffer⁶)

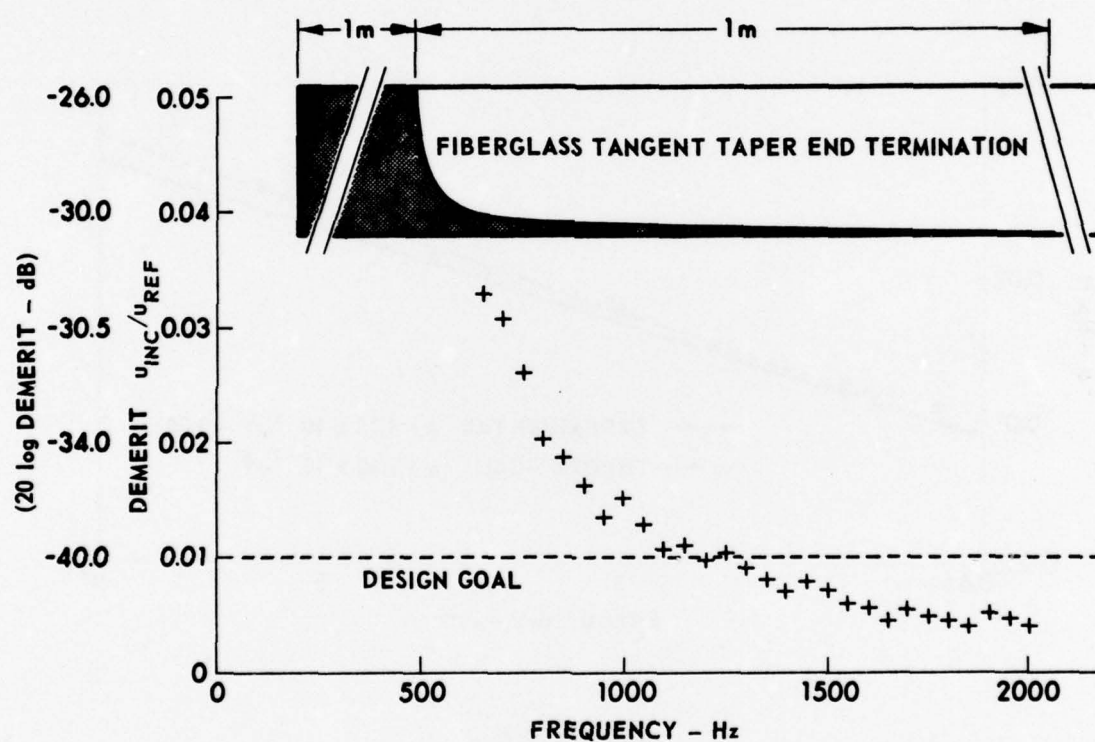


FIGURE 4.7
DEMERIT OF THE FIBERGLASS TANGENT TAPER
AND INSERT OF TANGENT TAPER IN PIPE

tangent taper termination made of fiberglass insulation material; the termination consisted of a meter long tangent taper section followed by a solid cylindrical section (see the insert in the figure). Frequency is plotted along the abscissa, and the demerit or reflection coefficient is plotted along the ordinate in the plot. Demerit is defined as the ratio of the amplitude of the reflected signal to that of the incident signal; the corresponding decrease in decibels of the reflected signal is written next to the demerit values. A demerit of 0.01 was the design goal (the dashed line in the figure); the fiberglass tangent taper provided a demerit of at least 0.01 for frequencies above 1250 Hz. In all the experimental runs the frequency of the pump was greater than 1250 Hz.

This thesis concerns the interaction of plane waves; under what conditions is the propagation of acoustic signals in a pipe planar? Planar propagation in pipes and ducts is certain only for frequencies below a cutoff frequency. The cutoff frequency for the various propagation modes in a circular tube of radius r is expressed by

$$f_{mn} = \frac{D_{mn} c_0}{2\pi r} \quad ,$$

where D_{mn} is the n th root of the following equation:

$$J_m'(D_{mn}) = 0 \quad .$$

The lowest cutoff frequency is the one for $m=1$, $n=0$. This frequency is 3960 Hz for the tube used in the experiments reported here. A signal of frequency greater than 3960 Hz will not necessarily propagate in a non-planar mode, and it was generally found that experiments with primary

frequencies above the lowest cutoff were run apparently without stimulating nonplanar modes. If a fundamental undergoes planar propagation, the higher harmonics of the fundamental that have frequencies greater than the lowest cutoff frequency will nevertheless also tend to have planar propagation, because the higher harmonics are produced by the propagation of the fundamental. The exception to this condition is provided by irregularities in the pipe, such as a poor flange connection and a protruding microphone or plug, which create a boundary condition different from the original one. These new boundary conditions require different modes of propagation of the signal to satisfy them. Thus, the pipe irregularities scatter energy out of the plane wave mode into higher order modes. If the irregularities are small, the amount of energy lost from the plane wave mode is small.

The actual propagation distances corresponding to the microphone locations are listed in Table 4.1.

TABLE 4.1

DISTANCES FROM SOURCES TO MICROPHONE
MEASURING LOCATIONS IN METERS

MIKE STATION	MONITOR	1	2	3	4	5	6	7
SINGLE YOKE	0.5	4.2	7.9	11.6	15.3	19.0	22.8	26.5
DOUBLE YOKE	0.1	3.8	7.6	11.3	15.0	18.7	22.4	26.1

The propagation distances are measured with respect to the finite amplitude producing drivers. When the single yoke was used, the propagation

distances were measured with respect to the face of the driver producing the pump signal. The propagation distances for the three-driver pump source (the double yoke) were measured with respect to the point of the yoke where the three individual pump signals merged. The source amplitudes for the two signals (pump and weak signal) were obtained through interpolation (by the use of the Fubini solution or small-signal theory) of their amplitudes observed at the monitor microphone location.

3. The Receive System

The receive system, treated as a single unit, was tested for distortion of the received signals and needed to be calibrated. The distortion test proceeded as follows. The microphone cartridge was removed from the preamplifier of the B&K 1/4 in. microphone. Two electrical signals of equivalent frequency and amplitude as produced in an experimental run were introduced to the preamplifier through an electronic signal summer. The spectrum of the signal produced was viewed on the spectrum analyzer for intermodulation distortion components located at frequencies where sidebands of the acoustical interaction would be. The results for the equivalent input of a signal of 4.5 kHz at a SPL of 150 dB and a signal of 1 kHz at a SPL of 110 dB were that no intermodulation distortion component had an amplitude larger than 70 dB. Since the amplitude of the sidebands recorded during an experiment were usually around 100 dB, they were therefore not produced in the receive system. This distortion test checked the distortion of the complete receive system except for the B&K microphone cartridge. It was believed that the distortion caused by the cartridge would be smaller than the distortion caused by the rest of the system. The calibration of the system was begun

by calibrating the spectrum analyzer, according to its manual, for frequency and amplitude response. The second part of the procedure was to calibrate the entire system with the B&K pistonphone. The receive system was calibrated before and after every experimental run.

CHAPTER V

COMPARISON OF EXPERIMENTAL RESULTS AND THEORETICAL PREDICTIONS

A representative sample of the experimental results for Case II are presented here and compared to the theory developed in Chapter II. For the weak signal the experiments covered a range of source SPL from 104 to 121 dB and a frequency range from 0.6 to 1 kHz. The corresponding ranges for the pump were 125 to 158 dB and 1.5 to 6.6 kHz, respectively. The measurement distances ranged from 3.9 m to 27 m. The largest value of σ_p for which a measurement was made was 30. A total of 25 independent experiments were run. Because of the similarity and conformity of the results, only three of the experimental runs are presented here. No experimental waveforms are presented. The relative amplitudes of the weak signal and the pump were such that the width of the oscillogram trace overshadowed the modulation of the pump by the weak signal (the modulation may be seen in the theoretical predictions, Figs. 1.2 and 3.5).

An example spectrum of an experimental waveform is shown in Fig. 5.1. Spectra for u_w' , u_p' , and u are shown in plots (a), (b), and (c), respectively. The ordinates are SPL and the abscissas are frequency. The values of the indices above a component identify its relative frequency (or its $u_{m,n}$ representation). The notation is that presented in Chapter II. Some components are the result of degeneracy, i.e., the addition of two or more components whose frequencies are the same. Distortion of the weak signal may be seen in plot (a) (the second harmonic of the weak signal is 26 dB down from the weak signal). The "spurious"

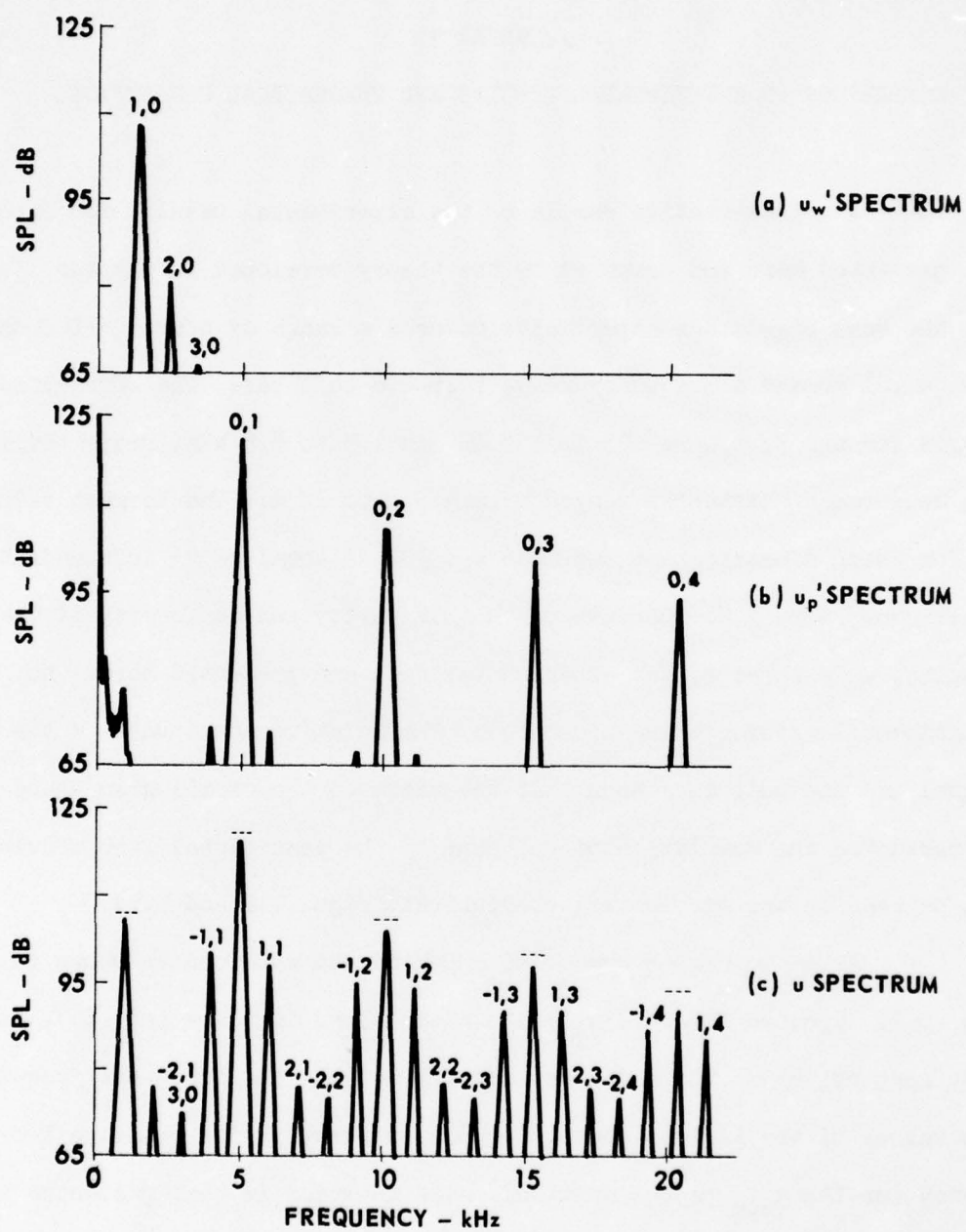


FIGURE 5.1
EXAMPLE SPECTRUM OF EXPERIMENTAL WAVEFORM

SOURCE $SPL_w = 118$ dB, $f_w = 1$ kHz

SOURCE $SPL_p = 146$ dB, $f_p = 5$ kHz

$X = 26.2$ m

weak signal and sidebands in plot (b), which should be the spectrum of the pump signal by itself, are caused by the presence of the weak signal in the signal to the pump drivers. The weak signal leaked into the pump transmit system even though the input to the weak signal amplifier was grounded. Leakage of the pump signal was avoided in plot (a) by grounding the input of the pump amplifier and disconnecting the pump signal from the grounding switch. The sidebands are caused by the interaction of the weak signal and its harmonics with the pump and its harmonics. The $-1,1$ component is the first lower sideband and the $1,1$ component is the first upper sideband. The dashed lines above the $1,0$ and $0,n$ components in plot (c) represent the SPL of the corresponding components in the other two plots. The difference between the dashed line and the amplitude of the components in plot (c) is 1 dB, 1 dB, 1.5 dB, 2.2 dB, and 3.2 dB for the components $1,0$ and $0,n$ ($n=1,2,3,4$), respectively. Little decrease of the weak signal is observed, but the pump and its harmonics are definitely reduced. The higher the harmonic of the pump, the larger the difference in SPL of the harmonic in plots (c) and (b); this trend was predicted in Chapter II (Eq. 2.26). The difference between the two SPLs is a measure of the amount of energy redistributed from the harmonics to the sideband formation.

Figure 5.2 shows a comparison of predictions and measurements for an experiment in which the source conditions were as follows:

$$\text{SPL}_p = 140 \text{ dB}, \text{SPL}_w = 115 \text{ dB}, f_p = 1.5 \text{ kHz}, \text{ and } f_w = 1 \text{ kHz}.$$

The changes in SPL of the weak signal ($u_{1,0}$), the first lower sideband ($u_{-1,1}$), the pump ($u_{0,1}$), and the first upper sideband ($u_{1,1}$) as a

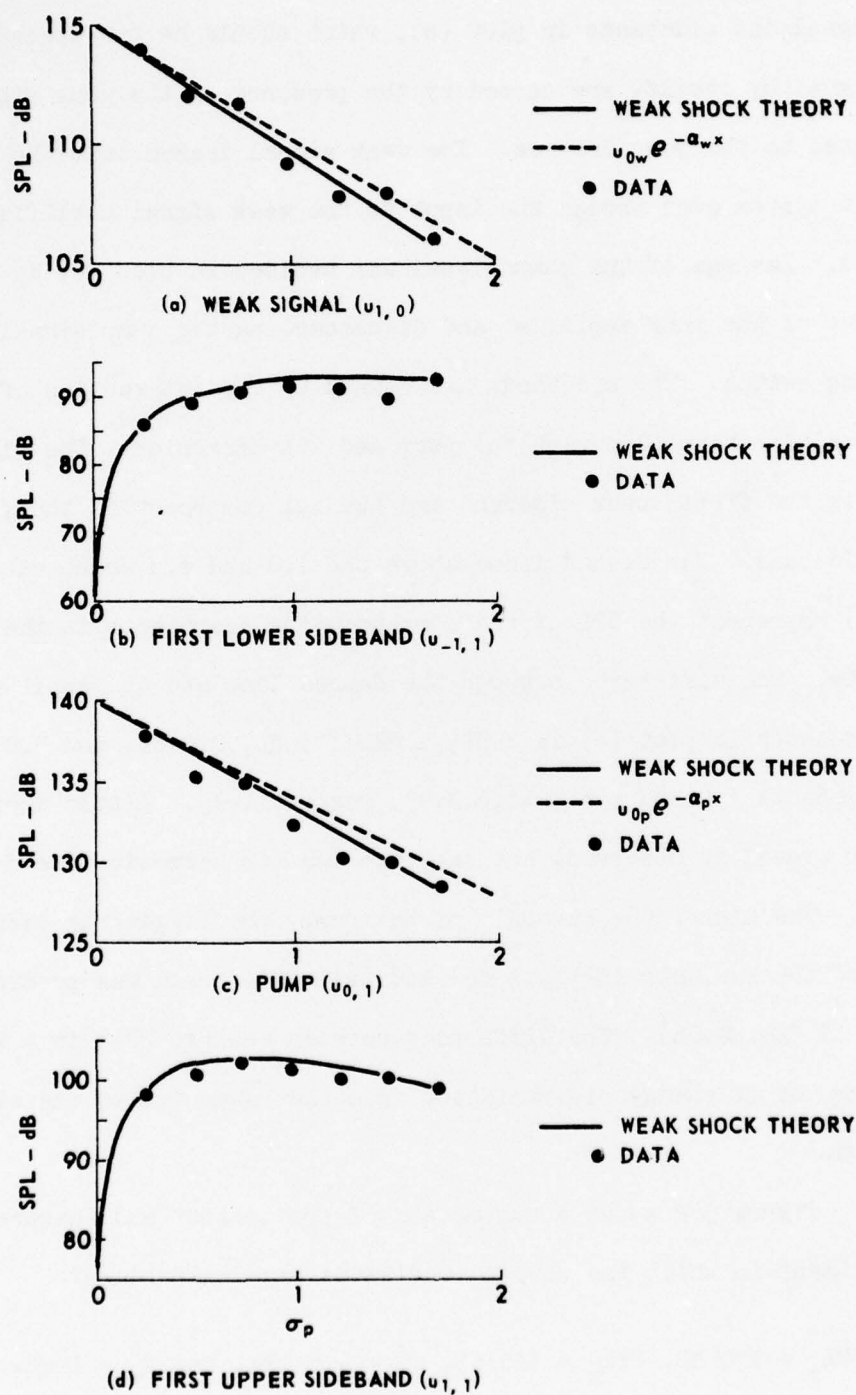


FIGURE 5.2
COMPARISON OF EXPERIMENTAL DATA WITH THEORY
SOURCE $SPL_w = 115$ dB, $f_w = 1.0$ kHz
SOURCE $SPL_p = 140$ dB, $f_p = 1.5$ kHz

function of σ_p are shown in plots (a), (b), (c), and (d), respectively. In plots (a) and (c) the dashed lines represent the decrease of the respective components based on small-signal absorption. The difference between the small-signal predictions and the weak shock theory predictions for the weak signal represents the suppression of the weak signal. In the case of the pump [plot (c)] the difference primarily represents the excess attenuation caused by the finite amplitude distortion of the pump itself. The particular experimental run shown in Fig. 5.2 is a little unusual because the first lower sideband is to the left of the weak signal in the frequency domain. The two primaries were chosen close in frequency so that the value of Ω would be near one. In Chapter II, in the analysis of the Case II preshock solutions, it was observed that the greatest predicted suppression of the weak signal occurs when Ω has a value of one. The agreement between theory and experiment is good; the standard deviation of the data about the theoretical curve has a value of 0.7 dB. Only 0.8 dB of suppression of the weak signal was achieved. The first upper sideband grows more rapidly and is larger than the first lower sideband. Such an asymmetry agrees with the theoretical predictions in Chapter II.

Figure 5.3 shows the comparison of predictions and measurements for an experiment with a smaller value of Ω . The source conditions were as follows:

$$\text{SPL}_p = 144 \text{ dB}, \text{SPL}_w = 113 \text{ dB}, f_p = 2.5 \text{ kHz}, \text{ and } f_w = 1 \text{ kHz}.$$

The weak signal does not undergo much suppression and, in fact, the suppression seems to taper off at approximately 1 dB, around $\sigma_p = 2$. From that point on, the predicted decrease in the weak signal parallels the

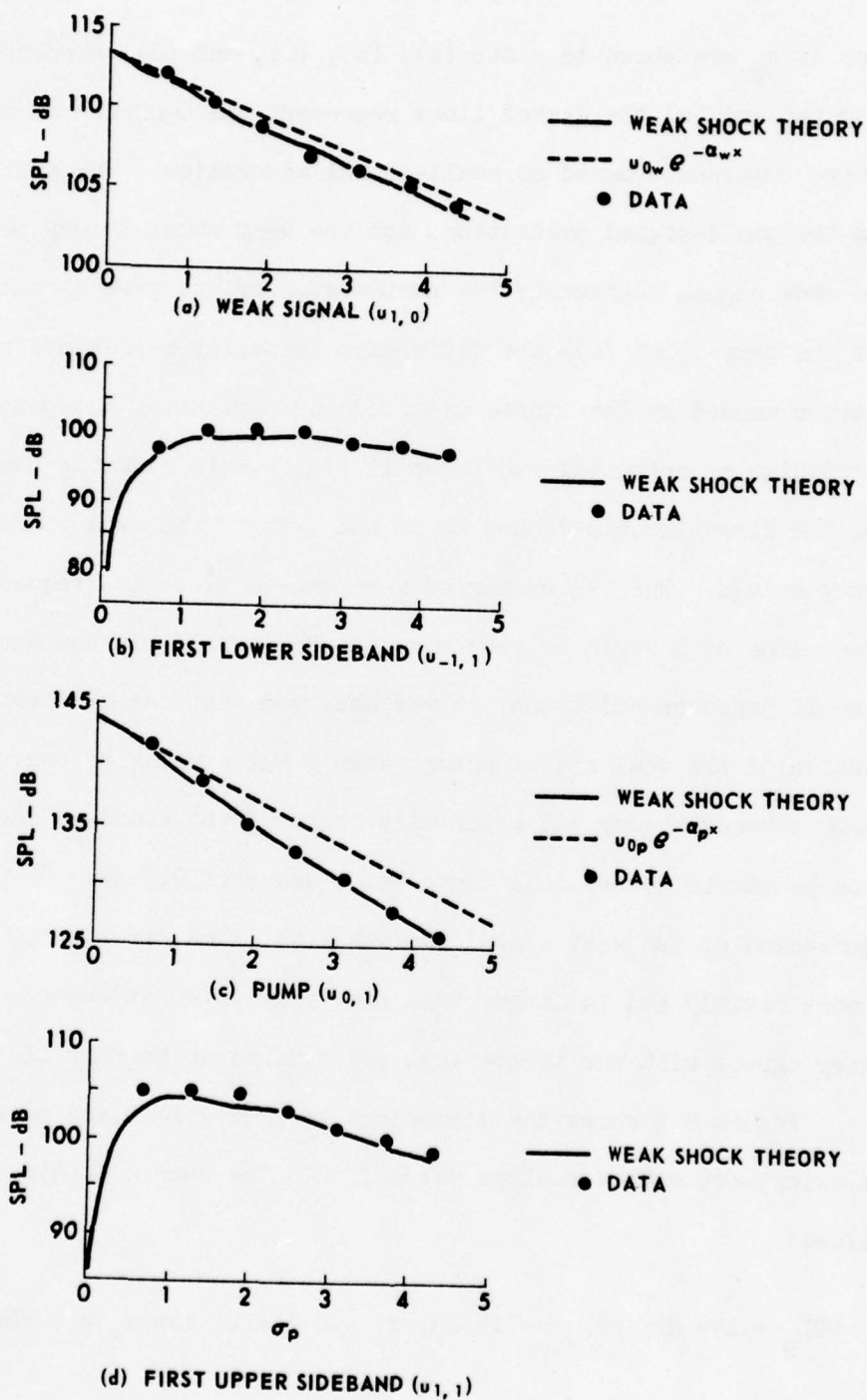


FIGURE 5.3
COMPARISON OF EXPERIMENTAL DATA WITH THEORY

SOURCE $SPL_w = 113$ dB, $f_w = 1.0$ kHz

SOURCE $SPL_p = 144$ dB, $f_p = 2.5$ kHz

linear theory curve. The agreement between theory and experiment is in general better than for the previous experiment; the standard deviation of the data about the theoretical curve is equal to 0.5 dB. Again the first upper sideband is seen to grow more rapidly and to be larger in amplitude than the first lower sideband. At the larger values of σ_p , however, the greater attenuation of the higher frequency sideband has its effect and the first lower sideband becomes the larger one. The squiggle in the weak shock theory curves is partially due to the polynomial fit performed in program GRAPH.

The majority of the experimental results and theoretical predictions were similar to Figs. 5.2 and 5.3; an exception is shown in Fig. 5.4. In this example (which shows the smallest value of Ω) the source conditions were:

$$\text{SPL}_p = 145 \text{ dB}, \text{SPL}_w = 114 \text{ dB}, f_p = 4 \text{ kHz}, \text{ and } f_w = 1 \text{ kHz}.$$

What sets this particular experimental run apart is the fact that the weak signal undergoes amplification (relative to the small-signal prediction) rather than suppression. The enhancement of the weak signal (approximately 1 dB) appears to occur between the values $\sigma_p = 1$ and $\sigma_p = 4$. Beyond the point $\sigma_p = 4$, the weak signal decays according to linear (small-signal) theory. The agreement between theory and experiment is good; the standard deviation of the data about the theoretical curve is equal to 0.7 dB. Again the upper sideband is more prominent at first; the lower sideband is more prominent later. An extensive experimental and theoretical investigation was undertaken to study the enhancement of the weak signal, but the results of the study were not conclusive. The theoretical work showed that,

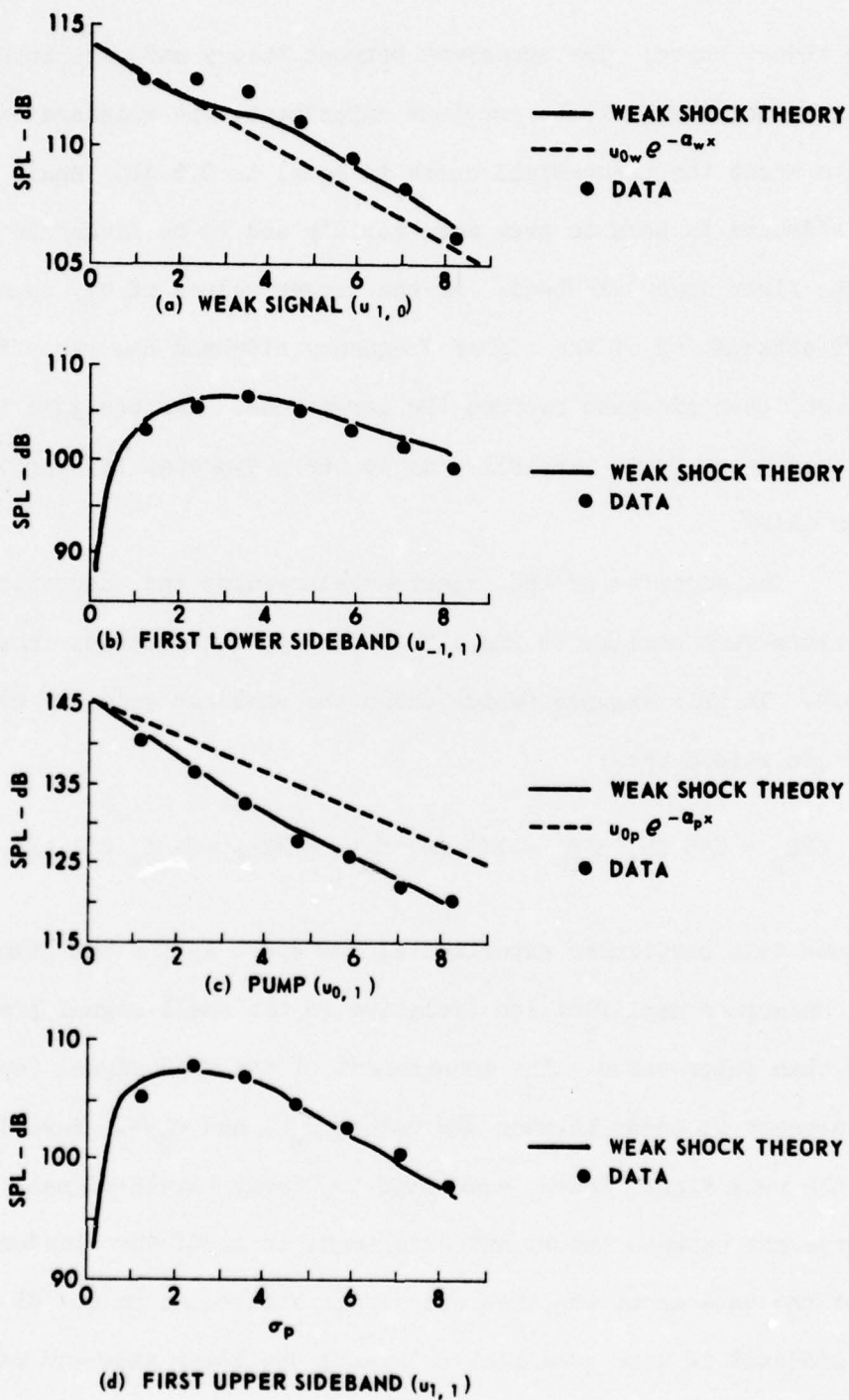


FIGURE 5.4
COMPARISON OF EXPERIMENTAL DATA WITH THEORY
SOURCE $SPL_w = 114$ dB, $f_w = 1.0$ kHz
SOURCE $SPL_p = 145$ dB, $f_p = 4.0$ kHz

whenever enhancement occurred, the pump frequency was a harmonic of the weak signal; the investigation also showed that this frequency condition was necessary but not sufficient. The predicted enhancement was amplitude dependent as well as frequency dependent. The experimental work was less edifying. No other experimental run demonstrated the enhancement of the weak signal to the degree seen in Fig. 5.4. Figure 5.4 is presented to show a result which was observed both experimentally and theoretically but which is not completely understood.

CHAPTER VI

CONCLUSIONS AND FINAL COMMENT

The purpose of this research has been to study the suppression of sound by sound of a higher frequency. More specifically, the planar propagation in air of a finite amplitude tone (the pump) and a smaller amplitude tone (the weak signal) of lower frequency has been investigated both theoretically and experimentally. A brief summary of the work completed and the conclusions drawn from those results follows.

Suppression is caused by a modulation of the weak signal by the pump. The acoustic energy of the weak signal is not lost (absorbed) but is rather redistributed to other parts of the spectrum. The amount of suppression depends qualitatively on whether the pump frequency is lower than the weak signal frequency (Case I) or vice versa (Case II). In Chapter II, Case I and Case II interactions were reviewed and compared. A general notation was introduced so that the various formulas could be used for either Case I or Case II. The exact solution valid before shock formation was reviewed, both for the time domain (Earnshaw solution) and for the frequency domain (Fenlon solution). A convenient way of writing Fenlon's solution was given. Various approximate solutions were formed from the exact solutions and compared with each other; analysis of these solutions led to many conclusions. Suppression before shock formation in Case I may easily exceed 40 dB, but for Case II suppression may never exceed 2.4 dB and in most practical cases is much less. The modulation process that causes suppression also leads to the formation of sidebands

about the high frequency signal. The primary energy source for the sideband formation in both Case I and Case II was observed to be the higher frequency signal and its harmonics, if any. In Case II, it was observed that the higher the harmonic of the pump, the greater the harmonic's amplitude is decreased in the interaction. The first upper sideband grows more rapidly (at least at first) and is larger than the first lower sideband.

Theoretical predictions valid beyond the shock formation distance were obtained. Included in these predictions are the effects of small-signal attenuation and dispersion. Weak shock theory, cast in difference equation form, was used to obtain the predictions. In Chapter III the difference equations were implemented in a computer algorithm. The computer program, referred to as program C500, incorporates attenuation and dispersion.

The agreement between the experimental results and the theoretical predictions shown in Chapter V was excellent and, in general, supported the conclusions drawn from the preshock solutions. The experiments, which were for Case II only, showed little suppression of the weak signal; the maximum suppression observed was about 1 dB. The suppression of the weak signal occurred at relatively small values of σ_p (σ_p is the shock formation distance of the pump); for values of σ_p approximately equal to 3, the suppression process halted and the weak signal propagated thereafter according to linear theory. The first upper sidebands were observed to be more prominent than the first lower sidebands for small values of σ_p but, because of absorption, for larger values of σ_p the lower sidebands were more prominent. In some cases the weak signal became

enhanced (relatively) rather than suppressed. Enhancement was observed both experimentally and theoretically; it appeared to occur when certain frequency and amplitude conditions were met by the primaries. In particular, the pump and weak signal had to be harmonically related. With the primaries so related, degeneracy occurs. Thus the enhancement may have been caused by the presence of sidebands equal in frequency to that of the weak signal.

The primary task undertaken, the investigation of Case II, was accomplished. The conclusion is that little suppression of a weak signal by a higher frequency pump is possible, before or after shock formation. It has been firmly established here that if large suppression of a tone is desired, the suppression may only be obtained through a Case I interaction, even though the Case II interaction is more attractive in respect to harmonic and sideband "pollution." The computer programs developed to implement the theoretical investigation of Case II are applicable for other purposes. The computer programs may easily be adapted to other types of propagation (spherical or cylindrical) and to other forms of attenuation (atmospheric or underwater).

The present work completed, what is the next step? A logical extension of the work presented here is the substitution of noise, either narrowband or wideband, for one or both of the two acoustic signals. The work with tones would seem to indicate that the most efficient way to suppress a band of noise would be a Case I interaction with a lower frequency pump. The theoretical work in this case could then be restricted to shock-free regions. The preshock solutions are, in general, easier to

apply than the postshock solutions. In any case, however, the application to suppression of random noise is not a trivial theoretical problem. Some work involving noise has already been done. Pestorius⁸ has studied the propagation of wideband finite amplitude noise (no tones present). Some theoretical work on the interaction of noise with a tone has been reported by Rudenko, Soluyan, and Khokhlov.³⁰ Work is presently being done at ARL on the interaction of a finite amplitude tone and a bandpass of noise (Ref. 26).

APPENDIX A
LISTINGS OF PROGRAM C500 AND
SUBROUTINES USED BY PROGRAM C500

```

PROGRAM C500
COMMON T(4200),U(4200),FT(1800)
DIMENSION JX(4200),LU(412)
EQUIVALENCE(U,JX)
REAL MAX1,MAX2
C*****
C THIS IS PROGRAM C500 WHICH PROPAGATES AN INPUT WAVEFORM BY INCRE
C MENTAL STEPS TO A DESIRED DISTANCE USING WEAK SHOCK THEORY. A11
C ENUTATION AND DISPERSION ARE APPLIED, FOR A DETAILED EXPLANATION
C SEE ARL-TR-77-8 BY RILL WILLSHIRE. THE FOLLOWING IS A LIST OF
C THE IMPORTANT PROGRAM PARAMETERS.
C A-SPL OF SMALL SIGNAL RE .00002 NT/MZ
C F1-FREQUENCY OF SMALL SIGNAL
C F2-SPL OF HIGH FREQUENCY PUMP
C F2- FREQUENCY OF PUMP
C DISTANCE- DESIRED PROPAGATION DISTANCE
C DISINC- INCREMENTAL PROPAGATION DISTANCE
C NEXP2- THE NO. OF ELEMENTS IN U AND T ARRAYS * 2**NEXP2
C FMAX- FREQUENCY OF LAST FOURIER COEFF. CALCULATED BY FFT
C SCAL- USED TO SCALE U ARRAY BEFORE FFT
C U- PARTICLE VELOCITY ARRAY
C T- CORRESPONDING TIME ARRAY
C USCAL=SCAL, USED FOR INITIALIZATION
C F2U=MAX, USED FOR INITIALIZATION
C NATDIS=NO OF PROP. STEPS BETWEEN ATEN AND DISPER CORRECTIONS *
C NATDIS=NDISTORS
C NATDIS=NATDIS, USED FOR INITIALIZATION
C NEXP2=NEXP2, THE NO OF ELEMENTS IN U AND T ARRAYS INITIALLY
C NPOINTS- NO OF ELEMENTS IN U AND T AFTER CALL TO SUB. WAVEPROP
C MPOINTS- USED TO INITIAL. NPOINTS WHEN ATT=DISP. NOT APPLIED
C LPOINTS- USED TO INITIAL. NPOINTS WHEN ATT=DIS NOT APPLIED
C NEXP2/2
C NEXP2/2 * IS THE NO. OF FOURIER COEFFS. CALCULATED BY FFT
C NPD=NO OF PUMP WAVELENGTHS IN INITIAL U ARRAY
C DELT- ORIGINAL WAVEFORM INCREMENT
C NOOL- NO OF ZEROS IN RIGHT ZERO BUFFER
C NOOL= NO OF ZEROS IN LEFT ZERO BUFFER
C NMO=NOOL+1, FIRST NON-ZERO ELE. IN U ARRAY
C NMO=NPOINTS+NOOL, LAST NON-ZERO ELE. IN U ARRAY
C NMO=NMO+1, FIRST ZERO ELE. IN RIGHT ZERO BUFFER
C NMO=NMO+NOOL, LAST ZERO ELE. IN U ARRAY IN RIGHT ZERO BUFFER
C NDISTORS= NO OF INCRE. PROP. STEPS PERFORMED BY ONE CALL TO
C SUBROUTINE WAVEPROP
C NO-NO OF CALLS TO WAVEPROP TO REACH DESIRED PROP. DISTANCE
C*****
250 READ 250,A,F1,F2,THETA
FORMAT(SF,2)
260 REAU 260,DISTANCE,DISINC,NEXP2
FORMAT(2F,2,IS)
270 REAU 270,FMAX,SCAL
FORMAT(2F16,4)
P1=J1+15
C*****
C AMP OF TONES CAST INTO PARTICLE VEL. FROM SPL RE .00002 NT/MZ
C*****
AA=(.0000000002)*10.**(A/20.)
BB=(.0000000002)*10.**(B/20.)
USCAL=SCAL
F2U=MAX
NATDIS=2
NDISTORS=2
MATDIS=NATDIS
NPOINTS=NEXP2
NEXP2=NEXP2
LPOINTS=NPOINTS
NMO=NMO/2
NMO=NMO/2+1
NPD=NPD*(N-1)/(2*FMAX)
PRINT 46,NPD
47 FORMAT( * NPD = *,110)
DELT=NPD/(F2*(NPOINTS-1))
NOOL=15
NMO=NOOL+1
NMO=NPOINTS+NOOL
NMO=NPOINTS+1+NOOL
NMO=NPOINTS+NOOL+NOOL
C*****
C DL 101 CREATES LEFT ZERO BUFFER
C*****
DO 101 J=1,NOOL
U(J)=0.
T(J)=J*DELT-DELT
101 CONTINUE
C*****
C DL 100 CREATES INITIAL WAVEFORM
C*****
DO 100 J=NMO,NEND
RUNT=(J-101)*DELT-DELT
RUNT=(J-101)*DELT-DELT
U(J)=AA*SIN(2*PI*F1*RUNT)-BB*SIN(2*PI*F2*RUNT+THETA)
T(J)=RUNT
100 CONTINUE
NMO=NMO+1
C*****
C DL 102 CREATES RIGHT ZERO BUFFER
C*****
DO 102 J=NMO,NEND
RUNT=(J-101)*DELT-DELT
RUNT=(J-101)*DELT-DELT
U(J)=0.
T(J)=RUNT
102 CONTINUE
CALL STORE(1,3,T,PAU,47)
CALL DISKWAIT
ZDISTANCE=(DISINC*NDISTORS)
NOI=ROUND(Z)
PRINT 5003,NOI
5003 FORMAT( * THE NUMBER OF DISINC = *,110)
DISTANCE=U.

FMAX=20000.
WRITE(12) A,F1,F2,THETA,DISTANCE,DISINC,NPD,FMAX,NOI
LPRINTS=NDISTORS
C*****
C DL 1016 IS THE MAJOR LOOP OF C500. EACH COMPLETION OF THE
C LOOP COMPLETES NDISTORS INCRE. PROP. STEPS.
C*****
DO 1016 I=1,NOI
DISTANCE=DISTANCE+DISINC*NDISTORS
CALL FFTCH(1,3,T,PAU,47)
CALL FFTCH(1,3,T,PAU,47)
CALL DISKWAIT
SCAL=USCAL
SIG=1.00000002*PI*F2*DISTANCE/(3*0.340.)
NPOINTS=NPOINTS
C*****
C SUB WAVEPROP PROPAGATES THE WAVEFORM VIA WEAK SHOCK THEORY
C*****
CALL WAVEPROP(U,T,DISTANCE,DISINC,NPOINTS,NDISTORS)
NPOINTS=NPOINTS
CALL STORE(1,3,T,PAU,47)
CALL DISKWAIT
C*****
C SUR TIME FRE REMOVES THE ZERO BUFFERS AND PERFORMS A FFT
C*****
CALL TIMEFRE(U,T,NPOINTS,N,NEXP2,IX,SCAL,NM,ITOT,THAX,LU,II,SIG,
CHARIF,IT,AREND)
C*****
C SUR WANGEN2 APPLIES A HANNING DATA WINDOW TO THE SPECTRUM OF THE
C INTERMEDIATE WAVEFORM
C*****
CALL WANGEN2(N,IX)
2227 SCAL=SCAL*U*FLOCAT(ITOT)
C*****
C DL 20 SCALES THE SPECTRUM COMPONENTS TO ABSOLUTE VALUES
C*****
DO 20 L=1,N
JX=L-L
U(J)=IX(J)/(IN*SCAL)
20 CONTINUE
SHOR=U(2)
C*****
C DL 315 CALCULATES THE FOURIER COEFFICIENTS
C*****
DO 315 I=2,NM
J2=I-1+1
J2=J2+1
AMP=SQRT(U(J)*U(J)+U(JJ)*U(JJ))
IF(AMP.EQ.0.) GO TO 880
U(I)=20.*ALOG10((415*AMP)/(1.00002*(1.414)))
GO TO 880
880 U(I)=0.
890 CONTINUE
IF(U(I).LT.0.0) U(I)=0.0
315 CONTINUE
IF(U(I).EQ.0.) GO TO 891
U(I)=20.*ALOG10(415*ABS(U(I))/(1.414*.00002))
GO TO 892
891 U(I)=0.
892 CONTINUE
IF(U(I).LT.0.0) U(I)=0.0
IF(SHOR.EQ.0.) GO TO 893
U(NM)=20.*ALOG10(415*ABS(SHOR)/(1.414*.00002))
GO TO 894
893 U(NM)=0.
894 CONTINUE
IF(U(NM).LT.0.0) U(NM)=0.0
C*****
C DL 888 CALCULATES THE FREQUENCIES OF THE FOURIER COEFFICIENTS
C*****
DO 888 J=1,NMI
T(J)=(J-1)/THAX
888 CONTINUE
ILM=1
C*****
C DL 5 SELECTS THE MAXIMUM FOURIER COEFF. AND FINDS CORRECTED
C VALUES FOR THE AMPLITUDE AND FOR THE FREQUENCY OF THE COEFF
C*****
DO 5 I=2,NMI
IF(U(I).GT.FMAX) GO TO 715
IF(U(I).LT.U(I-1)) GO TO 5
IF(U(I).LT.U(I-1)) GO TO 5
IF(U(I-1).GT.U(I+1)) GO TO 6
KATT=I
GO TO 7
6 KATT=I
7 CONTINUE
IF(KATT.LT.019*14
9 MAX2=U(I)
MAX1=U(I-1)
GO TO 11
14 MAX2=U(I-1)
MAX1=U(I)
11 CONTINUE
ILM=ILM+2
MAX2=U(0.**(MAX2/20.))
MAX1=U(0.**(MAX1/20.))
HUMAX1=MAX2
HUMAX2=MAX1
D=(2-NOI)/(1+NOI)
ALPHA=MAX1*PI*NOI*(1-NOI)/SIN(PI*NOI)
IF(KATT.LT.0) GO TO 45
U(I)=20.*ALOG10(ABS
P1=ILM+1-1+1)/THAX

```

```

      FT(1LW)=1.0/11
      GO TO 94
95  U(1)=20.*ALOG(0.1AB)
      FT(1LW)=(1-2.0)/TMAX
      FT(1LW)=U(1-1)
96  CONTINUE
97  CONTINUE
715 CONTINUE
      PRINT 701,11,1LW
701  FORMAT(10X,'THE INDEX IS =',15.0, 1LW =',15.0)
      WRITE(2) SIG,1LW,FT
      LPOINTS=NPOINTS
C*****
C  IF ATT-DIS ARE TO BE APPLIED DL B15 APPLIES THEM IF NOT CONTROL
C  RETURNS TO THE BEGINNING OF DL 8016
C*****
C  IF (11,NE,NATDIS) GO TO 8016
      CALL FETCH(1,U,1400,47)
      CALL DISKWAIT
      NPOINTS=NPOINTS
      NSCAL=SCAL
C*****
C  TIMEFRE REMOVES ZERO BUFFERS AND PERFORMS FFT ON WAVEFORM
C*****
      CALL TIMEFRE(U,T,NPOINTS,N,NEXPZ,1A,SCAL,NH,ITOT,TMAX,LU,11,SIG,
      CHAGIF,DT,NBEND)
C*****
C  DL B15 APPLIES ATTENUATION AND DISPERSION CORRECTIONS
C*****
      DO 815 1=2,NH
        J=2*(1-1)+1
        J2=J+1
        FRE=(1-1)/TMAX
        ARG=(.80137)*SQRT(FRE)-.005577)*NDISTONS*DISINC*NATDIS
        Z=1X(1)
        IX(J)=EXP(-ARG)*IX(J)*COS(ARG)+IX(J2)*SIN(ARG)
        IX(J2)=EXP(-ARG)*IX(J2)*COS(ARG)-Z*5SIN(ARG)
815  CONTINUE
      IX(1)=0
      IOP=ISC=0
C*****
C  PERFORMS BACKWARD FFT TO GET BACK INTO THE TIME DOMAIN
C*****
      ITOTR=IFFTDB(IX,NEXPZ,IOP,ISC,LU)
C*****
C  DL 816 SCALES WAVEFORM TO ABSOLUTE VALUES AFTER BACKWARD FFT
C*****
      DO 816 J=1,NH
        L=N*1-J
        U(L)=IX(L)/(NH*NSCAL*2.0**((ITOT-1)/1016))
816  CONTINUE
C*****
C  DL 818 SHIFTS ELE. OF U AND T FORWARD TO MAKE ROOM FOR LEFT
      ZERO BUFFER.
C*****
      DO 818 1=1,LH
        N1=NH-1
        N1=N1-NDOL
        U(N1)=U(N1)
        T(N1)=T(N1)+DT*(FLOAT(NDOL))
818  CONTINUE
C*****
C  DL 821 CREATES LEFT ZERO BUFFER
C*****
      DO 821 1=1,NDOL
        U(1)=0
        T(1)=(-1)*DT
821  CONTINUE
      LPOINTS=NPOINTS
      NBUFF=LPOINTS-NDOL
C*****
C  DL 817 CREATES RIGHT ZERO BUFFER
C*****
      DO 817 J=NHGO,NHEND
        U(J)=0
        T(J)=T(N1)+(J-NHGO)*DT
817  CONTINUE
      CALL STORE(1,U,1400,47)
      CALL STORE(1,T,1400,47)
      CALL DISKWAIT
      NATDIS=NATDIS
      LPOINTS=N*1016
8016 CONTINUE
      PRINT 1,SIG
      1  FORMAT(10X,'THE LAST SIGMA IS =',15.0)
      END

SUBROUTINE WAVEPROP(U,T,DISTANCE,DISINC,NPOINTS,NDISTONS)
  DIMENSION U(1),T(1)
  COMMON DUM(1200),TS(1200),DCS(1200)
C*****
C  SEE ARL 78-73 FOR DETAILS ON THIS SUBROUTINE
C*****
C*****
  WAVEPROP IS THE WAVE-SHOCK WAVE PROPAGATION ALGORITHM.
  *****
  CALL PARAMETERS ---
  U      -- U IS A REAL ONE DIMENSIONAL ARRAY DESCRIBING THE PARTIAL
          VELOCITY OF A POINT ON THE WAVE FORM IN EITHER ENGLISH
          OR METRIC UNITS. IF METRIC UNITS ARE USED CO, THE SMALL
          SIGNAL SPEED OF SOUND, MUST BE SUPPLIED IN METRIC UNITS.
  T      -- T IS A REAL ONE DIMENSIONAL ARRAY DESCRIBING THE TIME (IN
          SECONDS) COORDINATE FOR A PARTICULAR POINT ON THE WAVEFORM.
          THE DOUBLET ((11,T(1))) THEN DESCRIBES A WAVEFORM POINT
          IN THE PARTIAL VELOCITY-TIME PLANE.
  DISTANCE -- A REAL VARIABLE. IT IS THE DISTANCE OVER WHICH THE WAVE
          IS TO BE PROPAGATED.
  DISINC  -- A REAL VARIABLE. IT IS THE INCREMENTAL STEP SIZE USED TO
          COVER THE DISTANCE.
  NPOINTS -- AN INTEGER VARIABLE. IT IS THE NUMBER OF POINTS USED TO
          DESCRIBE THE WAVE FORM TO BE PROPAGATED.
  C  NDISTONS-- THE NUMBER OF INCREMENTAL STEPS PROPAGATED BY ONE
          CALL TO WAVEPROP.
  *****
  PERIOD = T(NPOINTS)
  R = 1.205
  CO=340.
  ETA = R/CO**2
  DISFACT=ETA*DISINC
  DO 140 NDISTUR=N,NDISTONS
    NS = NSHIFT + 0
    TLOW = T(1)-1.0
    C*****
    THIS LOOP TESTS FOR SHOCKS AND SHIFTS OUT POINTS
    IN THE DOUBLED VALUED REGION
    C*****
    DO 30 INDEX=N,NPOINTS
      NPOINT = INDEX-NSHIFT
      T(NPOINT)=T(INDEX)-U(INDEX)*DISFACT
      U(NPOINT)=U(INDEX)
      IF (T(NPOINT).GT,TLOW) GO TO 30
      TAVG = (T(NPOINT)+T(NPOINT-1))/2.0
      DO 10 I=1,NS
        IF (TAVG.LE-TS(I)) GO TO 20
        CONTINUE
        NS = NS+1
        TS(NS) = TAVG
        LOC(NS) = NPOINT
        GO TO 30
      NSHIFT = NSHIFT+NPOINT-LOC(NS)
      LOC = LOC(1)-1
      T(LOC)=T(NPOINT)
      U(LOC)=U(NPOINT)
      TS(1) = (T(NPOINT)+T(LOC))/2.0
      NS = 1
      IF (NS.GT,1199) GO TO 200
      GO TO 241
    200 PRINT 202
    202 FORMAT(10X,'NS IS TOO LARGE')
    201 CONTINUE
    30  TLOW = T(NPOINT)
        NPOINTS = NPOINTS-NSHIFT
        TLEFT = ANINT(T(1),T(NPOINTS))
        IF (TLEFT.LT,0.0) GO TO 50
        PRINT 150, DISTANCE,NDISTUR
        STOP
      TBIG = ANINT(T(1)+T(NPOINTS))
      IF (TBIG.GT,PERIOD) GO TO 70
      PRINT 160, DISTANCE,NDISTON
      STOP
      70  CONTINUE
          IFLAG = NSHIFT + 0
          TLOW = T(1)-1.0
          C*****
          THIS LOOP ADJUSTS VELOCITIES AT THE SHOCKS AND SHIFTS OUT POINTS
          IN THE OVERLAP REGION THAT OCCURS WHEN SHOCKS OVERTAKE
          C*****
          DO 130 INDEX=N,NPOINTS
            NPOINT = INDEX-NSHIFT
            T(NPOINT) = T(INDEX)
            U(NPOINT) = U(INDEX)
            IF (IFLAG.EQ,1) GO TO 100
            IF (T(NPOINT).GT,TLOW) GO TO 120
            TAVG = (T(NPOINT)+T(NPOINT-1))/2.0
            IFLAG = 1
            I = NPOINT-2
            GO TO 90
          I = I-1
          NSHIFT = NSHIFT+1
          T(1+2) = T(NPOINT)
          U(1+2) = U(NPOINT)
          90  IF (TAVG.LT,T(1)) GO TO 80
              U(1+1) = U(1)+U(1+2)-U(1)*((TAVG-T(1))/(T(1+1)-T(1)))
              T(1+1) = TAVG
              GO TO 130
            IF (T(NPOINT).LT,TAVG) GO TO 110
            U(NPOINT-1) = U(NPOINT-1)+U(NPOINT)-U(NPOINT-1)*((TAVG-
            (NPOINT-1))/(T(NPOINT)-T(NPOINT-1)))
            T(NPOINT-1) = TAVG
            IFLAG = 0
            GO TO 120
          110  NSHIFT = NSHIFT+1
              GO TO 130
            120  TLOW = T(NPOINT)
              CONTINUE
              NPOINTS = NPOINTS-NSHIFT
              RETURN
          C*****
          150  FORMAT(10X,'EXCEEDED TIME BASE TO THE LEFT',/,10X,
              S=DISTANCE**E15,S=10X,15X,ITERATIONS')
          160  FORMAT(10X,'EXCEEDED TIME BASE TO THE RIGHT',/,10X,
              S=DISTANCE**E15,S=10X,15X,ITERATIONS')
          END

```



```

SUBROUTINE TIMEPRE(U,T,NPOINTS,N,NEXP2,IX,SCAL,NH,ITOT,TMAX,LU,II)
CS10=HAFIO(OT,NBEND)
DIMENSION U(1),T(1),IX(1),LU(1)
DIMENSION HELP(513)
C*****
C
C SUB. TIMEPRE REMOVES THE ZERO BUFFERS FROM AN INTERMEDIATE
C WAVEFORM AND PERFORMS A FFT. THE ZERO BUFFERS ARE ALSO
C CHECKED TO SEE IF THEY STILL EXIST.
C*****
PRINT 251,NPOINTS
251 FORMAT(' NPOINTS = ',I10)
IF(UINBEND).NE.0.) GO TO 375
GO TO 376
375 CONTINUE
PRINT 378
378 FORMAT(' RIGHT ZERO BUFFER NOT LARGE ENOUGH')
STOP
376 CONTINUE
LETNPOINTS
C*****
C NL 266 REMOVES THE RIGHT ZERO BUFFER. LET IS EQUAL TO THE
C NUMBER OF ZEROS REMOVED.
C*****
DO 266 I=1,NPOINTS
J=NPOINTS+1-I
IF(U(J).EQ.0.) GO TO 267
GO TO 268
267 LET=LET+1
266 CONTINUE
268 LET=LET+1
LETNPOINTS=LET
PRINT 1001,LET
1001 FORMAT(' LET = ',I10)
LET=LET
IF(LU(1).NE.0.) GO TO 475
GO TO 38A
475 PRINT 476
476 FORMAT(' LEFT ZERO BUFFER NOT LARGE ENOUGH')
STOP
38A CONTINUE
MET=0
C*****
C NL 366 REMOVES THE LEFT ZERO BUFFER. MET IS EQUAL TO THE
C NUMBER OF ZEROS REMOVED.
C*****
DO 366 I=1,NPOINTS
IF(U(I).EQ.0.) GO TO 367
GO TO 368
367 MET=MET+1
366 CONTINUE
368 MET=MET+1
PRINT 3001,MET
3001 FORMAT(' MET = ',I10)
TNO=MET*(LET)-T(MET)
NPOINTS=LET-MET
LU=MET+1
TSLIDE=T(LUVE)
C*****
C
C NL 500 RENUMBERS THE ELE. IN THE U AND T ARRAYS AND MAINTAINS
C THE CORRECT TIME RELATIONSHIP BETWEEN THE U ELE.
C*****
DO 500 K=1,NPOINTS
L=K-MET
U(K)=U(L)
T(K)=T(L)-TSLIDE
500 CONTINUE
DT=(T(NPOINTS)-T(1))/(N-1)
C*****
C
C RESAMPLE PRODUCES N EQUALLY SPACED POINTS FROM THE NPOINTS
C UNEQUALLY SPACED POINTS OBTAINED FROM WAVEPROP.
C*****
CALL RESAMPLE(U,T,N,NPOINTS,DT,HELP)
TOP=ISC+0
TMAX=T(N)-T(1)
DT=TMAX/(N-1)
C*****
C
C NL 10 SCALES THE FLOATING PT. ELE. OF U BEFORE AN INTEGER FFT
C*****
DO 10 J=1,N
IX(J)=U(J)*SCAL
10 CONTINUE
C*****
C
C A FORWARD INTEGER FFT IS TAKEN ON THE WAVEFORM
C*****
ITOT=IFFTOP(IX,NEXP2,TOP,ISC,LU)
END

```

```

SUBROUTINE RESAMPLE(U,T,N,NPOINTS,DT,HELP)
DIMENSION U(1),T(1),HELP(1)
COMMON DIM(800),FT(1800)
C*****
C
C RESAMPLE PRODUCES N EQUALLY SPACED POINTS FROM THE NPOINTS
C UNEQUALLY SPACED POINTS OBTAINED FROM WAVEPROP.
C SEE APL TP-73-23 FOR DETAILS ON THIS SUBROUTINE
C*****
LCP=(N-2313)/2
NN=2
DO 430 I=1,N
TLIM=T(NN)
TT=(I-1)*DT
IF((TT-TLIM).LE.1.0E-12) GO TO 420
NN=NN+1
420 CONTINUE
IF(I.GT.1800) GO TO 445
FT(I)=(TT-T(NN-1))*U(NN)-U(NN-1)/(T(NN)-T(NN-1))*U(NN-1)
GO TO 430
445 CONTINUE
HELP(I-1800)=(TT-T(NN-1))*U(NN)-U(NN-1)/(T(NN)-T(NN-1))*U(NN-1)
GO TO 430
10 CONTINUE
CH=I/2
ICH=CH
ICH=2*ICH
RAT=ICH-1
IF(RAT.EQ.0.) GO TO 443
LM=(I-2313)/4
T(LM)=(TT-T(NN-1))*U(NN)-U(NN-1)/(T(NN)-T(NN-1))*U(NN-1)
GO TO 430
443 CONTINUE
ML=(I-2313)/2+1
U(ML)=(TT-T(NN-1))*U(NN)-U(NN-1)/(T(NN)-T(NN-1))*U(NN-1)
430 CONTINUE
DO 442 J=2313,4096,2
KIN=(J-2313)/2+1
U(J)=U(KIN)
442 CONTINUE
DO 441 J=2313,4095,2
JIN=(J-2313)/2
U(J)=U(JIN)
441 CONTINUE
DO 15 J=1801,2313
U(J)=HELP(J-1800)
15 CONTINUE
DO 447 J=1,1800
U(J)=FT(J)
447 CONTINUE
DO 448 L=1,N
TLIM=T(L)*DT
448 CONTINUE
GO TO 460
450 PRINT 470
PRINT 500,1
500 FORMAT(' ',I10)
STOP
460 RETURN
470 FORMAT('IM,10MNN EXCEEDED NPOINTS')
END

```

APPENDIX B
LISTINGS OF PROGRAM GRAPH

```

PROGRAM GRAPH
DIMENSION MIP(6)
DIMENSION FT(1000)
DIMENSION W(100)
DIMENSION AMP(6,200),SIGMA(6,200),YAMP(200),XSIGMA(200)
DIMENSION XP(55)
COMMON VFC(20,6)
C*****
C
PROGRAM GRAPH SELECTS CERTAIN FREQUENCY COMPONENTS FROM THE
SPECTRA FROM PROGRAM C500 AND PLOTS THE AMPLITUDES OF THE
FREQUENCY COMPONENTS ASSOCIATED TO A PARTICULAR FREQUENCY
VERSUS THE SIGMA OF THE PUMP OF EACH FREQUENCY COMPONENT.
FOR MORE EXPLANATION SEE AHL-TR-77-8. THE FOLLOWING IS A
LIST OF IMPORTANT PROGRAM PARAMETERS.
XYZ - THE BANDWIDTH OF THE NUMERICAL FILTER.
SIGMA - THE MAXIMUM SIGMA-2 TO BE PLOTTED.
SISCAL=SIGMA/5 -SCALING FACTOR FOR HON. AXIS.
DBGO -THE MIN. VALUE ON VERT. AXIS IN DB RE .00002 N/M
DBEND -THE MAX VALUE OF VERT AXIS IN DB RE 2*10**5N/M
UBSCAL=(DBEND-DBGO)/3-SCALING FACTOR FOR VERT. AXIS.
LPST -SPECTRAL NUMBER OF FIRST FRE. COMPONENT PLOT.
LPEND -SPECTRAL NO OF LAST FRE. COMPONENT PLOT.
NO -THE NO OF SPECTRA PASSED TO GRAPH BY C500.
MX -(MX=-4) NO OF FRE. COMP. FOUND FOR EACH SPECTRAL NO.
C*****
READ (2) A,F1,B,F2,THETA,DISTANCE,DISINC,NPD,FHAX,NO
PRINT 1000,F1,F2,NO
1000 FORMAT( * F1 = *F10.2* F2 = *F10.2* NO = *,I10)
FA=F2-F1
FB=F2-F1
XYZ=50.
SIGMA=50.
LPST=1
LPEND=6
DBGO=60.
DBEND=100.
SISCAL=SIGMA/5.
UBSCAL=(DBEND-DBGO)/3.
W(1)=F1
C*****
C
DL 6005 CALCULATES THE CENTER FRE. OF THE FILTER AND STORES
THFM IN THE W ARRAY.
C*****
DO 6005 J=3,50.3
W(J)=(J/3)*F2
W(J-1)=W(J)-F1
W(J+1)=W(J)+F1
IF (W(J+1).GT.FHAX) GO TO 6006
6005 CONTINUE
6006 LOT=J
M1=M2=M3=M4=0
C*****
C
DL 200 BEGINS THE FILTERING OF EACH SPECTRUM BY READING IT FROM
MAG TAPE.
C*****
DO 200 J=1,NO
JAY=1
READ (2) SIG,ILM,FT
IF (SIG.GT.SIGMA) GO TO 201
C*****
C
DL 100 IS THE ACTUAL NUMERICAL FILTER.
C*****
DO 100 I=1,ILM*2
101 CONTINUE
CHECK=ABS(W(JAY)-FT(I))
IF (CHECK.LT.XYZ) GO TO 203
IF (FT(I).LT.W(JAY)) GO TO 100
JAY=JAY+1
GO TO 101
203 CHECK2=ABS(W(JAY)-FT(I+2))
IF (CHECK2.LT.XYZ) GO TO 204
GO TO 205
204 IF (CHECK.LT.CHECK2) GO TO 206
GO TO 100
206 IF (FT(I+1).LT.FT(I+3)) GO TO 100
206 CONTINUE
IF (JAY.EQ.1) GO TO 210
IF (JAY.EQ.2) GO TO 211
IF (JAY.EQ.3) GO TO 213
M4=M4+1
MRUN=M4
GO TO 214
210 M1=M1+1
MRUN=M1
GO TO 214
211 M2=M2+1
MRUN=M2
GO TO 214
213 M3=M3+1
MRUN=M3
214 CONTINUE
AMP(JAY,MRUN)=FT(I+1)
SIGMA(JAY,MRUN)=SIG
JAY=JAY+1
IF (JAY.GT.5) GO TO 200
100 CONTINUE
200 CONTINUE
201 CONTINUE
C*****
C
DL 801 PLOTS THE DESIRED SPECTRAL NO. PLOTS.
C*****
DO 801 I=LPST,LPEND
IF (I.EQ.1) MRUN=M1
IF (I.EQ.2) MRUN=M2
IF (I.EQ.3) MRUN=M3
IF (I.EQ.4) MRUN=M4
LH=2*DBH
LRL=3*HSTG
CALL PLOT (6.5,-12.,*3)
CALL ORIGIN(1.,3,0)
CALL PLTARIS(0.,0.,5.,0.,0.0,SIGMA,1.,LRL,-3.5)
CALL PLTARIS(0.,0.,3.,90.,IRGO,DBEND,5.,LB,2*4)
C*****
C
DL 800 TRANSFERS THE PARTICULAR DATA OF ONE SPECTRAL NO. TO BE
PLOTTED TO THE PLOTTING ARRAYS.
C*****
DO 800 J=1,MRUN
VEC(J,2)=YAMP(J)*AMP(I,J)
VEC(J,1)=XSIGMA(J)*SIGMA(I,J)
800 CONTINUE
XBAR=GAMMA*TOL*0.
MM=MRUN
IVEC=200
KK=10
K3=KK*1
KIP=2
C*****
C
PERFORMS A POLYNOMIAL OF ORDER KK LEAST SQUARES BEST FIT ON THE
DATA TO BE PLOTTED.
C*****
CALL PFITLSO(IVEC,IVEC,XP,MM,KK,K3,KIP,XBAR,GAMMA,TOL,YAV,YBAR,
CYSO,YMAX)
DO 114 J=1,MRUN
YAMP(J)=VEC(J,5)
814 CONTINUE
PRINT 444,MRUN
444 FORMAT( * MRUN = *,I15)
CALL PLTDATA(XSIGMA,YAMP,MRUN,0.0,0.0,SISCAL,DBGO,UBSCAL,0.08)
CALL PLOT(0.0,0.0,3)
801 CONTINUE
END

```

APPENDIX C
LISTINGS OF PROGRAM TIMEPLOT


```

PROGRAM TIMEPLOT
DIMENSION T(4200),U(4200)
C*****
C
PROGRAM TIMEPLOT REMOVES THE LEFT ZERO BUFFERS FROM SELECTED
WAVEFORMS AND PLOTS THE FIRST PORTION OF THE SELECTED
WAVEFORMS. FOR MORE DETAIL SEE AML-77-8, THE
FOLLOWING IS A LIST OF IMPORTANT PROGRAM PARAMETERS.
NO- THE NO OF WAVEFORMS TO BE CONSIDERED.
IMOP- THE NO OF WAVEFORMS SKIPPED BETWEEN THE PLOTTED ONES IS
IMOP-1
MMOP=IMOP USED FOR INITIALIZATION.
TMAX=.002*.66 THE LENGTH OF THE PLOTTED PORTION OF THE WAVEFORM
TSCAL=TMAX/S SCALING FACTOR FOR HOR. AXIS.
TTC=.00004 SPACING IN SEC. ON HOR. AXIS TIC MARKS.
AMP=. MAX. PARTICLE VELOCITY IN M/S.
AMPSCL=2*AMP/2.5 SCALING FACTOR FOR VERT. AXIS.
IFNOT USED TO PRINT THE TIC SPACING AT THE BOTTOM OF THE PLOT
PAPER.
IFLIT- USED TO POSITION THE PLOTS ON THE PLOTTING PAPER.
C*****
C
NO=100
IMOP=66
MMOP=IMOP
TMAX=.002*.66
TSCAL=TMAX/S.
TTC=.00004
AMP=.
AMPSCL=2*AMP/2.5
IFNOT=5
HOR=0.
IFLIT=1
C*****
C
A ORIGIN IS ESTABLISHED ON THE PLOTTING PAPER.
C*****
C
CALL PLOT(0.,-12.,-3)
CALL ORIGIN(0.,0.)
C*****
C
NL 100 IS THE MAJOR LOOP OF THE PROGRAM. THE LOOP HEADS A
WAVEFORM FROM MAG TAPE AND DECIDES TO PLOT IT UN TO READ
ANOTHER ONE.
C*****
C
DO 100 I=1,NO
READ (3) T,U,N,I+1,SIG
IF (I+1.EQ.IMOP) GO TO 999
GO TO 100
999 CONTINUE
IMOP=IMOP+MMOP
C*****
C
NL 300 COUNTS THE ZEROS IN THE LEFT ZERO BUFFER. THE NO. OF
ZEROS EQUALS J-1.
C*****
C
DO 300 J=1,N
IF (U(J).EQ.0.) GO TO 308
GO TO 309
308 CONTINUE
309 CONTINUE
TSLIP=T(J)
NNON=J-1
C*****
C
NL 310 REMOVES THE LEFT ZERO BUFFER AND SLIPS THE TIME AXIS
BACKWARD BY TSLIP TO MAINTAIN THE ORIGINAL TIME RELATION-
SHIP BETWEEN THE ELES. OF THE U ARRAY.
C*****
C
DO 310 I=1,NN
NAN=J-1
U(I)=U(NAN)
T(I)=T(NAN)-TSLIP
310 CONTINUE
C*****
C
NL 555 SELECTS THE NO. OF U ELES. NECESSARY FOR A PLOT THAT
LONG.
C*****
C
DO 555 J=1,N
IF (TMAX+T(I)) GO TO 600
555 CONTINUE
600 CONTINUE
IF (IFLIT.EQ.1) GO TO 4
IF (IFLIT.EQ.2) GO TO 4
GO TO 6
4 CALL ORIGIN(7.,-7.)
IFLIT=2
GO TO 7
5 CALL ORIGIN(0.,3.5)
IFLIT=3
GO TO 7
6 CALL ORIGIN(0.,3.5)
IFLIT=1
7 CONTINUE
LW=3*AMP
LWL=4*TIME
CALL PLTARIS(0.,-1.25+2.5*00.-AMP,AMP,1.,LW,3,1)
CALL PLTARIS(0.,0.,0.,0.,0.,TMAX,TTC,LWL,4,0)
CALL PLDATA(T,U,0+0+0+0,TSCAL,0.,AMPSCL,0.00)
CALL PLOTLINE(3,-1.,4.,14+0.)
PRINT 33,I+1,SIG
33 FORMAT(1X,INDEX = 0,I4, SIGMA = 0,F6,3)
IF (IFNOT.EQ.3) GO TO 444
GO TO 100
888 CONTINUE
IFNOT=10
CALL PLOTLINE(3,-1.7.,14+0.)
PRINT 34,TTC
34 FORMAT(10,6,0 SECONDS BETWEEN TIC MARKS ON HOR. AXIS)
100 CONTINUE
END

```

APPENDIX D

ALTERNATE REPRESENTATION OF THE IMPROVED FM SOLUTION

The Earnshaw solution for the two-frequency boundary condition,

$$u(0,t) = u_{op} \sin \omega_p t + u_{ow} \sin \omega_w t, \quad (2.10)$$

is

$$u(x,t') = u_{op} \sin \omega_p \varphi + u_{ow} \sin \omega_w \varphi, \quad (2.11a)$$

where

$$\varphi = t' + \frac{\beta x}{c_o} \left(u_{op} \sin \omega_p \varphi + u_{ow} \sin \omega_w \varphi \right). \quad (2.11b)$$

The weak signal term of the Earnshaw solution is

$$u_w = u_{ow} \sin \omega_w \varphi. \quad (D.1)$$

The improved FM solution (Eq. 2.19, a time domain solution) was obtained from Eq. D.1 by using the following approximation of Eq. 2.11b,

$$\varphi = t' + \frac{\beta x}{c_o} u_{op} \sin \omega_p \varphi. \quad (2.16)$$

A dimensionless representation of Eqs. D.1 and 2.16 is used to derive a frequency domain representation for the improved FM solution. The weak signal term becomes

$$V_w = \sin \Omega \Phi, \quad (D.2)$$

where

$$V_w = \frac{u_w}{u_{ow}} \quad (D.3a)$$

and

$$\Phi = y + \sigma_p \sin \Phi \quad (D.3b)$$

with

$$y = \omega_p t' \quad . \quad (D.4)$$

Equation D.2 may also be represented as

$$V_w = \text{Im } e^{j\Omega\Phi} \quad , \quad (D.5)$$

if the imaginary part of the result at the end of the derivation is taken to equal V_w . The Laplace transform is taken from Eq. D.5,

$$\overline{V_w(s)} = \int_0^\infty V_w(y) e^{-sy} dy \quad . \quad (D.6)$$

The transform becomes, after one integration by parts and a change from an integration over y to one over Φ ,

$$\overline{V_w(s)} = \frac{-V_w(y) e^{-sy}}{s} \Big|_0^\infty + \int_0^\infty \frac{j\Omega e^{-sy} e^{j\Omega\Phi}}{s} d\Phi \quad . \quad (D.7)$$

With the substitution of an expression for y obtained from Eq. D.3b, Eq. D.7 becomes

$$\overline{V_w(s)} = \frac{1}{s} + j \frac{\Omega}{s} \int_0^\infty e^{(-s+j\Omega)\Phi} e^{s\sigma_p \sin \Phi} d\Phi \quad . \quad (D.8)$$

A Bessel function identity is needed to evaluate Eq. D.8. A generating function for the modified Bessel function of first kind, I_n , is

$$e^{\frac{1}{2} z(t+1/t)} = \sum_{n=-\infty}^{\infty} I_n(z) t^n \quad . \quad (D.9)$$

Let $t = je^{j\theta}$; Eq. D.9 becomes

$$e^{z \sin \theta} = \sum_{n=-\infty}^{\infty} I_n(z) (-j)^n e^{jn\theta} \quad . \quad (D.10)$$

Equation D.8 becomes, with the application of Eq. D.10,

$$\overline{V_w(s)} = \frac{1}{s} + \frac{j\Omega}{s} \sum_{n=-\infty}^{\infty} I_n(\sigma_p s) (-j)^n \int_0^\infty e^{[-s + (\Omega+n)]j\phi} d\phi \quad . \quad (D.11)$$

Evaluation of the integral in Eq. D.11 is straightforward and yields

$$\overline{V_w(s)} = \frac{1}{s} + \frac{j\Omega}{s} \sum_{n=-\infty}^{\infty} (-j)^n \frac{I_n(\sigma_p s)}{s - j(\Omega+n)} \quad . \quad (D.12)$$

The inverse Laplace transform of Eq. D.12 is expressed as

$$V_w(y) = \frac{1}{2\pi j} \int_{Br} \left[\frac{1}{s} + j\Omega \sum_{n=-\infty}^{\infty} (-j)^n \frac{I_n(\sigma_p s)}{s - j(\Omega+n)} \right] e^{sy} ds \quad . \quad (D.13)$$

The integrand of Eq. D.13 has simple poles at $s=0$ and at $s=j(\Omega+n)$. Using the theorem of residues to evaluate the boundary integral of Eq. D.13 yields

$$V_w(y) = \sum_{n=-\infty}^{\infty} \frac{\Omega}{\Omega + n} J_n \left[(\Omega+n)\sigma_p \right] e^{j(\Omega+n)y} \quad , \quad (D.14)$$

where the Bessel function identity

$$I_n(jx) = j^n J_n(x) \quad (D.15)$$

has been used. Taking the imaginary part of Eq. D.14, the final result

is obtained

$$V_w(y) = \sum_{n=-\infty}^{\infty} \frac{\Omega}{\Omega + n} J_n(\Omega + n)\sigma_p \sin(\Omega + n)y \quad . \quad (D.16)$$

Equation D.16 is an alternate representation for the improved FM solution presented in Chapter II (Eq. 2.19) and is equivalent to Eq. 2.20. The derivation presented here is due to Blackstock. A similar approach was used by Lockwood¹⁶ in his derivation of a solution equivalent to Fenlon's solution.

Equation D.16 shows an asymmetry structure similar to the approximate Fenlon solution (Eq. 2.23); the argument of the Bessel function is $\Omega + n$, not simply Ω like in the FM solution. The amplitude factor for Eq. D.16 is $\Omega/(\Omega + n)$ rather than an amplitude factor similar to the one in Eq. 2.23. The reason for the difference in amplitude factors is that Eq. 2.23 incorporates to some degree the mutual sideband formation from both signals, while Eq. D.16 incorporates only the sidebands from the effect of the pump on the weak signal.

BIBLIOGRAPHY

1. A. L. Thuras, R. T. Jenkins, and H. T. O'Neil, "Extraneous Frequencies Generated in Air Carrying Intense Sound Waves," J. Acoust. Soc. Am. 6, 173-180 (1935).
2. U. Ingard and D. E. Pridmore-Brown, "Scattering of Sound by Sound," J. Acoust. Soc. Am. 28, 367-369 (1956).
3. P. J. Westervelt, "Scattering of Sound by Sound," J. Acoust. Soc. Am. 29, 934-935 (1957).
4. P. J. Westervelt, "Parametric End-Fire Array," J. Acoust. Soc. Am. 32, 934(A) (1960). Paper presented at the 59th meeting of the Acoustical Society of America, Brown University, Providence, Rhode Island (1960).
5. P. J. Westervelt, "Absorption of Sound by Sound," J. Acoust. Soc. Am. 53, 384(A) (1973). Paper presented at the 84th meeting of the Acoustical Society of America, Miami Beach, Florida (1972).
6. M. E. Schaffer, "The Suppression of Sound with Sound," Applied Research Laboratories Technical Report No. 75-64 (ARL-TR-75-64), Applied Research Laboratories, The University of Texas at Austin (1975). ADA 023 128.
7. M. B. Moffett, W. L. Konrad, and A. T. Corcella, "An Experimental Demonstration of the Absorption of Sound by Sound in Water," Naval Underwater Systems Center Technical Memorandum No. TD124-92-7f, Naval Underwater Systems Center, New London Laboratory, New London, Connecticut (1975).
8. F. M. Pestorius, "Propagation of Plane Acoustic Noise of Finite Amplitude," Applied Research Laboratories Technical Report No. 73-23 (ARL-TR-73-23), Applied Research Laboratories, The University of Texas at Austin (1973). AD 778 868.
9. F. H. Fenlon, "An Extension of the Bessel-Fubini Series for a Multiple-Frequency CW Acoustic Source of Finite Amplitude," J. Acoust. Soc. Am. 51, 284-289 (1972).
10. K. A. Naugol'nykh, S. I. Soluyan, and R. V. Khokhlov, "Nonlinear Interaction of Sound Waves in an Absorbing Medium," Sov. Phys. Acoust. 9, 155-159 (1963).
11. M. B. Moffett, W. L. Konrad, and L. F. Carlton, "An Experimental Demonstration of the Absorption of Sound by Sound in Water," submitted for publication in J. Acoust. Soc. Am. (1977).

12. E. D. Banta, "Lossless Propagation of One-Dimensional Finite Amplitude Sound Waves," *J. Math. Anal. Applications* 10, 6-13 (1964).
13. D. T. Blackstock, "Propagation of Plane Sound Waves of Finite Amplitude in Nondissipative Fluids," *J. Acoust. Soc. Am.* 34, 9-30 (1962).
14. D. T. Blackstock, "Nonlinear Acoustics (Theoretical)," in *Amer. Inst. Phys. Handbook*, D. E. Gray, ed. (McGraw-Hill Book Co., Inc., New York, 1972), 3rd ed., pp. 3-183/ - /3-205.
15. R. T. Beyer, *Nonlinear Acoustics* (Naval Sea Systems Command, Washington, D. C., 1975, copies available from John Neely, N.S.S.C. 06H1, Washington, D. C. 20360), pp. 98-101.
16. J. C. Lockwood, "Two Problems in High-Intensity Sound," Applied Research Laboratories Technical Report No. 71-26 (ARL-TR-71-26), Applied Research Laboratories, The University of Texas at Austin (1971). AD 740 498.
17. D. T. Blackstock, "Connection between Fay and Fubini Solutions for Plane Sound Waves of Finite Amplitude," *J. Acoust. Soc. Am.* 39, 1019-1026 (1966).
18. A. B. Carlson, *Communications Systems: An Introduction to Signals and Noise in Electrical Communications* (McGraw-Hill Book Co., New York, 1968), pp. 225-228.
19. M. J. Lighthill, "Viscosity Effects in Sound Waves of Finite Amplitude," in *Surveys in Mechanics*, G. K. Batchelor and R. M. Davies, eds. (Cambridge Univ. Press, Cambridge, England, 1956), pp. 250-352.
20. H. Lamb, *Hydrodynamics* (Daves Publications, New York, 1945), pp. 619-621.
21. G. Kirchhoff, "Ueber der Einfluss der Warmeleitung in Gase auf die Schallbewegung," *Ann. Physik* 134, 177-193 (1868). ["On the Influence of Heat Conduction on Sound Propagation in Gases."]
22. D. E. Weston, "The Theory of the Propagation of Plane Sound Waves in Tubes," *Proc. Phys. Soc. (London)* B66, 695-709 (1953).
23. L. B. Evans, H. E. Bass, and L. C. Sutherland, "Atmospheric Absorption of Sound: Theoretical Predictions," *J. Acoust. Soc. Am.* 51, 1565-1575 (1972).
24. D. A. Webster, "Saturation of Plane Acoustic Waves and Notes on the Propagation of Finite Amplitude Spherical Waves," Master's Thesis, The University of Texas at Austin (1976), Applied Research Laboratories Technical Report No. 77-4 (ARL-TR-77-4), Applied Research Laboratories, The University of Texas at Austin (1977). ADA 035 694.

25. John C. Burgess, "On Digital Spectrum Analysis of Periodic Signals," J. Acoust. Soc. Am. 58, 556-567 (1975).
26. D. A. Webster, M. A. Theobald, and D. T. Blackstock, "Nonlinear Propagation Effects in Noise," Paper presented at the DOT/FAA Jet Noise/Core Noise Status Review, Washington, D. C., 22-24 February 1977 (ARL-TP-77-12).
27. J. L. McKittrick, D. T. Blackstock, and W. M. Wright, "Profile of Repeated Shock Waves in a Tube," J. Acoust. Soc. Am. 42, 1153(A) (1967).
28. S. H. Burns, "Rational Design of Matched Absorbing Terminations for Tubes," J. Acoust. Soc. Am. 49, 1693-1697 (1971).
29. J. Jessup, "A Study of Terminations for Progressive Wave Tubes," internal report on summer research project under Dr. D. T. Blackstock, Applied Research Laboratories, The University of Texas at Austin (1976).
30. O. V. Rudenko, S. I. Soluyan, and R. V. Khokhlov, "Problems in the Theory of Nonlinear Acoustics," Sov. Phys. Acoust. 20, 271-275 (1974).

March 1977

DISTRIBUTION LIST FOR
ARL-TR-77-22
UNDER CONTRACTS F44620-76-C-0040
and N00014-75-C-0867
UNCLASSIFIED

Director	(3)	Office of Naval Research	(6)
Defense Advanced Research Projects Agency		Code 102 1P (ONR/L)	
Attn: Technical Library		800 North Quincy Street	
1400 Wilson Blvd.		Arlington, VA 22217	
Arlington, VA 22209			
Office of Naval Research	(3)	Commanding Officer	(3)
Physics Program Office (Code 421)		Office of Naval Research Branch Office	
800 North Quincy Street		1030 East Green Street	
Arlington, VA 22217		Pasadena, CA 91101	
Naval Research Laboratory	(3)	Commanding Officer	(3)
Department of the Navy		Office of Naval Research Branch Office	
Attn: Technical Library		495 Summer Street	
Washington, DC 20375		Boston, MA 02210	
Office of Naval Research	(1)	Director	(1)
Assistant Chief for Technology (Code 200)		U.S. Army Engineering Research	
800 North Quincy Street		and Development Laboratories	
Arlington, VA 22217		Attn: Technical Documents Center	
		Fort Belvoir, VA 22060	
Office of the Director of Defense	(3)	ODDR&E Advisory Group on Electron Devices	(3)
Research and Engineering		201 Varick Street	
Information Office Library Branch		New York, NY 10014	
The Pentagon			
Washington, DC 20301		New York Area Office	(1)
U.S. Army Research Office	(2)	Office of Naval Research	
Box CM, Duke Station		715 Broadway, 5th Floor	
Durham, NC 27706		New York, NY 10003	
Director, National Bureau of Standards	(1)	Air Force Weapons Laboratory	(1)
Attn: Technical Library		Technical Library	
Washington, DC 20234		Kirtland Air Force Base	
		Albuquerque, NM 87117	
Commanding Officer	(3)	Air Force Avionics Laboratory	(1)
Office of Naval Research Branch Office		Air Force Systems Command	
536 South Clark Street		Technical Library	
Chicago, IL 60605		Wright-Patterson Air Force Base	
		Dayton, OH 45433	
San Francisco Area Office	(3)	Naval Weapons Center	(1)
Office of Naval Research		Technical Library (Code 753)	
760 Market Street, Room 447		China Lake, CA 93555	
San Francisco, CA 94102			

Dist. List for ARL-TR-77-22 under Contracts F44620-76-C-0040 and N00014-75-C-0867 (cont'd)

Lawrence Livermore Laboratory Attn: Dr. W.F. Krupke University of California PO Box 808 Livermore, CA 94550	(1)	Naval Electronics Laboratory Center Technical Library San Diego, CA 92152	(1)
Harry Diamond Laboratories Technical Library Connecticut Ave. at Van Ness, N.W. Washington, DC 20008	(1)	Naval Undersea Center Technical Library San Diego, CA 92132	(1)
Naval Air Development Center Attn: Technical Library Johnsville Warminster, PA 18974	(1)	Naval Surface Weapons Center Technical Library Dahlgren, VA 22448	(1)
Naval Training Equipment Center Technical Library Orlando, FL 32813	(1)	Naval Ship Research and Development Center Central Library (Code L42 and L43) Bethesda, MD 20084	(1)
Naval Underwater Systems Center Technical Library New London, CT 06320	(1)	Naval Surface Weapons Center Technical Library Silver Spring, Maryland 20910	(1)
Commandant of the Marine Corps Scientific Advisor (Code RD-1) Washington, DC 20380	(1)	Naval Avionics Facility Technical Library Indianapolis, IN 46218	(1)
Naval Ordnance Station Technical Library Indian Head, MD 20640	(1)	AFOSR/NA Attn: L/C L.W. Ormand Bldg 410 Bolling AFB, DC 20332	(16)
Naval Postgraduate School Technical Library (Code 0212) Monterey, CA 93940	(1)	USAFA (Library) USAFA CO 80840	(1)
Naval Missile Center Technical Library (Code 5632.2) Point Mugu, CA 93010	(1)	AFIT Library (AU) AFIT, Area B, Bldg 640 Wright-Patterson AFB OH 45433	(1)
Naval Ordnance Station Technical Library Louisville, KY 40214	(1)	NASA Langley Research Center Attn: Library Hampton, VA 23365	(1)
Commanding Officer Ocean Research & Development Activity National Space Technology Laboratories Bay St. Louis, MS 39520	(1)	AFAPL Attn: Paul Shahady Wright-Patterson AFB OH 45433	(1)
Naval Explosive Ordnance Disposal Facility Technical Library Indian Head, MD 20640	(1)	Aeronautical Research Associates of Princeton, Inc 50 Washington Road Princeton, NJ 08540	(1)
		Case Western University School of Engineering Attn: Prof. Greber University Circle Cleveland, OH 44106	(1)

Dist. List for ARL-TR-77-22 under Contracts F44620-76-C-0040 and N00014-75-C-0867 (cont'd)

Stanford University Department of Aeronautics & Astronautics Attn: K. Karamcheti Stanford, CA 94305	(1)	Naval Postgraduate School Physics and Chemistry Department Attn: A.B. Coppens J.V. Sanders Monterey, CA 93940	(1) (1)
NEAR, Inc 510 Clyde Ave Mountain View, CA 94043	(1)	Naval Research Laboratory Underwater Sound Reference Division Attn: P.H. Rogers PO Box 8337 Orlando, FL 32806	(1)
University of Southern California Department of Aerospace Engineering Attn: Dr. Ho, Chih-Ming University Park Los Angeles, CA 90007	(1)	New London Laboratory Naval Underwater Systems Center Attn: M.B. Moffett W.L. Konrad R.H. Mellen	(1) (1) (1)
University of Toronto Institute of Aerospace Studies Attn: H.S. Ribner I.I. Glass 4925 Dufferin St Downsview, Ontario Toronto Canada, M3H 5T6	(1) (1)	New London, CT 06320 Office of Naval Research Attn: R.F. Obrochta (Code 222) 800 North Quincy Street Arlington, VA 22217	(1)
U.S. Department of Commerce National Oceanic and Atmospheric Administration Environmental Research Laboratories Attn: Freeman Hall Boulder, CO 80302	(1)	Pennsylvania State University Applied Research Laboratory Attn: F. H. Fenlon PO Box 30 State College, PA 16801	(1)
Brown University Department of Physics Attn: P.J. Westervelt Providence, RI 02912	(1)	Raytheon Company Attn: J.C. Lockwood R.G. Pridham W. Main Road Portsmouth, RI 02871	(1) (1) (1)
NASA Langley Research Center Acoustics and Noise Reduction Division Attn: J.M. Seiner, Mail Stop 460 Hampton, VA 23365	(1)	University of Tennessee Department of Physics Attn: M.A. Breazeale Knoxville, TN 37916	(1)
Georgia Institute of Technology School of Mechanical Engineering Attn: A.D. Pierce Atlanta, GA 30332	(1)	Cambridge University University Engineering Department Attn: J.E. Ffowcs-Williams Trumpington Street Cambridge CB 2 1PZ ENGLAND	(1)
Hendrix College Department of Physics Attn: R.L. Rolleigh Conway, AR 72032	(1)		
Kalamazoo College Department of Physics Attn: W.M. Wright Kalamazoo, MI 49008	(1)	The Clayton H. Allen Corporation 651 Concord Avenue Attn: Dr. Clayton H. Allen Cambridge, MA 02138	(1)

Dist. List for ARL- TR-77-22 under Contracts F44620-76-C-0040 and N00014-75-C-0867 (cont'd)

Defence Research Establishment Atlantic Attn: H.M. Merklinger PO Box 1012 Dartmouth, Nova Scotia B2Y 3Z7 CANADA	(1)	Virginia Polytechnic Institute and State University Department of Engineering Science and Mechanics Attn: John Kaiser Ali Nayfeh	(1) (1)
Technical University of Denmark Fluid Mechanics Department Attn: L. Bjørnø Building 404 DK-2800 Lyngby DENMARK	(1)	Blacksburg, VA 24061 University of Göttingen Attn: M.R. Schroeder 42-44 Burger Ctr. Göttingen, Germany	(1) (1)
The University of Birmingham Electronic and Electrical Engineering Department Attn: H.O. Berkday P.O. Box 36 B Birmingham B15 2TT ENGLAND	(1)	University of Toronto Mechanical Engineering Department Attn: David S. Scott Toronto, Ontario, Canada M5S 1A4 Institute of Sound Vibration Research The University	(1) (1)
Paul S. Veneklasen and Associates 1711 Sixteenth Street Attn: Mark E. Schaffer Santa Monica, CA 90404	(1)	Attn: Dr. C.L. Morfey Southampton S09 5NH ENGLAND	
A & B Science Consultants, Inc PO Box 443 Attn: Henry E. Bass, President University, MS 38677	(1)	Dr. J.H. Ginsberg School of Mechanical Engineering Purdue University West Lafayette, IN 47907	(1)
Applied Physics Department Royal Melbourne Institute of Technology 124 La Trobe Street Attn: John D. Buntine Melbourne, Victoria, 3000, AUSTRALIA	(1)	Dr. Akira Nakamura The Institute of Scientific & Industrial Research Osaka University Yamadakami, Suita-Shi Osaka 565 JAPAN	(1)
Yale University Mason Laboratory M4 Attn: R. E. Apfel New Haven, CT 06511	(1)	Dr. R.B. Thompson Science Center Rockwell International 1049 Camino Dos Rios Thousand Oaks, CA 91360	(1)
University of Leeds Department of Mathematics Attn: David G. Crighton Leeds, Yorkshire, LS2 9JT ENGLAND	(1)	Centre Universitaire, 59326 Laboratoire d'Opto-Acousto-Electronique Attn: J.M. Rouvaen Valéncienes	(1)
M.I.T. Ocean Engineering Department Attn: W.L. Harris Cambridge, MA 02139	(1)	FRANCE	

Dist. List for ARL-TR-77-22 under Contracts F44620-76-C-0040 and N00014-75-C-0867 (cont'd)

Louis C. Sutherland Wyle Labs 128 Maryland St. El Segundo, CA 90245	(1)
Francis J. Jackson Bolt Beranek and Newman, Inc. 1701 North Fort Myer Drive Arlington, VA 22209	(1)
William L. Willshire Rt 10 Box 306 Gulfport, MS 39501	(6)
David R. Kleeman IIT Research Institute ECAC P.O. Box 1711 Annapolis, MD 21404	(1)
Bolt Beranak and Newman, Inc. Attn: Mark Theobald 1740 Ogden Avenue Downers Grove, IL 60515	(1)
H.G. Frey, ARL/UT	(1)
T.G. Goldsberry, ARL/UT	(1)
J.M. Huckabay, ARL/UT	(1)
T.G. Muir, ARL/UT	(1)
D.A. Webster, ARL/UT	(1)
J.J. Truchard, ARL/UT	(1)
W. Cobb, ARL/UT	(1)
R.T. Beyer, ARL/UT	(1)
D.T. Blackstock, ARL/UT	(8)